VegET evapotranspiration for Africa: continental-scale simulation, multi-product evaluation, and drought assessment

Komlavi Akpoti, Naga Manohar Velpuri, Mansoor Leh, Stefanie Kagone, Kirubel Mekonnen, Afua Owusu, Mulugeta Tadesse, Paranamana Thilina Prabhath, Lahiru Madushanka, Tharindu Perera, Gabriel E. L. Parrish, Vinay Nangia, Souleymane Sy, Jan Bliefernicht, Samuel Guug, Abdulkarim H. Seid, Gabriel B. Senay

Angaben zur Veröffentlichung / Publication details:

Akpoti, Komlavi, Naga Manohar Velpuri, Mansoor Leh, Stefanie Kagone, Kirubel Mekonnen, Afua Owusu, Mulugeta Tadesse, et al. 2026. "VegET evapotranspiration for Africa: continental-scale simulation, multi-product evaluation, and drought assessment." *Journal of Hydrology: Regional Studies* 66: 103511. https://doi.org/10.1016/j.ejrh.2026.103511.

Journal of Hydrology: Regional Studies 66 (2026) 103511

Contents lists available at ScienceDirect

Journal of Hydrology: Regional Studies

journal homepage: www.elsevier.com/locate/ejrh

VegET evapotranspiration for Africa: Continental-scale simulation, multi-product evaluation, and drought assessment

Komlavi Akpoti [a,*], Naga Manohar Velpuri [b], Mansoor Leh [b], Stefanie Kagone [d], Kirubel Mekonnen [c], Afua Owusu [a], Mulugeta Tadesse [c], Paranamana Thilina Prabhath [b], Lahiru Madushanka [b], Tharindu Perera [b], Gabriel E.L. Parrish [e], Vinay Nangia [f], Souleymane Sy [g], Jan Bliefernicht [g], Samuel Guug [h], Abdulkarim H. Seid [c], Gabriel B. Senay [i]

[a] International Water Management Institute (IWMI), Accra, Ghana
[b] International Water Management Institute (IWMI), Colombo, Sri Lanka
[c] International Water Management Institute (IWMI), Addis Ababa, Ethiopia
[d] ASRC Federal Data Solutions LLC, Contractor to the US Geological Survey (USGS) Earth Resource Observation and Science (EROS) Center, Sioux Falls, SD 57198, USA
[e] KBR, Contractor to the USGS Earth Resources Observation and Science (EROS) Center, Sioux Falls, SD 57198, USA
[f] International Center for Agricultural Research in the Dry Areas (ICARDA), Rabat, Morocco
[g] Institute of Geography, University of Augsburg, Augsburg, Germany
[h] West African Science Service Centre on Climate Change and Adapted Land Use, WASCAL Competence Centre, Ouagadougou, Burkina Faso
[i] US Geological Survey EROS Center, Sioux Falls, SD, USA and North Central Climate Adaptation Science Center, Fort Collins, CO 80526, USA

ARTICLE INFO

Keywords:
Hydrological modeling
Evapotranspiration (*ETa*)
Africa
VegET model
Remote sensing
Drought monitoring
Climate zones
Land use

ABSTRACT

Study region: Continental Africa, encompassing diverse climatic zones—tropical, arid, and temperate—and spanning major transboundary river basins such as the Nile, Niger, Congo, Volta, and Zambezi River Basins. The region exhibits pronounced hydroclimatic gradients and heterogeneous land use systems ranging from rainfed croplands and rangelands to dense tropical forests and irrigated schemes.

Study focus: Actual evapotranspiration (ETa) is a central component of the terrestrial water balance, governing the redistribution of water and energy between the land surface and the atmosphere. Accurate estimation of ETa at continental scale is critical for hydrological monitoring, water resource management, and climate adaptation, as well as for quantifying water, energy, and carbon fluxes that underpin sustainable development. In this study, we applied the agro-hydrologic VegET v2 model to simulate a new, high-resolution, continental-scale ETa dataset for Africa (2000–2021). The model results were benchmarked against four widely used remote sensing-based products—MODIS16 v6.1, SSEBop v6.1, WaPOR v3, and GLEAM v4.1a—across major climate zones, land use types, and River Basins, providing a comprehensive multi-product evaluation of evapotranspiration dynamics across the continent.

New hydrological insights for the region: Validation against eddy covariance flux tower observations at eight representative sites confirmed that VegET v2 accurately reproduces the seasonal dynamics of observed ETa, achieving a correlation (r) of 0.8 and an RMSE of 25 mm month^{-1} —accuracy that is comparable to or higher than accuracies of satellite-based products

* Corresponding author.
E-mail address: k.akpoti@cgiar.org (K. Akpoti).

https://doi.org/10.1016/j.ejrh.2026.103511
Received 6 October 2025; Received in revised form 23 April 2026; Accepted 30 April 2026
Available online 15 May 2026

MODIS16, SSEBop, and GLEAM. This study represents one of the first Africa-wide hydrological simulations of ETa, extending the VegET model beyond basin-scale applications. Intercomparisons reveal that VegET aligns closely with MODIS16, SSEBop, and GLEAM in humid and tropical regions ($r = 0.80–0.90$; RMSE < 20 mm month^{-1}), while greater discrepancies appear in arid and semi-arid zones, where WaPOR tends to overestimate ETa (RMSE ≥ 28 mm month^{-1}). Despite these differences, VegET effectively captures spatial and temporal ETa variability across rainfed croplands, forests, and savannas, supporting its utility in regional water balance assessments, water accounting, and drought monitoring. A key application of VegET v2 is the Evapotranspiration Deficit Index (ETDI), derived by integrating VegET-based ETa with potential evapotranspiration (PET) to quantify water stress. ETDI successfully captured major drought episodes across Africa, including persistent Sahelian and southern African dry spells, the 2020–2021 winter drought in the Maghreb, and the 2018–2019 austral summer drought in southern Africa, while identifying positive anomalies over central Africa indicative of recurrent wetness. These results underscore VegET's capability as a hydrologically consistent, operational tool for continental ETa monitoring and drought assessment, offering support for basin-scale water balance studies, food security planning, and climate resilience across Africa's diverse hydrological environments.

1. Introduction

Actual evapotranspiration (ETa) is a central component of the terrestrial water balance that directly controls partitioning of precipitation into soil moisture, groundwater recharge, and river discharge (Bayat et al., 2021; Pokorny, 2009). Beyond its hydrological role, ETa links the water, energy, and carbon cycles (for more detail, refer to (Katul et al., 2012)), influencing atmospheric dynamics and ecosystem productivity. Water vapor released through ETa also acts as a greenhouse gas, making ETa a sensitive diagnostic variable for climate change (Wang and Dickinson, 2012). Globally, terrestrial ETa accounts for approximately 70% of precipitation (Oki and Kanae, 2006; K. Zhang et al., 2016), and in Africa, nearly 50% of annual rainfall originates from land-surface transpiration (Te Wierik et al., 2022, Van Der Ent et al., 2010), underscoring the central role ETa plays in regional hydrological cycles (Werth and Avissar, 2004). In most African catchments, ETa represents the largest consumptive use of rainfall, often exceeding 70% of annual precipitation (Blatchford et al., 2020; Fuentes et al., 2024; Kiptala et al., 2013; Weerasinghe et al., 2020). Accurate continental-scale estimation of ETa is therefore essential for hydrological monitoring (Velpuri et al., 2013a; Xu and Singh, 2005), water resources management, and climate adaptation (Hssaine et al., 2018; Vinukollu et al., 2011).

Despite its importance, ETa is inherently difficult to measure and predict at large spatial scales (Zhang et al., 2016) due to complex interactions at the soil–vegetation–atmosphere interface. Under- or over-estimation of ETa propagates directly into errors in river discharge projections (Thompson et al., 2014), compromises agricultural drought monitoring that depends on ET-based indices (Narasimhan and Srinivasan, 2005), and distorts water balance assessments that underpin regional water resource planning (Bo et al., 2011; Jin et al., 2009). ETa also affects groundwater recharge (Jin et al., 2009; Pool et al., 2021) and soil moisture dynamics (Dong et al., 2020; Huang et al., 2021) with direct implications for agricultural productivity (Blatchford et al., 2019) and environmental sustainability. In agriculture, ETa governs crop water requirements and irrigation scheduling (Nagappan et al., 2020), while at landscape scale, ETa is an indicator of ecosystem health and carbon sequestration (Lan et al., 2021; Liu et al., 2024; Yang et al., 2021; Zhao et al., 2022). Variations in ETa can signal changes in vegetation cover, land use, and climate conditions (Akpoti et al., 2016), making ETa an essential climate variable for environmental monitoring (Bayat et al., 2021).

Remote sensing offers a unique capacity to monitor ETa over vast and heterogeneous landscapes where ground-based measurements are sparse or absent, a condition that characterizes much of Africa (Glenn, Neale, et al., 2011). These techniques integrate visible, near-infrared, and thermal-infrared spectral bands to retrieve parameters such as vegetation indices, surface temperature, and albedo, from which ETa can be estimated (Zhang et al., 2016). Sensors including the Moderate Resolution Imaging Spectroradiometer (MODIS), the Visible Infrared Imaging Radiometer Suite (VIIRS), Landsat, and Sentinel-2 provide spatially explicit and temporally continuous ETa estimates at varying resolutions (Guerschman et al., 2022). Building on these observations, energy-balance models such as the Surface Energy Balance Algorithm for Land (SEBAL) (Bastiaanssen, 2000) and Mapping EvapoTranspiration at high Resolution with Internalized Calibration (METRIC), Allen et al., (2007) further constrain ETa by incorporating thermal infrared data.

When validated against eddy covariance (EC) flux tower measurements—widely regarded as the benchmark for ETa evaluation—remote sensing products typically achieve accuracies within 15 to 20% (Chen et al., 2009) or 11 to 14% in some studies (Ha et al., 2015). However, the reliability of these validations is itself constrained by well-documented limitations of EC data, including energy-budget non-closure of 10 to 30% (Glenn et al., 2010) and the restricted spatial footprint of tower measurements, which typically cover fetches of 100–1000 m (Vinukollu et al., 2011). Moreover, the accuracy of remote sensing-based ETa models depends on the quality of ground-based calibration data because errors or biases in reference measurements propagate into model parameterization and ultimately into ETa estimates (Glenn et al., 2010; Ha et al., 2015). Despite advances in satellite technology—such as MODIS Collection 6 (Wan, 2014; Wan et al., 2021), VIIRS (Justice et al., 2013; Hulley and Hook, 2018), and Sentinel-2 (Drusch et al., 2012; European Space Agency (ESA), 2021)—that have improved spatial and temporal resolution, remote sensing-based ETa models remain sensitive to cloud cover, which limits observation frequency in tropical and cloud-prone regions (Awada et al., 2022). Integrated approaches combining remote sensing with surface energy balance and soil moisture modeling have been proposed to construct

continuous ETa time series under such data-limited conditions (Awada et al., 2024).

Given the availability of multiple ETa estimation methods (Zhang et al., 2016), systematic intercomparison of algorithms and products is essential for understanding the strengths and limitations of each approach across diverse climatic and land cover conditions. While remote sensing approaches provide critical spatial coverage, they are primarily diagnostic and rely on empirical or energy-balance relationships. Hydrological models, in contrast, explicitly account for soil water storage, precipitation inputs, and vegetation phenology in simulating ETa, thereby offering complementary value for water balance analysis and drought monitoring. Continental-scale hydrological simulations of ETa remain rare in Africa (Trambauer et al., 2013), where most VegET applications to date have focused on the U.S. (Senay, 2008; Senay et al., 2011; Velpuri et al., 2013) and the Horn of Africa (Senay et al., 2023).

At the global scale, several reviews and intercomparisons have highlighted both the progress and persistent limitations of existing ETa products. Tang et al., (2024) reviewed 25 global ETa datasets and found that remote sensing-based and hybrid products generally outperform reanalysis-based estimates, though significant inter-product variability persists due to differences in spatial resolution, temporal coverage, and underlying algorithms. Zhang et al., (2016) similarly underscored persistent uncertainties arising from model parameterization and reliance on ground-based calibration data, noting that different models yield varying results depending on climatic and land cover conditions. To address these challenges, multi-model comparisons have become indispensable. Vinukollu et al., (2011) evaluated process-based models including SEBS, PM-Mu, and PT-Fi using NASA Aqua satellite inputs, highlighting the strengths of energy-balance approaches but also the sensitivity of models like SEBS to simplistic assumptions. Velpuri et al., (2013a) compared MODIS16 and SSEBop across the conterminous United States and demonstrated that SSEBop's integration of thermal data increased accuracies of estimates in forested regions and varying climate zones, with uncertainties ranging from 15 to 30% at basin scales. Studies using two-source energy balance and vegetation-index approaches have further demonstrated that dynamic models incorporating stomatal resistance or crop-coefficient relationships outperform simpler vegetation-index-only methods, which fail to adequately capture moisture stress conditions (Gonzalez-Dugo et al., 2009; Ha et al., 2015). Pòças et al., (2020) confirmed the utility of spectral vegetation indices such as the Normalized Difference Vegetation Index (NDVI) and Soil Adjusted Vegetation Index (SAVI) for correlating with crop coefficients in irrigation management, despite limitations in cloud-prone regions. However, the consistent underestimation by MODIS ETa products remains a concern requiring further refinement (Gonzalez-Dugo et al., 2009; Ha et al., 2015). Commonwealth Scientific and Industrial Research Organisation (CSIRO) MODIS Reflectance Scaling Evapotranspiration (CMRSET) (Guerschman et al., 2022) offer flexible alternatives by integrating data from multiple satellite platforms. Collectively, these findings underscore the need for comprehensive multi-product evaluations, particularly in data-scarce regions like Africa (Tang et al., 2024), where such assessments are essential to improving ETa estimation accuracy and informing effective water resource management (Wang and Dickinson, 2012).

Several studies have evaluated ETa models and products across Africa, revealing substantial spatial and temporal variability driven by the continent's diverse climates and landscapes. In West Africa, Adeyeri and Ishola, (2021) analyzed ETa trends using Global Land Evaporation Amsterdam Model (GLEAM), CSIRO Penman-Monteith Leuning (PML), and FLUXNET-MTE products and found significant inter-product differences across ecological zones, with rainfall identified as the primary driver of ETa variability in semi-arid regions like the Sahel. Jung et al., (2019a) further investigated ETa uncertainties in West Africa and showed that land surface model parameterization contributed over 90% of total uncertainty in humid zones, emphasizing the need for improved modeling approaches in data-scarce regions. At continental scale, Trambauer et al., (2014) documented notable discrepancies among PCRaster Global Water Balance (PCR-GLOBWB), ERA-Interim, and MOD16, particularly in arid and semi-arid regions where input data variability and model uncertainties are most pronounced. Sun et al. (2012) combined The MODerate resolution Imaging Spectroradiometer (MODIS) and The Spinning Enhanced Visible InfraRed Imager (SEVIRI) data to increase accuracies of daily ETa estimates across Africa but found that satellite-based estimates underestimated ETa by 13 to 35% during wet periods, illustrating the difficulty of achieving accurate measurements across diverse climatic conditions. In sub-Saharan and East Africa, Marshall et al. (2013a) demonstrated increased accuracies from integrating remote sensing with land surface models in humid regions but identified persistent difficulties in semi-arid areas where traditional models often face challenges (Dile et al., 2020). Kiptala et al., (2013) showed that SEBAL, when integrated with ground-based meteorological data, provided more accurate ETa estimates than MODIS16 in the upper Pangani River Basin, especially during dry periods. Across South Africa, Majozi et al. (2017) conducted an intercomparison of satellite-based daily ETa estimates and found that no single model consistently outperformed others across all biomes and seasons, with significant underestimations during wet periods. Dzikiti et al. (2019) evaluated the Penman-Monteith based MODIS16 and the modified Priestley-Taylor (PT-JPL) in seasonally arid ecosystems and confirmed that both performed adequately primarily during periods of severe water stress. These studies collectively reveal the persistent challenges in estimating ETa accurately across Africa's varied landscapes and highlight the need for comprehensive multi-product and multi-model evaluations across major basins, land use classes, and climate zones.

The VegET model (Senay, 2008; Senay et al., 2023) is a large-scale agro-hydrological model that estimates ETa through a daily soil-water balance approach. It uses NDVI-derived landscape crop coefficients (Kcp) to represent vegetation water demand without requiring a land cover map or site-specific crop coefficients. A soil water stress function (Ks) modulates ETa based on root-zone moisture availability, ensuring that estimates are dynamically constrained by precipitation inputs and soil storage capacity. Unlike purely remote sensing-based ETa products that rely on empirical or energy-balance relationships, VegET's hydrological foundation provides explicit linkages between precipitation, soil moisture, and evapotranspiration, making it well suited for basin-scale water accounting and drought monitoring.

Building on this background, we applied and calibrated the enhanced VegET v2 at the scale of the entire African continent (2000–2021). This represents one of the first continental-scale hydrological simulations of ETa for Africa and moves beyond basin-level applications using VegET, thus provides a basis for intercomparison with existing remote sensing ETa products and a hydrologically

grounded dataset for continental water balance analysis.

The main objectives of this study are to: (i) apply and evaluate VegET v2 to simulate continental-scale ETa for Africa (2000–2021) and validate it against eddy-covariance (EC) flux-tower observations across representative ecosystems; (ii) benchmark VegET v2 against four widely used remote sensing-based ET products—MODIS16 v6.1 (Mu et al., 2011), SSEBop v6.1 (Senay et al., 2013, 2022), WaPOR v3 (FAO and IHE Delft, 2019), and GLEAM v4.1a (Martens et al., 2017; Miralles et al., 2011) —through systematic intercomparison across major river basins, land-use classes, and climate zones; and (iii) demonstrate the suitability of VegET v2 for operational drought monitoring using the Evapotranspiration Deficit Index (ETDI). Through the combination of modeling, validation, intercomparison, and drought applications, this research advances the understanding of evapotranspiration dynamics in Africa and strengthens the basis for basin-scale water accounting, agricultural planning, and climate adaptation strategies.

2. Materials and methods

This study applies the VegET v2 model (Senay et al., 2023) across the entire African continent to generate spatially explicit, daily ETa estimates for the period 2000–2021. The implementation builds on recent continental-scale hydrological applications of VegET within Africa (Akpoti et al., 2024), but here we focus specifically on the ETa component and its evaluation. The detailed model description, including root-zone soil moisture dynamics and water balance partitioning, is presented in Section 2.4.

2.1. Study area description

The study area encompasses the entire African continent, characterized by a wide range of climatic zones, major river basins, diverse land use patterns, and significant cropland areas. Accurately estimating ETa across Africa is complicated by pronounced climate variability that ranges from hyper-arid Saharan conditions to humid equatorial forests with highly heterogeneous land cover, and a persistent scarcity of ground-based hydrometeorological observations (Weerasinghe et al., 2020; Trambauer et al., 2014). The continent is divided into multiple Köppen-Geiger climate zones (Fig. 1a), ranging from tropical (Af, Am, Aw) to arid (BWh, BWk) and temperate (Cfa, Cfb) (Beck et al., 2018). These zones significantly influence evapotranspiration processes due to variations in temperature, humidity, and precipitation patterns. The tropical regions, for example, are characterized by high temperatures and humidity, resulting in higher *ETa* while the arid regions exhibit lower *ETa* due to limited water availability. The study focuses on 10 major River Basins across Africa, including the Nile, Niger, Congo, Volta, Senegal, Chad, Okavango, Zambezi, Limpopo, and Orange River Basins (Fig. 1b). These basins are relevant for understanding regional water balances because they represent diverse hydrological conditions, from the humid tropics of the Congo River Basin to the arid conditions of the Chad River Basin. The comparison of *ETa* across these basins helps in understanding the spatial variability of water availability and usage across the continent. Land use and land cover (LULC) across Africa are highly heterogeneous, with major categories including forests, shrublands, grasslands, and croplands (Fig. 1c). Croplands are further categorized into rainfed and irrigated systems (Fig. 1d). The distinction between rainfed and irrigated agriculture is important for *ETa* estimation because irrigation significantly alters the water balance and evapotranspiration rates. Understanding how different land cover types, especially croplands, influence *ETa* is key for effective water resource management, in water-scarce regions.

2.2. Data Sources and Spatio-Temporal Characteristics

When applied across the entire African continent, VegET version 2.0 integrates various datasets including precipitation, reference evapotranspiration (ET_o), land surface phenology (LSP), and soil properties (detailed in Table 1). Building on the findings from a prior comprehensive evaluation of satellite and reanalysis of rainfall products over Africa (Mekonnen et al., 2023), we selected the Climate Hazards Group InfraRed Precipitation with Station Data (CHIRPS) dataset (Funk et al., 2015) for this study. The model derives its LSP data from MODIS NDVI, provided by NASA's Land Processes Distributed Active Archive Center (LP DAAC) (Didan, 2015). We computed a daily median NDVI for the years 2003–2017, using linear interpolation from the 8-day composite data of the Aqua and Terra satellites. Reference ETo data was sourced from NOAA (Hobbins et al. 2023). The interception fraction layer in the model was developed using the MODIS Vegetation Continuous Fields (VCF) (Hansen et al., 2003), which estimates interception as a function of tree, herbaceous, and bare ground coverage in each pixel, following Eq. 1 as outlined in (Senay et al., 2023):

$$Interception = 0.15 \times Tcover + 0.1 \times Hcover \quad (1)$$

Here, Tcover represents the percentage of tree cover, assigned a maximum interception value of 15% based on published canopy interception studies for tropical and subtropical forests (Miralles et al., 2011; De Groen, Savenije, 2006). Hcover represents herbaceous cover with a maximum interception of 10%, consistent with values reported for grasslands and croplands (Senay et al., 2023; Gerrits et al., 2010). Bare ground does not contribute to interception. Soil data used to generate layers for Water Holding Capacity (WHC), Field Capacity (FC), and Porosity (POR) were obtained from the International Soil Reference and Information Centre (ISRIC) through their Soil Data Hub (Batjes, 2005). The POR layer was specifically used to determine saturation (SAT) levels in the model. To convert these raster data from a volumetric percentage (m^3/m^3) to depth (mm) per meter of the root-zone, we applied a conversion factor of 10 (Senay et al., 2023). Moreover, SAT values were calibrated to ensure they did not fall below the FC thresholds. ET_o datasets were also transformed from their original NetCDF format into GeoTiff format for use in the model.

Table 2 summarizes the characteristics of the four remote sensing-based ETa products used as benchmarks in this study. SSEBop

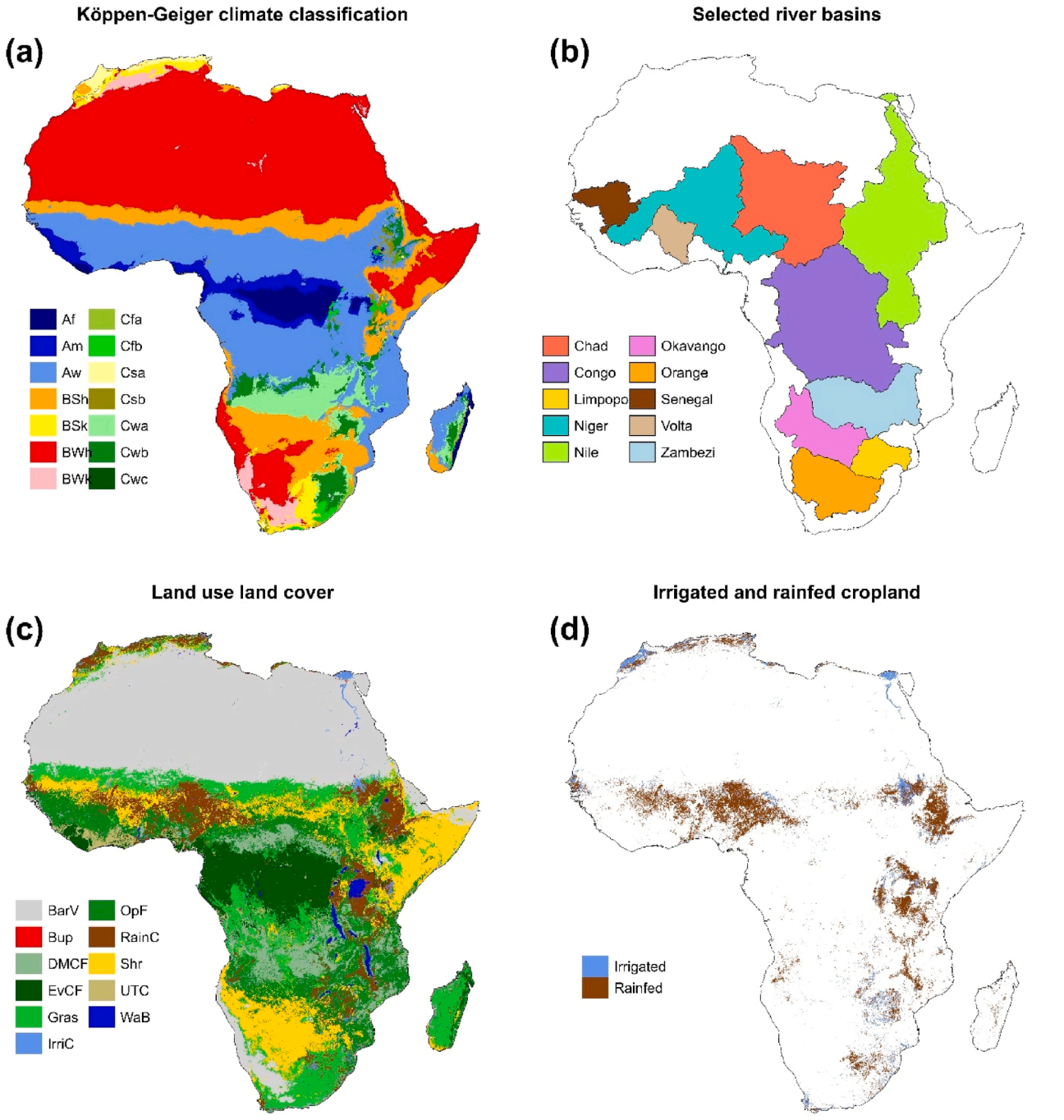

Fig. 1. Overview of the study area for *ETa* comparison across Africa. (a) Köppen-Geiger climate classification showing the diverse climatic zones across the continent, with data obtained from (Beck et al., 2018). (b) Selected major river basins used for *ETa* comparison, highlighting the Nile, Niger, Congo, Volta, Senegal, Chad, Okavango, Zambezi, Limpopo, and Orange Basins. (c) Land use and land cover (LULC) map illustrates the distribution of various vegetation and land cover types, including forests, shrublands, grasslands, and croplands, based on WaPOR v2 2021 land use data. (d) Focus on cropland distribution, distinguishing between rainfed and irrigated agricultural systems, for understanding regional *ETa* dynamics. This cropland distribution is obtained from (Owusu et al., 2024) cropland disaggregation assessment. For the climate zones legend: Af = Tropical, rainforest, Am = Tropical, monsoon, Aw = Tropical, savannah, BSh = Arid, steppe, hot, BSk = Arid, steppe, cold, BWh = Arid, desert, hot, BWk = Arid, desert, cold, Cfa = Temperate, no dry season, hot summer, Cfb = Temperate, no dry season, warm summer, Csa = Temperate, dry summer, hot summer, Csb = Temperate, dry summer, warm summer, Cwa = Temperate, dry winter, hot summer, Cwb = Temperate, dry winter, warm summer, Cwc = Temperate, dry winter, cold summer. For the land use legend: Shr = Shrubland, Gras = Grassland, RainC = Rainfed/Fallow Cropland, IrriC = Irrigated Cropland, Bup = Built-up, BarV = Bare/Sparse Vegetation, WaB = Water Bodies, EvCF = Evergreen Closed Forest, DMCF = Deciduous/Mixed Closed Forest, UTC = Unknown Tree Cover, OpF = Open Forest.

Table 1
Summary of data used in this study.

Parameters	Spatial Resolution	Temporal Resolution	Reference
Precipitation: CHIPRS	0.05 °	Daily; 1981—current	CHIRPS (Funk et al., 2015)
Land Surface Phenology	1 km	Every 8 days (Aqua and Terra); 2003–2017	MODIS NDVI (Didan, 2015)
Reference Evapotranspiration	0.625° x 0.5 °	daily; 1980-present	NOAA ETo (Hobbins et al. 2023)
Soil Properties	250 m	Static	ISRIC (Batjes, 2005)
Interception	250 m	Static	MODIS Vegetation Continuous Field (VCF) (Hansen et al., 2003)

v6.1 (Senay et al., 2023) estimates ETa by combining VIIRS thermal imagery with predefined reference temperature differences, operating at 10-day temporal and 1-km spatial resolution. MODIS16 v6.1 (Mu et al., 2011) applies the Penman-Monteith equation using MODIS vegetation indices and meteorological reanalysis data at 500-m resolution. WaPOR v3 (FAO and IHE Delft, 2019), uses the ETLook model with satellite thermal and optical data, providing ETa at 300-m global and 100-m Africa-specific resolutions. GLEAM v4.1a (Martens et al., 2017; Miralles et al., 2011) combines satellite observations with the Priestley-Taylor equation at 0.25° resolution. All products provide continental-scale coverage with varying spatial and temporal resolutions, as detailed in Table 2.

2.3. Eddy covariance data

For validation, we used eddy covariance (EC) flux tower measurements of latent heat flux (LE) from FLUXNET and complementary regional networks (Table 3). Eight sites were selected across major ecological zones in Africa: Dahra (Senegal), Ankasa, Kayoro, and Sumbrungu (Ghana), Demokeya (Sudan), Mongu (Zambia), Nazinga (Burkina Faso), and an irrigation site in Tunisia, spanning forests, savannas, croplands, and irrigated systems. The dataset consists of monthly aggregated LE fluxes covering periods between 2007 and 2021, harmonized across sites and filtered for data quality following standard FLUXNET protocols.

2.4. Overview of VegET modeling framework

The VegET model, a large-scale agro-hydrological model (Fig. 2), functions as a bucket-type model (Senay et al., 2023). Soil moisture (SM) simulations start with initial levels set to zero, followed by a stabilization or spin-up period lasting one year. For simulations covering 2000–2021, the year 2000 is used as the spin-up period. The model's handling of soil water storage is dictated by the physical characteristics of the soil, with soil properties derived from ISRIC's gridded datasets for Africa (ISRIC; (Batjes, 2005), as detailed in Table 1). In this model, soil porosity (POR) represents the saturation level (SAT), while the field capacity (FC) indicates the maximum amount of water that the soil can retain for plant use. The permanent wilting point (WP) marks the threshold below which

Table 2
Remote sensing *ETa* products characteristics.

ET Products	Major Characteristics of Model	Spatio-temporal availability	Reference
MODIS16 v6.1	Global ET estimation using the Penman-Monteith equation, integrating MODIS-derived vegetation indices and meteorological data at 500 m resolution. Provides 8-day and annual *ETa* composites since 2000.	Global coverage, 8-day, and annual composites from 2000 to present at 1 km spatial resolution	(Mu et al., 2011)
SSEBop v6.1	Simplified surface energy balance model estimates actual ET by predefining temperature differences between "hot" and "cold" reference conditions for each pixel. Version 6.1 introduces the Forcing And Normalizing Operation (FANO) algorithm to establish a dynamic wet-bulb boundary condition, enhancing model accuracy across diverse landscapes and seasons, and utilizes ET fractions derived from VIIRS thermal imagery updated every 10 days to refine spatiotemporal ETa estimates	Global coverage, monthly since 2012 (version6) at 1 km spatial resolution	(Senay et al., 2013, 2022)
WaPOR v3	Remote sensing-based *ETa* estimation using the ETLook model. Version 3 introduces higher spatial resolution by switching from MODIS to VIIRS for thermal infrared data, enhancing land surface temperature (LST) detail to 375 m, and incorporates a thermal sharpening method to improve *ETa* accuracy across diverse scales	Africa and Near East, decadal, seasonal, monthly, and annual data from 2009 to present for at 250 m, 100 m, 30 m for version 2. Version 3 starts from 2018, at 300 m resolution, with higher resolutions of 100 m for Africa and the Near East and 20 m for specific irrigation areas.	(FAO and IHE Delft, 2019)
GLEAMv4.1a	Global *ETa* estimation using the Priestley-Taylor equation and satellite-derived inputs like soil moisture and vegetation indices.	Global coverage, daily, monthly, and annual data from 1980 to present at 0.25-degree resolution.	(Martens et al., 2017; Miralles et al., 2011)

Table 3
Overview of eddy covariance flux tower sites used for ETa validation. Sites span diverse ecosystems across Africa, including savanna, forest, cropland, grassland, and irrigated systems. References indicate the original site descriptions and publications documenting each flux tower dataset.

Longitude	Latitude	Site name	Country	Site description	Reference
-15.4322	15.4028	Dahra	Senegal	Savanna, characterized by 10–30% forest canopy cover with trees exceeding 2 m in height and a predominantly herbaceous understory layer	(Tagesson et al., 2015, 2016)
-2.6942	5.2685	Ankasa	Ghana	Evergreen broadleaf forest site is characterized by > 60% woody vegetation cover with trees exceeding 2 m in height and year-round green canopy foliage	(Chiti et al., 2010; Valentini et al., 2016)
30.4783	13.2829	Demokeya	Sudan	Savanna, characterized by 10–30% forest canopy cover with trees exceeding 2 m in height and a predominantly herbaceous understory layer	(Ardö et al., 2008, 2016)
23.2525	-15.4391	Mongu	Zambia	Deciduous broadleaf forest site characterized by > 60% woody vegetation cover with trees exceeding 2 m in height and annual leaf-on/leaf-off phenological cycles	(Kutsch et al., 2016; Merbold et al., 2009)
9.013889	36.54662	Gendouba	Tunisia	Irrigation scheme (wheat, maize, faba bean, sorghum)	(Biradar et al., 2022)
-1.5857	11.15156	Nazinga	Burkina Faso	Near-natural savanna site located within the protected Nazinga Game Ranch wildlife area in Burkina Faso. Features mixed vegetation with shrubs, medium-sized trees (averaging 4.5 m height), and tall grass that can reach 2.5 m during rainy season.	(Bliefernicht et al., 2018; Hingerl et al., 2025; Nadolski et al., 2024)
-1.3209	10.9181	Kayoro	Ghana	Cropland site characterized by agricultural use with livestock grazing. Dominated by rainfed crops including sorghum, groundnut, and pearl millet, with maximum vegetation height typically under 1 m.	(Bliefernicht et al., 2018; Hingerl et al., 2025; Nadolski et al., 2024)
-0.9174	10.8466	Sumbrungu	Ghana	Degraded grassland is used primarily as rangeland for livestock. Features severely degraded soils with sparse grass typically not exceeding 10 cm height even during rainy season. Surrounded by scattered medium-sized trees and shrubs.	(Bliefernicht et al., 2018; Hingerl et al., 2025; Nadolski et al., 2024)

plants can no longer effectively extract water. The water holding capacity (WHC), defined as the difference between FC and WP, denotes the volume of water available to plants. As soil moisture decreases below the maximum allowable depletion (MAD) level, the model anticipates an increase in water stress on plants.

VegET enhances the management and understanding of agricultural water needs, in regions where defining crop coefficients (Kc values) over extensive areas is challenging (Senay et al., 2023). This challenge stems from uncertainties regarding crop types and the limited generalizability of published Kc values beyond their original experimental contexts. To overcome these issues, VegET incorporates land surface phenology (LSP) data derived from remotely sensed NDVI. The NDVI data, sourced from MODIS (Aqua and Terra – 1-km, 8-day composites) (Didan, 2015); Table 1), provide a more accurate and dynamic depiction of vegetation conditions and growth stages. Using this approach, VegET simulates crop water demands in a manner that accounts for regional specifics and landscape characteristics, thereby improving the precision of water requirement estimates. This method can be used to manage water resources in regions with complex agricultural practices and diverse environmental conditions. The model replaces the traditional crop coefficient (Kc) values, as proposed by (Allen et al., 1998), with a landscape coefficient (Kcp) derived from NDVI. This phenology-based Kcp is assumed to represent the collective water needs of the landscape in areas with stable land cover. Utilizing NDVI within a climatological framework provides more reliable and accurate seasonal water usage patterns compared to traditional Kc values (Senay et al., 2023). When soil moisture exceeds the saturation level (SAT), the model simulates surface runoff. Additionally, moisture within the zone between SAT and FC is distributed between surface runoff and deep drainage. The model simulates runoff (R) when soil moisture surpasses the WHC, with the excess classified as either surface runoff or deep drainage, depending on its position relative to SATfc, the volume between SAT and FC.

The same VegET v2 modeling system was used to generate the runoff and discharge fields (Akpoti et al., 2024), where simulated 1-km runoff was routed with mizuRoute to produce discharge for > 64,000 river segments across Africa. In this study, we leverage that same hydrological modeling framework but focus on the ETa outputs as the primary water balance flux, enabling direct evaluation against flux tower data and intercomparison with remote sensing ET products. We implemented the VegET model using a cloud-based infrastructure on Amazon Web Services (AWS), facilitating the preparation of both dynamic and static inputs necessary for the model's operation. The selected timeframe for the dataset, 2000–2021, was chosen to represent current hydrological conditions, allowing for a better understanding and management of present-day water resources. The choice of this period is influenced by the availability of high-quality remote sensing data, from the Moderate Resolution Imaging Spectroradiometer (MODIS), which has been consistently available since 2000. This time span is for capturing the climate and hydrological dynamics relevant to the study.

2.5. VegET ETa calculation methodology

For full model description, refer to (Akpoti et al., 2024; Senay et al., 2023). The VegET model calculates actual evapotranspiration (*ETa*) using a water balance approach that integrates vegetation dynamics and climatic factors, effectively simulating soil moisture and associated fluxes over time. The *ETa* is derived daily using the following formulation:

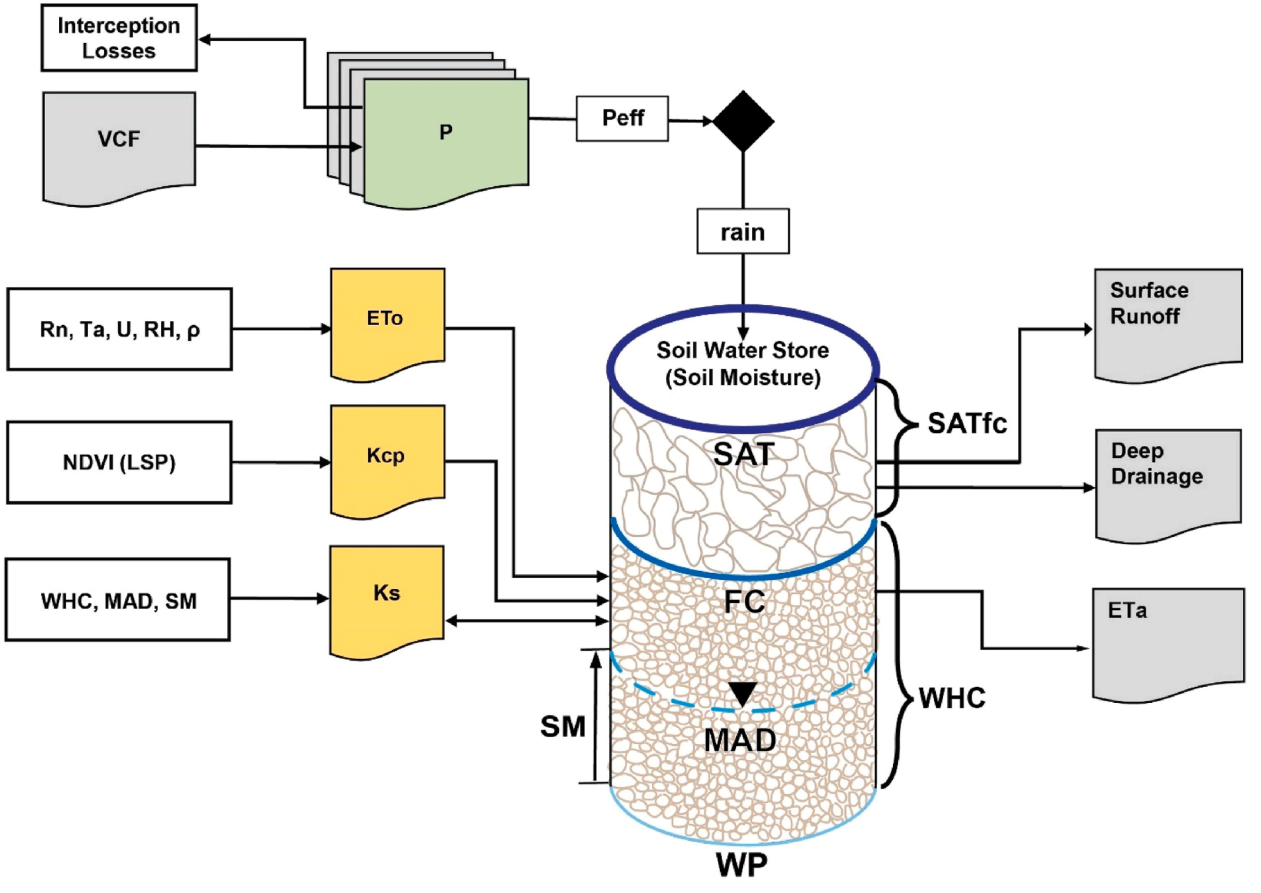

Fig. 2. Overview of the VegET model version 2.0 as adopted from (Senay et al., 2023) and (Akpoti et al., 2024). The main components of the model encompass vegetation and climatic inputs that influence soil water dynamics. It differentiates between gravity water, which accumulates when soil moisture exceeds field capacity (FC), and plant-available water, which lies between FC and the permanent wilting point (WP). The model incorporates various datasets, including MODIS Vegetation Continuous Fields (VCF) for deriving the interception fraction layer, precipitation (P), reference evapotranspiration ([illegible]), landscape water uses coefficient (K_{cp}), land surface phenology (LSP), soil stress coefficient (K_s), water holding capacity (WHC), maximum allowable depletion (MAD), soil saturation (SAT), and the volume between SAT and FC (SAT_{fc}). The model's output includes gridded data for surface runoff, deep drainage, soil moisture (SM), and actual evapotranspiration. R_n = net radiation; T_a = air temperature; U = wind speed; RH = relative humidity; ρ = air pressure; NDVI = Normalized difference vegetation index; ET_a = Actual evapotranspiration; P = precipitation; P_{eff} = effective precipitation.

$$ET_a = K_{cp} \times K_s \times ET_0 \tag{2}$$

Where K_{cp} is the landscape crop coefficient, derived from land surface phenology (LSP) based on Normalized Difference Vegetation Index (NDVI) data, K_s is the soil water stress coefficient, which varies between 0 and 1 depending on the soil moisture levels, ET_0 is the reference evapotranspiration, representing the potential evapotranspiration under optimal water conditions.

The calculation of K_{cp} depends on the NDVI values and follows these equations:

$$K_{cp} = \begin{cases} 1.25 \times NDVI + 0.20 \quad if\ (NDVI > 0.4) \\ 1.25 \times NDVI\ if\ (NDVI \leq 0.4) \end{cases} \tag{3,4}$$

This approach allows the VegET model to dynamically adjust the crop coefficient based on the real-time vegetative conditions of the landscape, ensuring that the ET_a calculations represent the actual water demands of the vegetation.

The soil water stress coefficient K_s is calculated as:

$$K_s = \begin{cases} \dfrac{SM_i}{MAD}\ if\ (SM_i < MAD) \\ 1 \quad if\ (SM_i \quad \geq MAD) \end{cases} \tag{5,6}$$

Where SM_i is the soil moisture at the current time step, MAD (Maximum Allowable Depletion) is the threshold below which vegetation starts to experience water stress, typically set as 50% of the Water Holding Capacity (WHC).

The VegET model simulates soil moisture (SM) by incorporating effective precipitation, ET_a, and other water balance components. Soil moisture is updated daily using Eq. 7:

$$SM_i = SM_{i-1} + Peff_i + ET_{ai} \tag{7}$$

Where SM_{i-1} is the soil moisture was from the previous day, $Peff_i$ is the effective precipitation for the current day, accounting for interception losses.

This continuous soil moisture calculation informs the daily *ETa*, ensuring that the model adjusts for changes in available water and vegetative demand throughout the growing season. The integration of these components allows VegET to provide accurate, spatially explicit estimates of *ETa.* This represents one of the first Africa-wide implementations of VegET at continental scale, with explicit calibration of soil hydraulic properties and phenology-based vegetation coefficients. By running VegET as a process-based hydrological model, we produce a new, consistent ETa dataset that complements existing satellite products but remains rooted in water balance closure principles.

2.6. Conversion of latent heat flux to actual ETa

Observed actual evapotranspiration from EC towers was derived by converting measured latent heat flux (LE, W m^{-2}) into equivalent water fluxes (mm $month^{-1}$). The conversion used the standard relation:

$$ET_a = \frac{LE}{\lambda} \times \Delta t \tag{8}$$

where λ is the latent heat of vaporization (2.45 MJ kg^{-1}), and Δt is the time conversion factor to express fluxes in mm per month (1 W $m^{-2} \approx 0.035$ mm h^{-1}). Monthly totals were computed by integrating daily values. Only positive LE values were considered, and data gaps were excluded from the analysis.

2.7. Evaluation metrics

In the evaluation of the VegET *ETa* product, several statistical metrics are used to assess its performance against reference *ETa* products, including MODIS16, SSEBop, GLEAM, and WaPOR. We focus on the Pearson correlation coefficient (r), the regression slope, and the Root Mean Square Error (RMSE) as indicators of model performance. The Pearson correlation coefficient (r) is used to measure the strength of the linear relationship between the simulated and reference *ETa* values. Values approaching 1 indicate a high degree of agreement between the simulated and reference data. The formula for r is given by:

$$r = \frac{\sum_{t=1}^{n}\left(X_{o,t} - \mu_o\right)\left(X_{s,t} - \mu_s\right)}{\sqrt{\sum_{t=1}^{n}\left(X_{o,t} - \mu_o\right)^2}\sqrt{\sum_{t=1}^{n}\left(X_{s,t} - \mu_s\right)^2}} \tag{9}$$

The regression slope provides insight into the scaling bias between the simulated and reference *ETa* values. A slope close to 1 is expected when the simulated *ETa* values are in good agreement with the reference values. The slope is calculated as:

$$Slope = \frac{\sum_{t=1}^{n}\left(X_{o,t} - \mu_o\right)\left(X_{s,t} - \mu_s\right)}{\sum_{t=1}^{n}\left(X_{o,t} - \mu_o\right)^2} \tag{10}$$

The Root Mean Square Error (RMSE) quantifies the average magnitude of the differences between the simulated and reference *ETa*

values, thereby providing a measure of the overall accuracy of the model. RMSE is computed using:

$$RMSE = \sqrt{\frac{1}{n}\sum_{t=1}^{n}\left(X_{s,t} - X_{o,t}\right)^2} \tag{11}$$

In these equations, n is the total number of time-steps, $X_{s,t}$ is the simulated VegET *ETa* value at time-step *t*, $X_{o,t}$ is the corresponding value of the reference *ETa* data (e.g., from MODIS16, SSEBop, GLEAM, or WaPOR), and μ_s and μ_o denote the means of the simulated and reference datasets, respectively.

While the VegET model simulates data from 2000 to 2021, the evaluation using the statistical metrics focuses on the period 2003–2021 for MODIS16, SSEBop, and GLEAM, and 2009–2021 for WaPOR. This alignment ensures consistency in data availability across the different ETa products, enabling a more accurate and meaningful comparison. In addition to these statistical measures, we use Taylor diagrams (Taylor, 2001) to facilitate the model intercomparison across climate zones, major basins, and land use/cover classes. The Taylor diagram graphically summarizes how closely the simulated *ETa* products (VegET, MODIS16, SSEBop, GLEAM, and WaPOR) match the reference data by simultaneously displaying three statistics: the correlation coefficient, the root mean square difference (RMSD), and the standard deviation. In changing the reference *ETa* product within the Taylor diagram, we can visualize the relative performance of each *ETa* model in capturing the spatial and temporal variability of evapotranspiration across diverse environmental conditions. The use of Taylor diagrams in this context provides a comprehensive overview of model performance briefly. This visual approach is essential for understanding the complex dynamics of evapotranspiration across Africa's varied landscapes, enabling a more nuanced assessment of how different models perform relative to one another in specific zones and under different scales. Beyond statistical agreement, these metrics are interpreted in hydrological terms, with RMSE values indicating the magnitude of water balance closure errors, correlation indicating consistency in seasonal flux dynamics, and Taylor diagrams providing an integrated view of spatial variability critical for basin-scale hydrology.

2.8. Drought assessment with VegET ETa

To assess agricultural drought across Africa during 2000–2021, we use the Evapotranspiration Deficit Index (*ETDI*) adapted from methodologies established by (Narasimhan and Srinivasan, 2005) and further evaluated in subsequent studies (e.g., (Wu et al., 2021). The *ETDI* is a robust metric for capturing the severity and spatial extent of drought by comparing *ETa* from VegET to potential evapotranspiration (PET), with the latter derived from GLEAM data in this study.

2.8.1. Calculation of Water Stress Ratio (WS)

The water stress ratio (WS) is a component in determining the *ETDI* and is calculated monthly as follows:

$$WS = \frac{PET - ET_a}{PET} \tag{12}$$

Where PET is the potential evapotranspiration derived from GLEAM and ***ETa*** is the actual evapotranspiration from the VegET model.

The WS ratio ranges from 0 to 1, where 1 indicates no evapotranspiration, signifying severe drought, and 0 indicates that *ETa* equals PET, indicating no drought stress.

2.8.2. Calculation of Water Stress Anomaly (WSA)

To quantify the anomaly in water stress for each month, we calculate the Water Stress Anomaly (WSA) by comparing the current WS to the historical median WS for that specific month:

$$WSA_{i,j} = \begin{cases} \dfrac{MWS_j - WS_{i,j}}{MWS_j - \min WS_j} \times 100 & if\ \left(WS_{i,j} \le MWS_j\right) \\ \dfrac{MWS_j - WS_{i,j}}{\max MWS_j - WS_j} \times 100 & if\ \left(WS_{i,j} \quad \ge MWS_j\right) \end{cases} \tag{13,14}$$

Where MWS_j is the long-term median water stress for month *j*, $\min WS_j$ and $\max MWS_j$ are the minimum and maximum WS for month *j* over the historical period.

The WSA values range from −100–100, indicating conditions from extremely wet to extremely dry, respectively.

2.8.3. Evapotranspiration Deficit Index (ETDI)

The *ETDI* for any given month is calculated incrementally, considering both the current WSA and the preceding month's *ETDI*:

$$ETDI_j = 0.5ETDI_{j-1} + \frac{WSA_{i,j}}{50} \tag{15}$$

Where $ETDI_{j-1}$ is the *ETDI* was from the previous month, $WSA_{i,j}$ is the water stress anomaly for the current month.

The *ETDI* values range from −4 to + 4, with negative and positive values indicating drought and wet conditions, respectively. This index provides a clear, temporally integrated measure of drought severity. The *ETDI* is calculated for each pixel across Africa using the spatially explicit VegET *ETa* data. This spatially distributed approach allows for a detailed analysis of drought trends and patterns over the 21-year period. In integrating the VegET model outputs with GLEAM PET data, this methodology offers a nuanced and dynamic

assessment of agricultural drought, considering both water supply (through precipitation and soil moisture) and demand (via evapotranspiration). The use of *ETDI* enables the identification of regions where water stress is most severe, supporting efforts in drought monitoring and mitigation.

ETDI classification presented in Table 4 categorizes drought and wetness severity into distinct classes following a similar approach by (Vicente-Serrano et al., 2010). The classification helps assess the extent of water stress or surplus by assigning negative values to drought conditions, with thresholds ranging from mild to extreme drought. Positive values indicate increasing levels of moisture, culminating in extremely wet conditions, which can lead to waterlogging or flooding. This *ETDI*-based classification provides a robust tool for monitoring agricultural drought across Africa, complementing other indices like the Standardized Precipitation Evapotranspiration Index (SPEI) by incorporating both water demand and availability. Because VegET is explicitly soil-water balance-based, the ETDI derived from VegET ETa and PET provides a physically consistent measure of water stress that is directly relevant for operational drought early warning and basin-scale hydrological monitoring.

3. Results

3.1. Validation against Eddy covariance observations

Validation against eddy covariance (EC) tower observations demonstrated that all *ETa* products reproduced the seasonal variability of observed *ETa* reasonably well, but with notable differences in magnitude and accuracy across sites (Fig. 3). Scatter plots comparing monthly observed *ETa* with product estimates indicated that VegET v2 showed the strongest correlation ($r = 0.80$, slope $= 0.96$, RMSE $= 25.5$ mm/month). SSEBop v6.1 and GLEAM v4.1a also demonstrated moderately strong correlations ($r = 0.67$ and 0.65, respectively), although with some bias at higher fluxes. MODIS16 v6.1 yielded moderately strong correlation ($r = 0.62$), while WaPOR v3 demonstrated the lowest correlation ($r = 0.56$), possibly due to limited data availability ($N = 21$). Time series analyses across the eight stations further revealed that VegET, SSEBop, and GLEAM generally captured seasonal cycles, whereas MODIS16 and WaPOR tended to underestimate peak *ETa* values (Fig. 4). Given that VegET explicitly simulates root-zone soil water balance, the *ETa* fields should be interpreted not only as flux estimates but also as integral components of basin water balance closure. This hydrological foundation distinguishes VegET from diagnostic satellite-based *ETa* products and explains its robust performance across diverse African climates. In particular, the strong correspondence between VegET and flux tower observations indicates that the model captures both the seasonal soil moisture control on *ETa* and the transition between water-limited and energy-limited regimes, which are critical to basin-scale hydrological monitoring.

3.2. Overall spatial comparison of VegET with remote sensing-based ETa products

Fig. 5 presents the spatial distribution of mean annual *ETa* across Africa for VegET v2, SSEBop v6.1, MODIS16 v6.1, WaPOR v3, and GLEAM v4.1a (Refer to Appendix A, Figures A1 to A5 for monthly climatology profiles). All products capture the broad climatological gradients, with higher *ETa* values in humid tropical regions (especially the Congo River Basin) and lower values in the arid and semi-arid zones (such as the Sahara, the Sahel, the Horn of Africa, southern Africa, and much of North Africa). VegET v2 and MODIS16 v6.1 exhibit particularly close agreement in many parts of the continent, including West Africa, the Sahel, the Congo River Basin, the Horn of Africa, southern Africa, and Madagascar, consistently identifying regions of high and low *ETa*. GLEAM v4.1a, MODIS16 v6.1, and, to a lesser extent, WaPOR v3 tend to produce slightly higher *ETa* estimates overall, most notably in the Congo River Basin and coastal West Africa. These differences likely stem from the underlying modeling assumptions, input data, and retrieval algorithms specific to each dataset. Nonetheless, the broad consistency among products in identifying major hydrological gradients highlights their collective utility for regional-scale assessment of evapotranspiration patterns.

3.3. Comparison of ET_a across major climate zones

The intercomparison across Köppen–Geiger climate zones highlights how water balance constraints dominate in arid/semi-arid regions, where VegET tends to yield lower *ETa* than some products. This demonstrates the model's explicit accounting of soil moisture limitations, consistent with drought-prone conditions, whereas satellite products relying on energy balance or VI-based upscaling

Table 4
Classification of the Evapotranspiration Deficit Index (*ETDI*) values into drought and wetness categories. Negative *ETDI* values indicate varying degrees of drought severity, while positive values reflect wet conditions, ranging from mild moisture increases to extreme waterlogging.

***ETDI* Value Range**	**Classification**	**Description**
< -3	Extreme Drought	Severe water deficit and vegetation stress. Very low evapotranspiration.
-3 to −2	Severe Drought	Significant moisture shortage, resulting in noticeable vegetation stress.
-2 to −1	Moderate Drought	Moderate water deficit, affecting vegetation and crop health.
-1–0	Mild Drought	Mildly below average moisture conditions. Some water stress is noticeable.
0–1	Normal	Average moisture conditions, no significant water stress.
1–2	Slightly Wet	Moist conditions and increased soil moisture are beneficial for vegetation growth.
2–3	Moderately Wet	Noticeably higher than average moisture conditions, potential for waterlogging.
> 3	Extremely Wet	Excessive moisture, waterlogged conditions, potential for flooding.

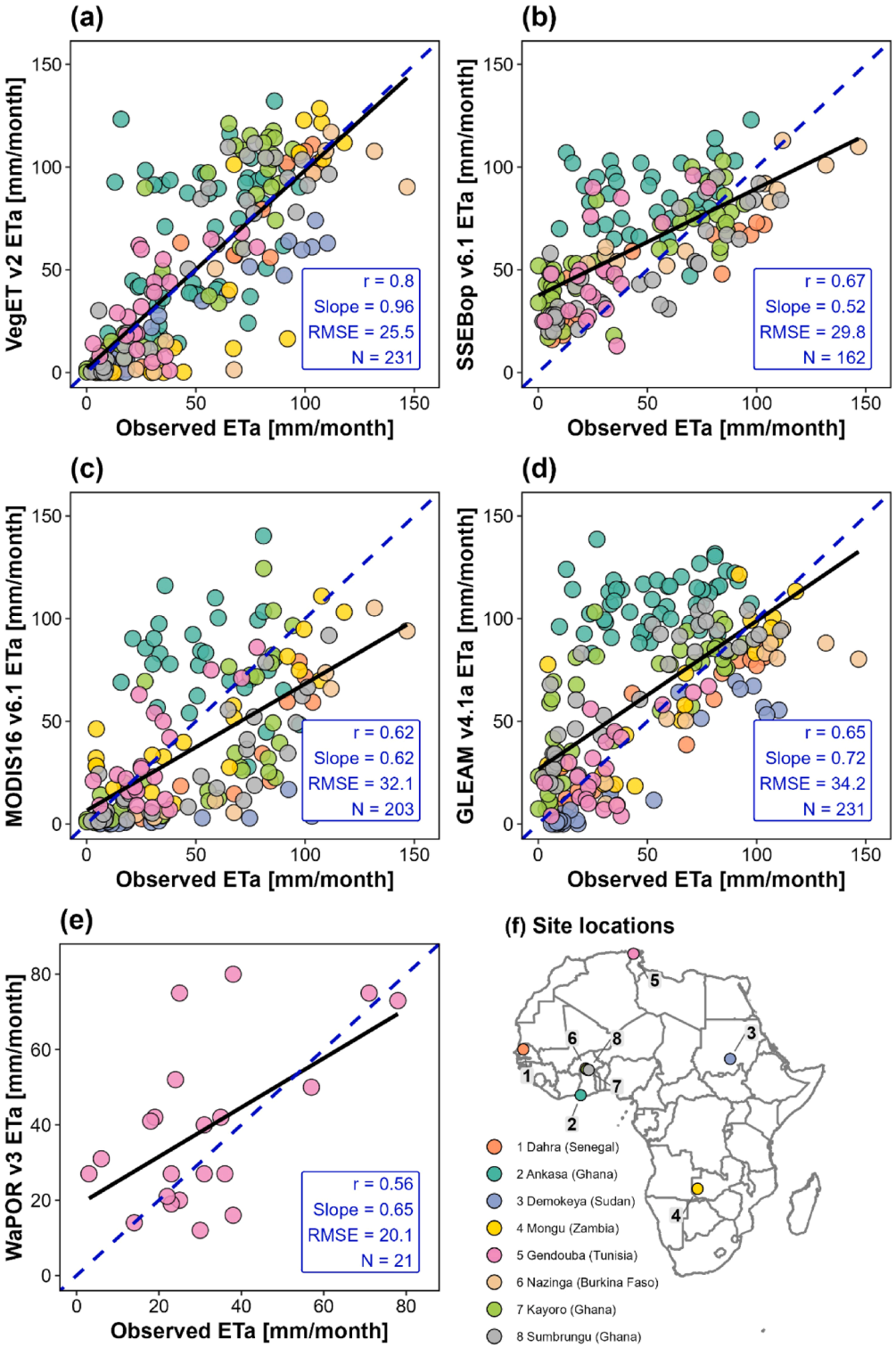

Fig. 3. Scatterplots of monthly observed ETa from eddy covariance towers versus ETa from (a) VegET v2, (b) SSEBop v6.1, (c) MODIS16 v6.1, (d) GLEAM v4.1a, and (e) WaPOR v3. Blue dashed line is the 1:1 line; black solid line is the regression fit. Reported statistics include Pearson correlation (r), regression slope, RMSE, and sample size (N).

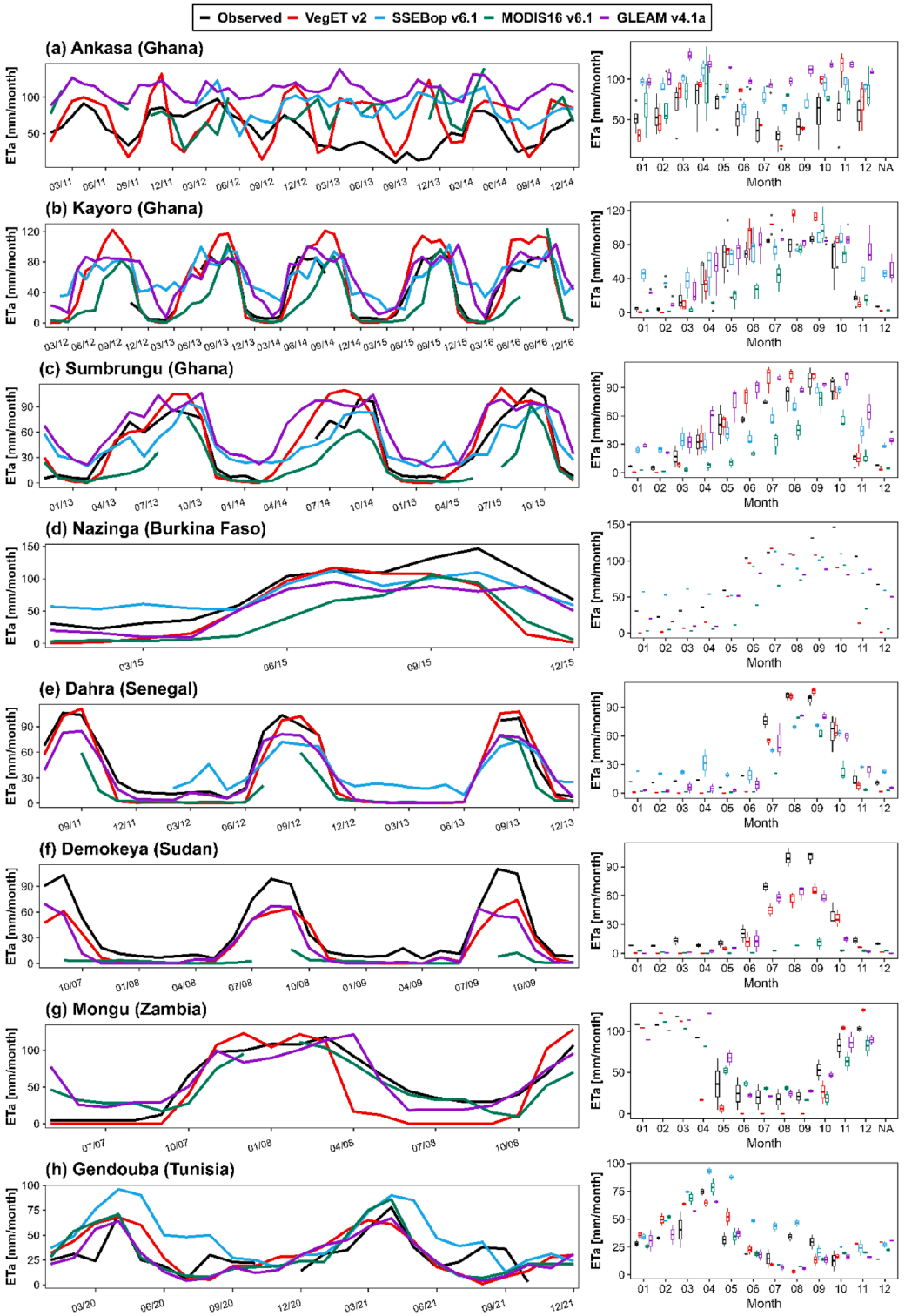

Fig. 4. Time series comparison of monthly observed ETa (black) with ETa from VegET v2, SSEBop v6.1, MODIS16 v6.1, and GLEAM v4.1a at eight eddy covariance sites across Africa. Boxplots (right panels) show seasonal variability of ETa (January–December) for each site.

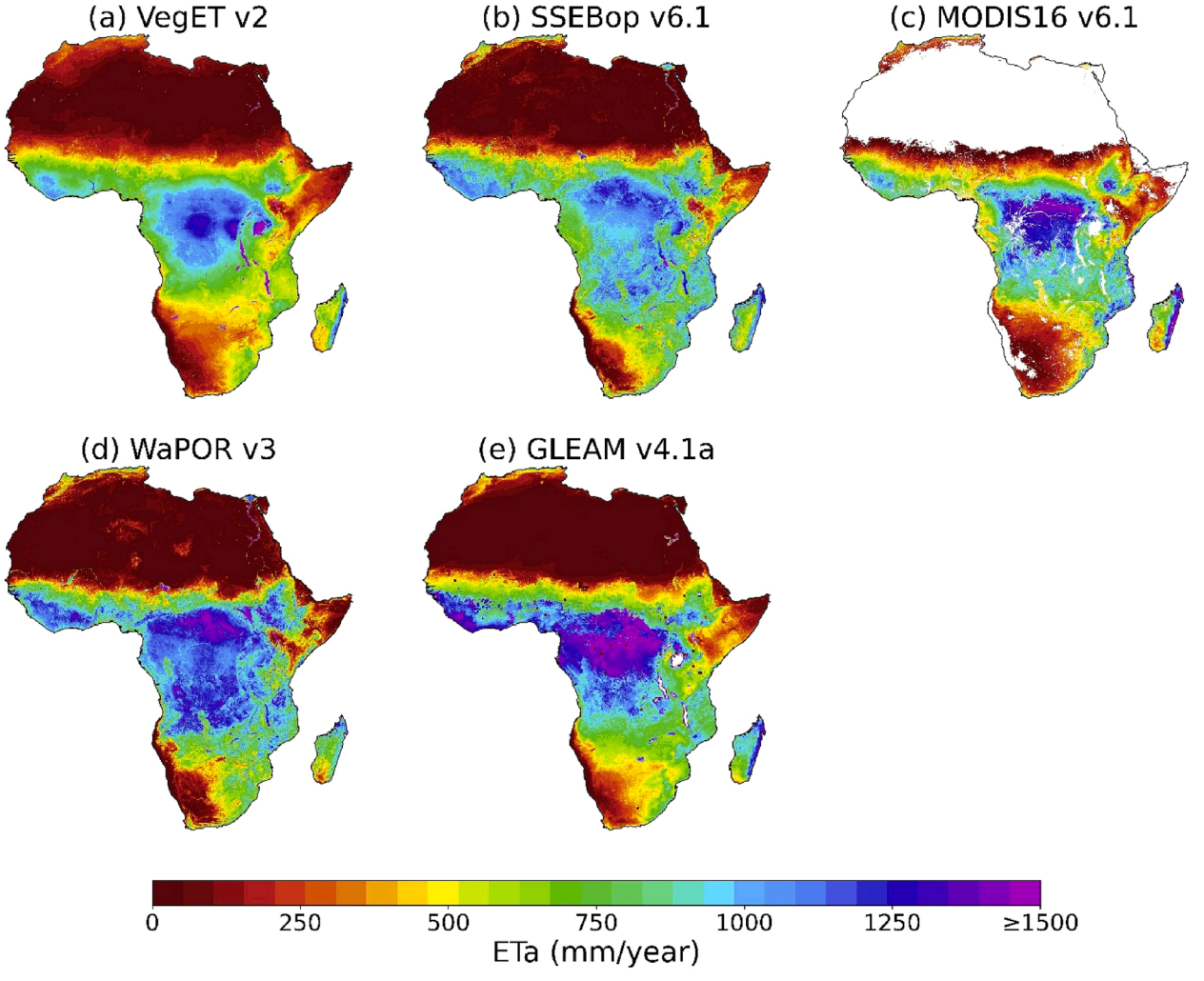

Fig. 5. Spatial distribution of total average annual ETa. The total annual is calculated for the period 2003–2021 for VegET v2, MODIS16 v6.1 and GLEAM v4.1a for comparison purposes and 2012–2021 for SSEBop v6.1, and 2018–2021 for WaPOR v3. White spaces in map c) represent no data pixels in MODIS16 product.

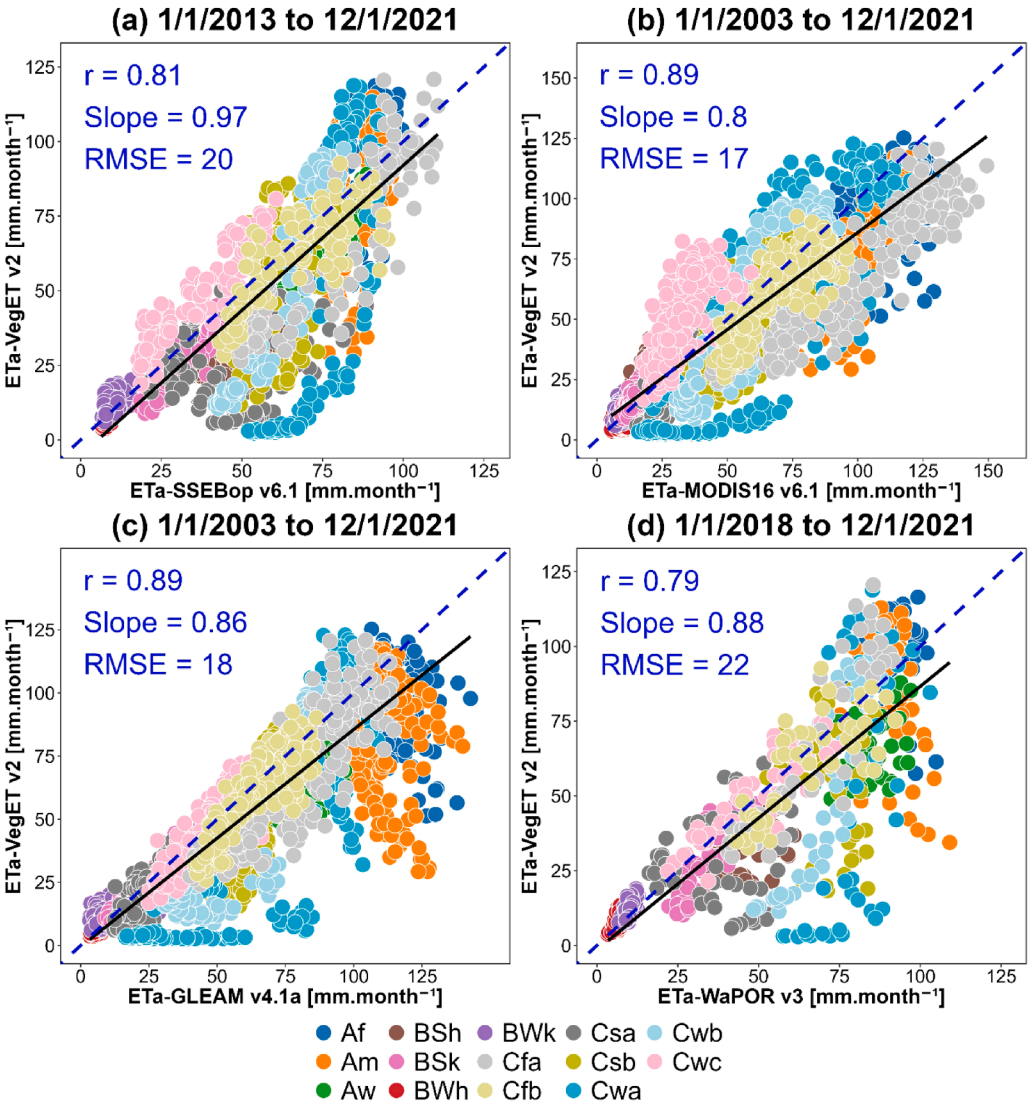

Fig. 6. Comparison of monthly *ETa* estimates from the VegET v2 model with four remote sensing *ETa* products (SSEBop v6.1, MODIS16 v6.1, WaPOR v3, and GLEAM v4.1a) across major climate zones. Each scatter plot represents the relationship between VegET and the corresponding remote sensing ET product. The solid black line shows the linear regression fit, while the dashed blue line indicates the 1:1 line. Climate zones are color-coded as indicated by the legend, with the following classifications: Af = Tropical, rainforest; Am = Tropical, monsoon; Aw = Tropical, savannah; BWh = Arid, desert, hot; BWk = Arid, desert, cold; BSh = Arid, steppe, hot; BSk = Arid, steppe, cold; Csa = Temperate, dry summer, hot summer; Csb = Temperate, dry summer, warm summer; Cwa = Temperate, dry winter, hot summer; Cwb = Temperate, dry winter, warm summer; Cwc = Temperate, dry winter, cold summer; Cfa = Temperate, no dry season, hot summer; Cfb = Temperate, no dry season, warm summer.

may overestimate *ETa* when soil water is limiting.

Fig. 6 presents scatter plots of monthly *ETa* estimates between VegET v2 and each remote sensing ETa product, stratified by Koppen–Geiger climate zones ranging from tropical (Af, Am, Aw) to arid (BWh, BWk, BSh, BSk) to temperate (e.g., Cfa, Cfb, Csa, Csb). Across most zones, VegET exhibits strong agreement with MODIS16 v6.1 and GLEAM v4.1a, indicated by relatively high correlation coefficients (e.g., $r \geq 0.79$), slopes approaching unity, and moderate RMSE values (~17–20 mm.month^{-1}). SSEBop v6.1 also shows robust performance ($r \approx 0.81$) with a slope near 1.0 and RMSE around 20 mm.month^{-1}, particularly in tropical and temperate regions. WaPOR v3 demonstrates some divergence in humid and semi-arid areas ($r \approx 0.79$ and RMSE= 22 mm.month^{-1}).

A more detailed view of product performance is shown in box plots (Fig. 7) that illustrate monthly *ETa* distributions across climate zones. In tropical rainforest (Af) and monsoon (Am) zones, most products cluster closely in both magnitude and seasonal pattern, yet WaPOR typically estimates higher peak *ETa* values as indicated by a broader interquartile range. In arid deserts (BWh, BWk) and steppe regions (BSh, BSk), the products display more variability—especially during the dry season—though VegET, SSEBop, and GLEAM generally align well, while WaPOR continues to exhibit larger *ETa* values in water-stressed conditions. MODIS16, conversely, tends toward slightly lower ETa during certain peak growing months, a pattern also observed in the time series (Figure A2). The time

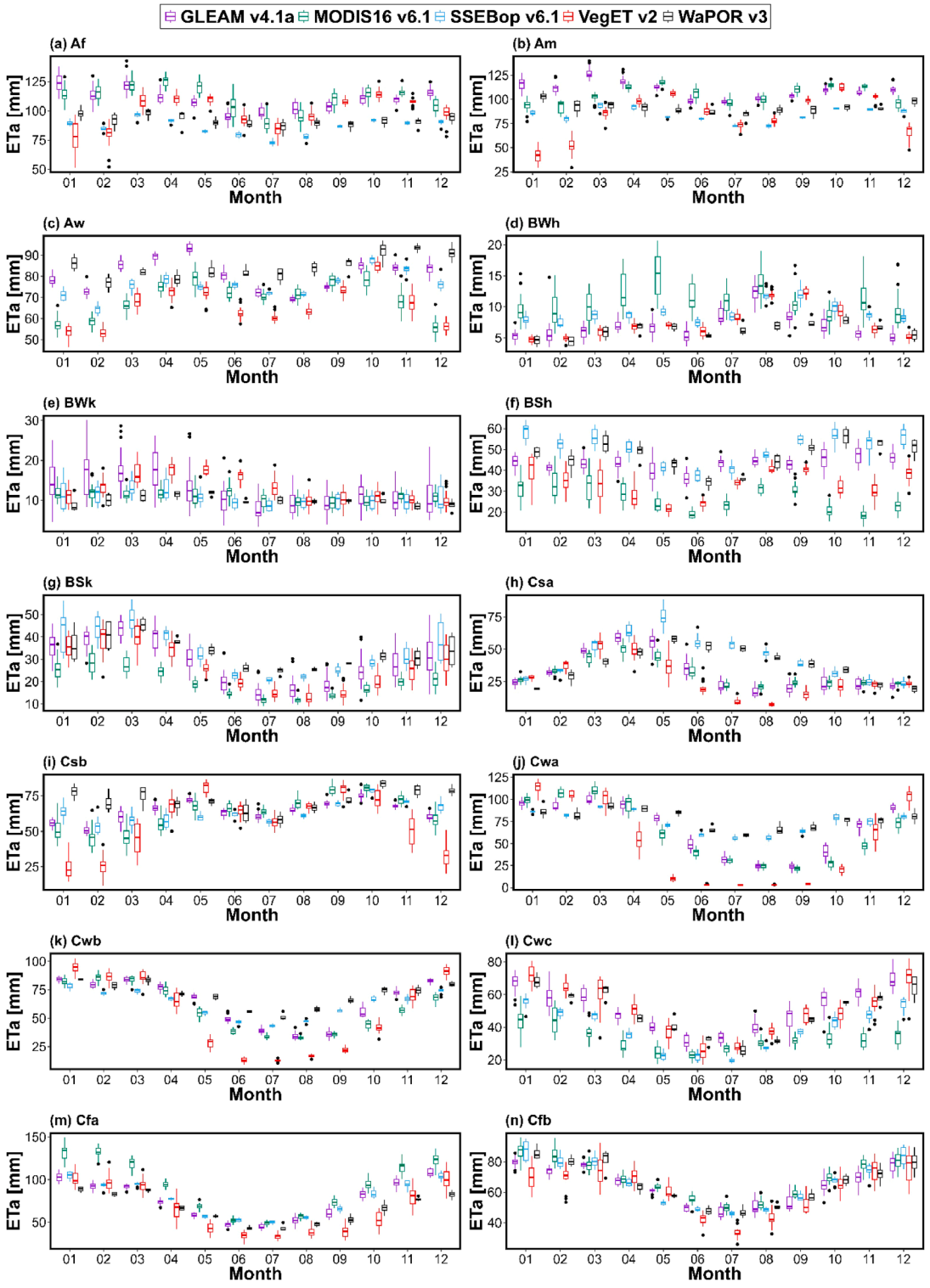

(caption on next page)

Fig. 7. Box plots of monthly actual evapotranspiration (*ETa*) estimates across major climate zones in Africa (see Fig. 1a for the climate zones). *ETa* estimates are compared between the VegET v2 model and four remote sensing *ETa* products for the period 2003–2021 (MODIS16 v6.1, and GLEAM v4.1a), 2018–2021 (WaPOR v3) and 2013–2021 (SSEBop v6.1). Each panel corresponds to a specific climate zone, including tropical (a) rainforest (Af), (b) monsoon (Am), (c) savannah (Aw); arid (d) hot desert (BWh), (e) cold desert (BWk), (f) hot steppe (BSh), (g) cold steppe (BSk); temperate (h) dry summer, hot summer (Csa), (i) dry summer, warm summer (Csb), (j) dry winter, hot summer (Cwa), (k) dry winter, warm summer (Cwb), (l) dry winter, cold summer (Cwc); and (m) no dry season, hot summer (Cfa), (n) no dry season, warm summer (Cfb). The interquartile range shows the variability of each product's estimates, with outliers represented by black dots.

series in Figure A2 underscore these seasonal cycles, showing how all datasets respond similarly to the major rainy and dry periods in tropical, arid, and temperate zones. WaPOR's higher *ETa* spikes in humid regions and semi-arid transitions are again evident, whereas VegET, GLEAM, SSEBop, and MODIS16 follow more moderate trajectories. These monthly cycles further highlight a notable convergence among VegET, GLEAM, and SSEBop, particularly in temperate climates (e.g., Cfa, Cfb, Csa, Csb), where the products' *ETa* estimates remain closely aligned throughout the year.

In the Cfb climate zone (temperate, no dry season, warm summer), the *ETa* estimates across all five models show a high degree of

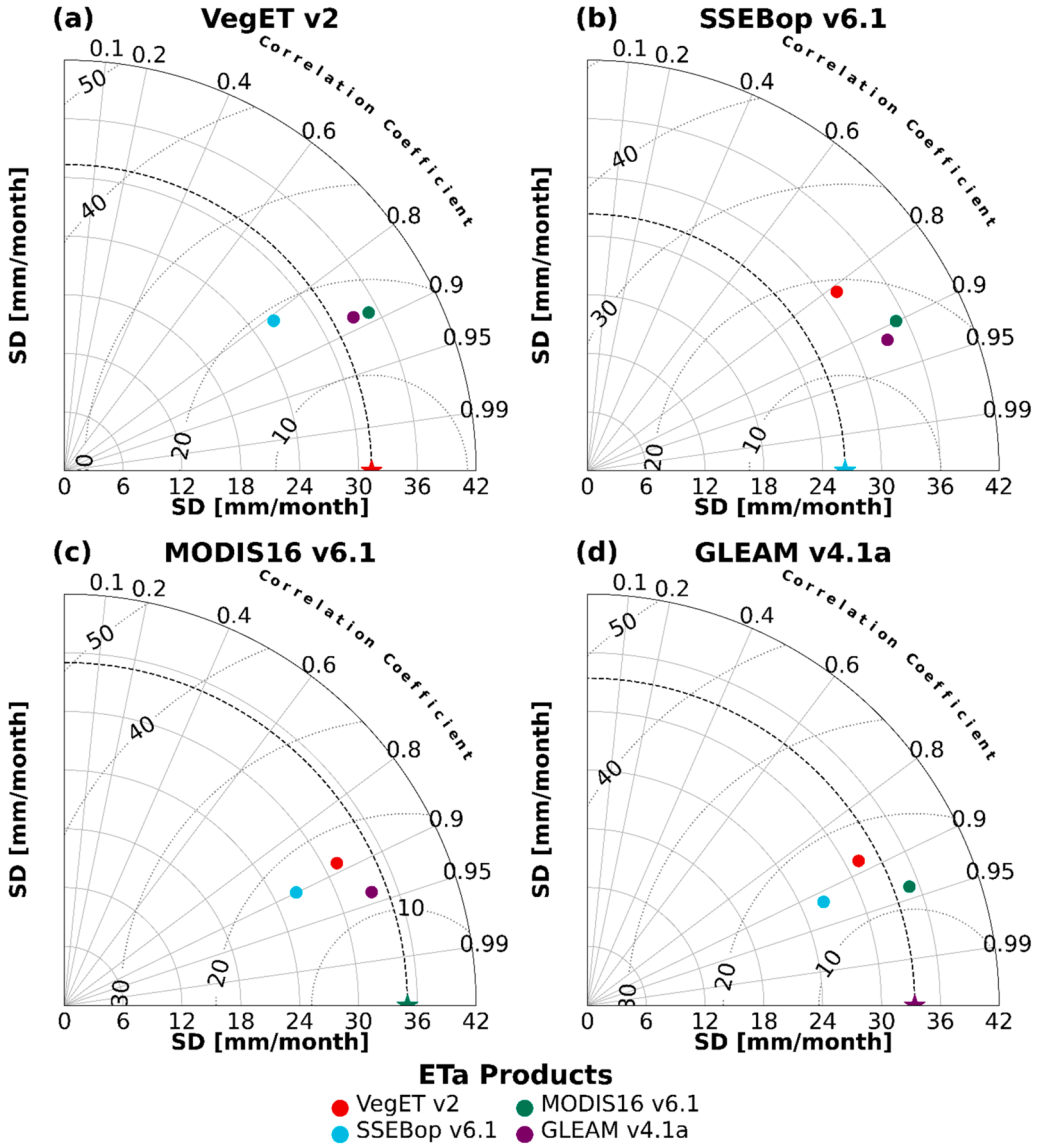

Fig. 8. Taylor diagrams comparing actual evapotranspiration (ETa) estimates for various products, combining all climate zones together, for the period 2013–2021. The diagram depicts the overall standard deviation (SD) and correlation coefficient (R), and Root Mean Square Error (RMSE) for each ETa product when averaged across all climate zones. The reference product is indicated in the title of the panel, and the other products are compared against this reference.

convergence. This can be attributed to the biophysical characteristics of this zone, which include evenly distributed precipitation throughout the year, moderate temperatures, and typically dense vegetation cover. These conditions reduce both water stress and the influence of energy extremes, resulting in stable and consistent evapotranspiration patterns. Consequently, model differences—such as those between water balance and energy balance approaches—become less pronounced, leading to similar *ETa* outputs.

The climate-zone-wise monthly *ETa* profiles reveal several features. First, the divergence among *ETa* products in Af (tropical rainforest), Am (monsoon), and Csb (temperate dry summer) zones occurs during the January–April period, which corresponds to key seasonal transitions (e.g., end of short rains or dry season onset). These periods are characterized by rapid shifts in rainfall, solar radiation, and vegetation phenology, which are handled differently by the models. For instance, VegET's water balance approach may be slower to respond to abrupt increases in vegetation activity following rainfall onset, whereas energy balance models (like SSEBop and GLEAM) are more responsive to changes in surface temperature and net radiation. Secondly, in the Csa climate zone (temperate with dry, hot summer), VegET v2 exhibits the lowest *ETa* during the core summer months (June to August), followed by GLEAM and MODIS16. This reduction likely indicates the model's sensitivity to water limitations during periods of high evaporative demand and minimal precipitation. VegET's estimates are constrained by soil moisture dynamics and a fixed 366-day NDVI climatology, which effectively captures seasonal vegetation phenology but does not capture interannual anomalies, such as intensified vegetation stress or premature senescence during exceptionally dry summers. In contrast, models like SSEBop and WaPOR maintain higher ETa during this

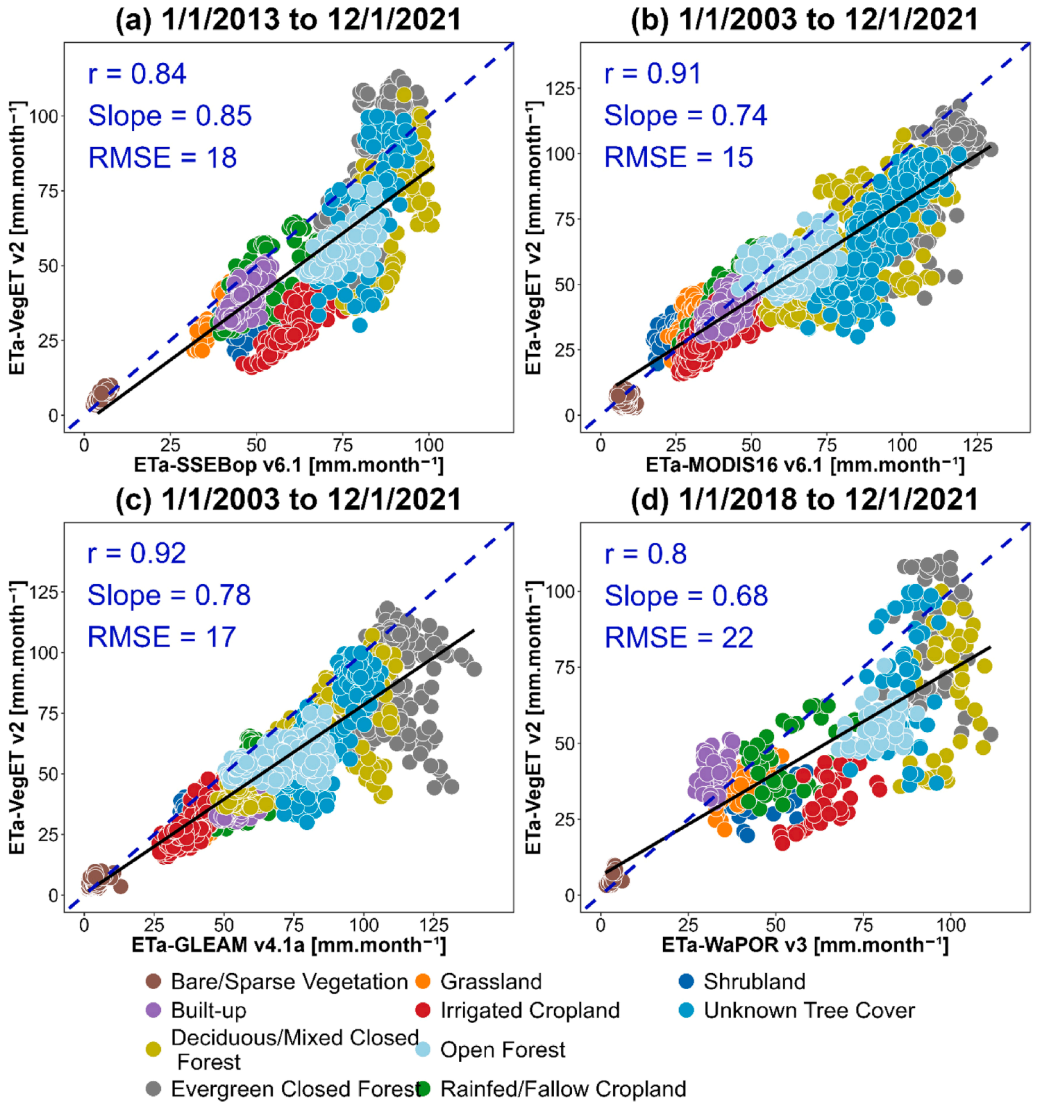

Fig. 9. Comparison of monthly *ETa* estimates from the VegET v2 model with four remote sensing *ETa* products (SSEBop v6.1, MODIS16 v6.1, WaPOR v3, and GLEAM v4.1a) across major land use classes, excluding water bodies. Each scatter plot represents the relationship between VegET and the corresponding remote sensing *ETa* product. The solid black line shows the linear regression fit, while the dashed blue line indicates the 1:1 line.

period, possibly due to differences in how they incorporate surface energy fluxes or assume water availability.

The Taylor diagrams in Fig. 8 (and Appendix Figure B1) integrate correlation, relative variability, and standard deviation, providing a succinct overview of agreement within each climate zone. When VegET is used as the reference, SSEBop, MODIS16, and GLEAM exhibit high r values (≳0.8) and standard deviations similar to VegET, underscoring their consistent performance across tropical and temperate areas. WaPOR's larger deviations in standard deviation and somewhat lower r demonstrate its distinctive spatial and temporal *ETa* patterns in more extreme environments. The diagrams also illustrate that although all products capture the main hydroclimatic gradients, each has unique characteristics—particularly in regions with strong seasonal transitions or intense agricultural activity—leading to differences in both slope and RMSE. VegET v2 aligns most closely with MODIS16 v6.1, GLEAM v4.1a, and SSEBop v6.1 across most climate zones, as evidenced by consistently high r (0.79–0.89), slopes near 1.0, and moderate RMSE values (17–20 mm.month−1). WaPOR v3 typically reports higher ETa in wetter and semi-arid zones, resulting in lower correlation (∼0.79) and a slightly higher RMSE (∼22 mm month^{-1}). Nevertheless, all products broadly capture the seasonal and spatial ETa dynamics across Africa's major climate regimes, with differences primarily manifesting in regions characterized by strong moisture gradients, intensive agriculture, or complex topography.

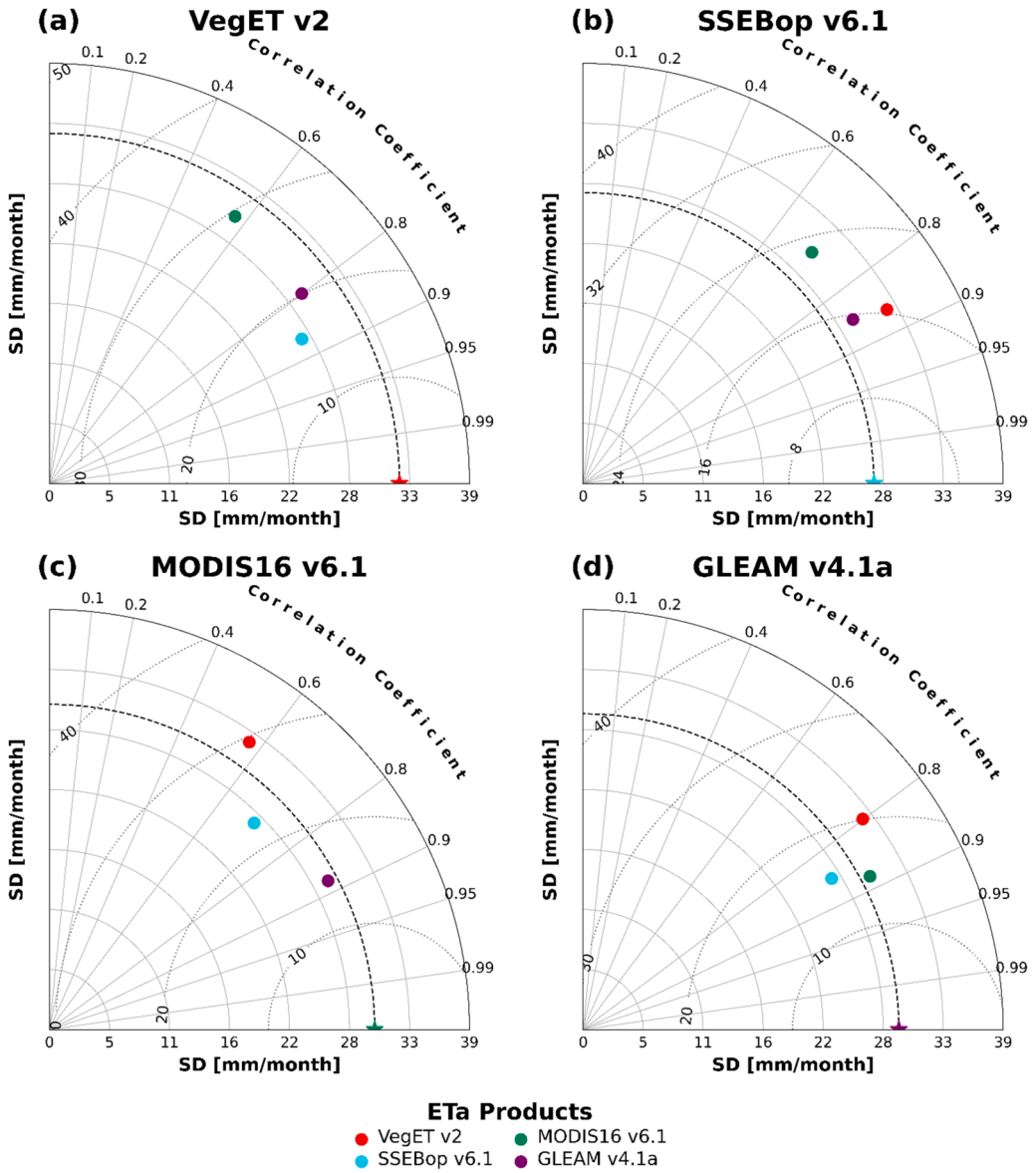

Fig. 10. Taylor diagrams comparing actual evapotranspiration (ETa) estimates for various products, combining all land use classes together, for the period 2013–2021. The diagram depicts the overall standard deviation (SD) and correlation coefficient (R), and Root Mean Square Error (RMSE) for each ETa product when averaged across all climate zones. The reference product is indicated in the title of the panel, and the other products are compared against this reference.

3.4. Comparison of Eta across major land use and land cover classes

Fig. 9 presents scatter plots illustrating the relationship between VegET v2 and each remote sensing *ETa* product over various LULC classes, including croplands, forests, grasslands, and urban/built-up areas. Overall, VegET shows the strongest alignment with MODIS16 v6.1 and GLEAM v4.1a as indicated by high correlation coefficients ($r \geq 0.90$ in some classes), near-unity slopes, and RMSE values generally in the range of 15–20 mm.month^{-1} . These findings are most evident in rainfed/fallow cropland, open forest, and grassland classes, where points cluster closely along the 1:1 line. SSEBop v6.1 also exhibits strong agreement ($r \approx 0.84$, slope ≈ 0.85, RMSE ≈ 18 mm.month^{-1}), particularly in shrubland and grassland areas. Its performance in forested zones, however, displays slightly elevated RMSE, suggesting higher uncertainty where dense vegetation might influence water fluxes. In contrast, WaPOR v3 deviates more markedly in irrigated cropland and built-up areas as indicated by lower correlation ($r \approx 0.80$) and higher RMSE (up to 22 mm. month^{-1}). These discrepancies imply a tendency to overestimate *ETa* in heavily managed agricultural zones or urban settings, possibly due to distinct water consumption patterns or complex surface characteristics that the retrieval algorithm interprets differently from other datasets.

Seasonal cycle analyses in Figure A4 reinforces these findings. Across grasslands, croplands, and forested areas, VegET, GLEAM, SSEBop, and MODIS16 display comparable median *ETa* values with relatively tight interquartile ranges. WaPOR, however, often exhibits higher or more variable *ETa* in irrigated cropland and built-up classes, manifesting as larger spread and higher outliers. This

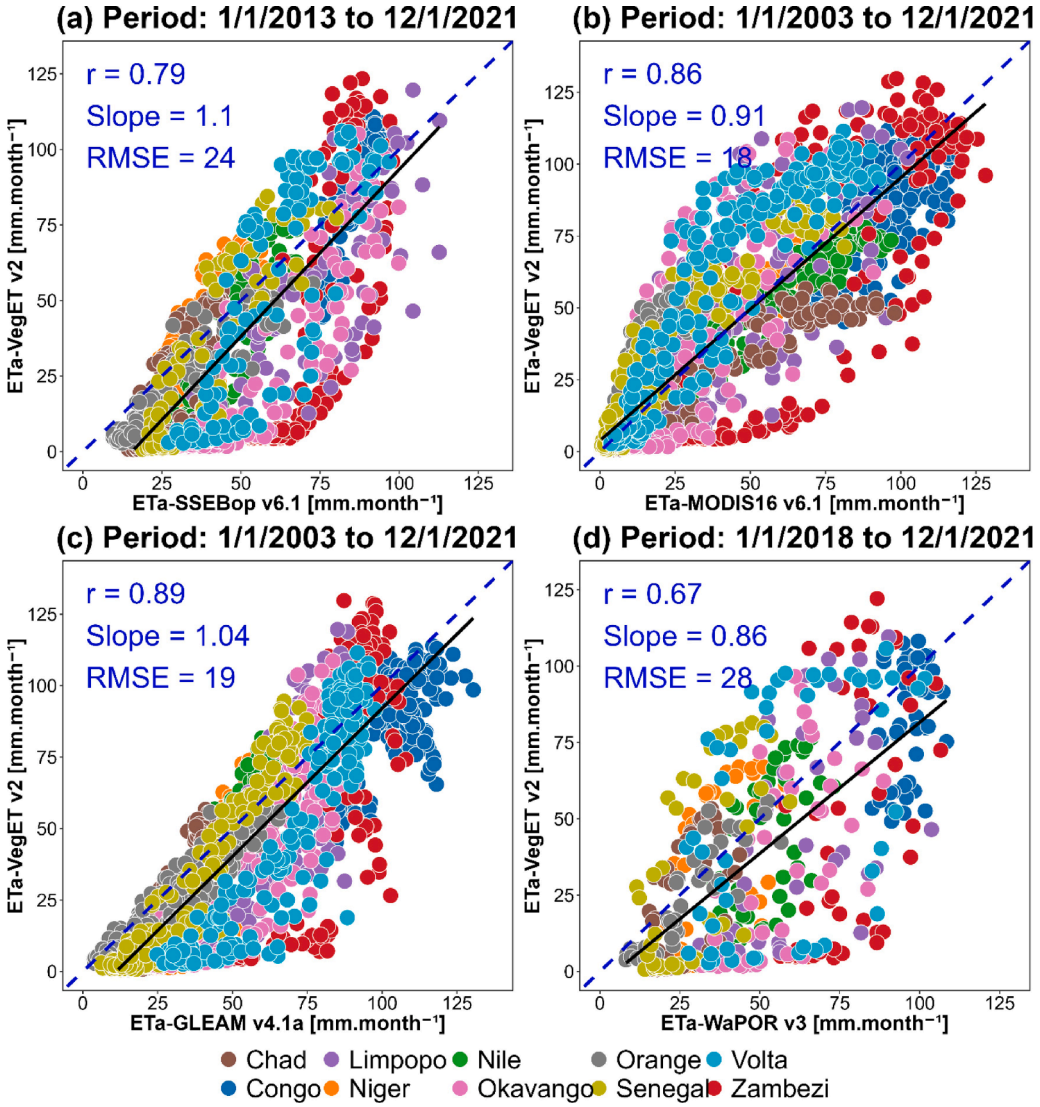

Fig. 11. Comparison of monthly *ETa* estimates from the VegET v2 model with four remote sensing *ETa* products (SSEBop v6.1, MODIS16 v6.1, WaPOR v3, and GLEAM v4.1a) across ten African river basins. Each scatter plot represents the relationship between VegET and the corresponding remote sensing *ETa* product. The solid black line shows the linear regression fit, while the dashed blue line indicates the 1:1 line.

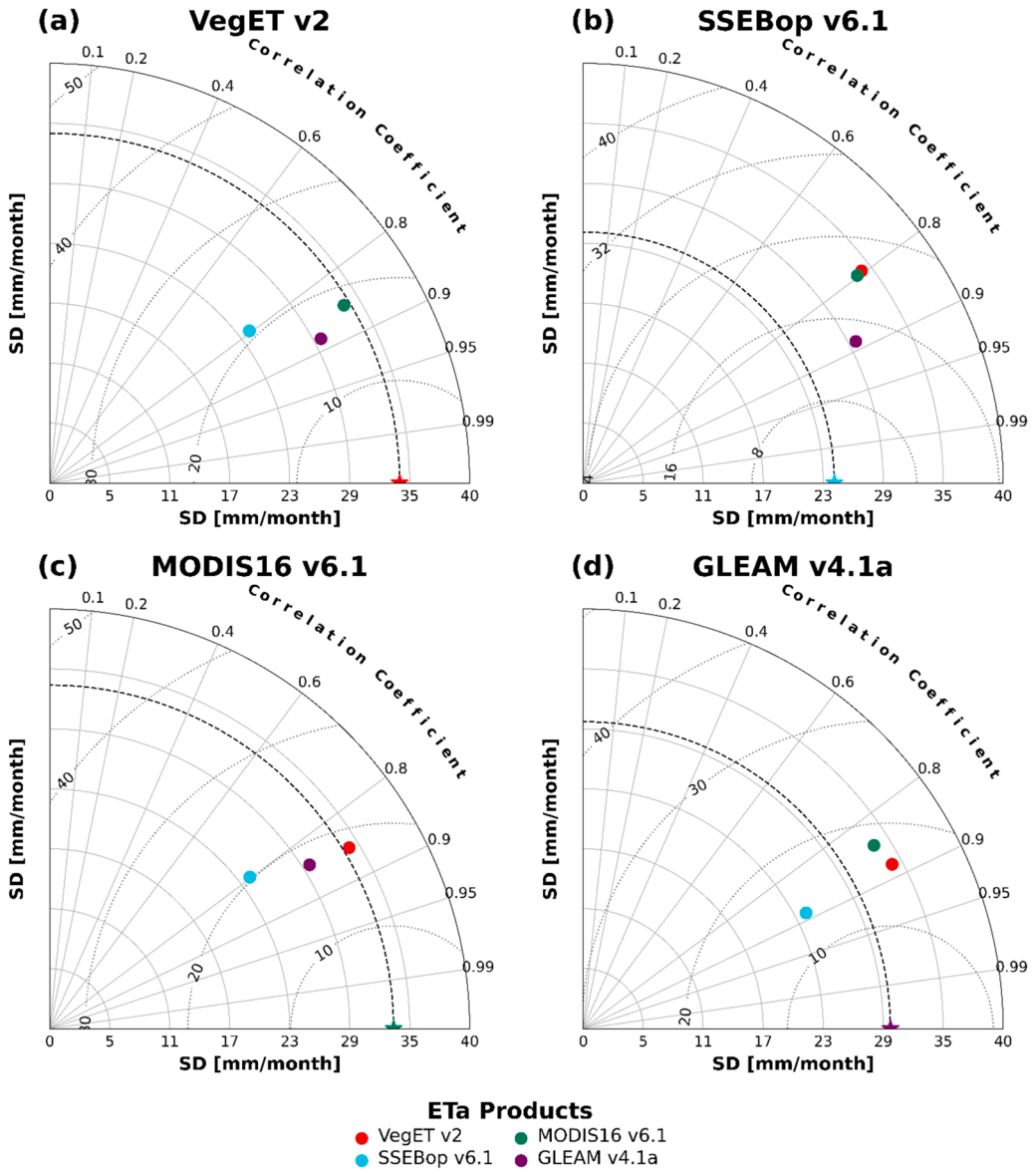

Fig. 12. Taylor diagrams comparing actual evapotranspiration (ETa) estimates for various products, combining all ten basins together, for the period 2013–2021. The diagram depicts the overall standard deviation (SD) and correlation coefficient (R), and Root Mean Square Error (RMSE) for each ETa product when averaged across all basins. The reference product is indicated in the title of each panel, and the other products are compared against this reference.

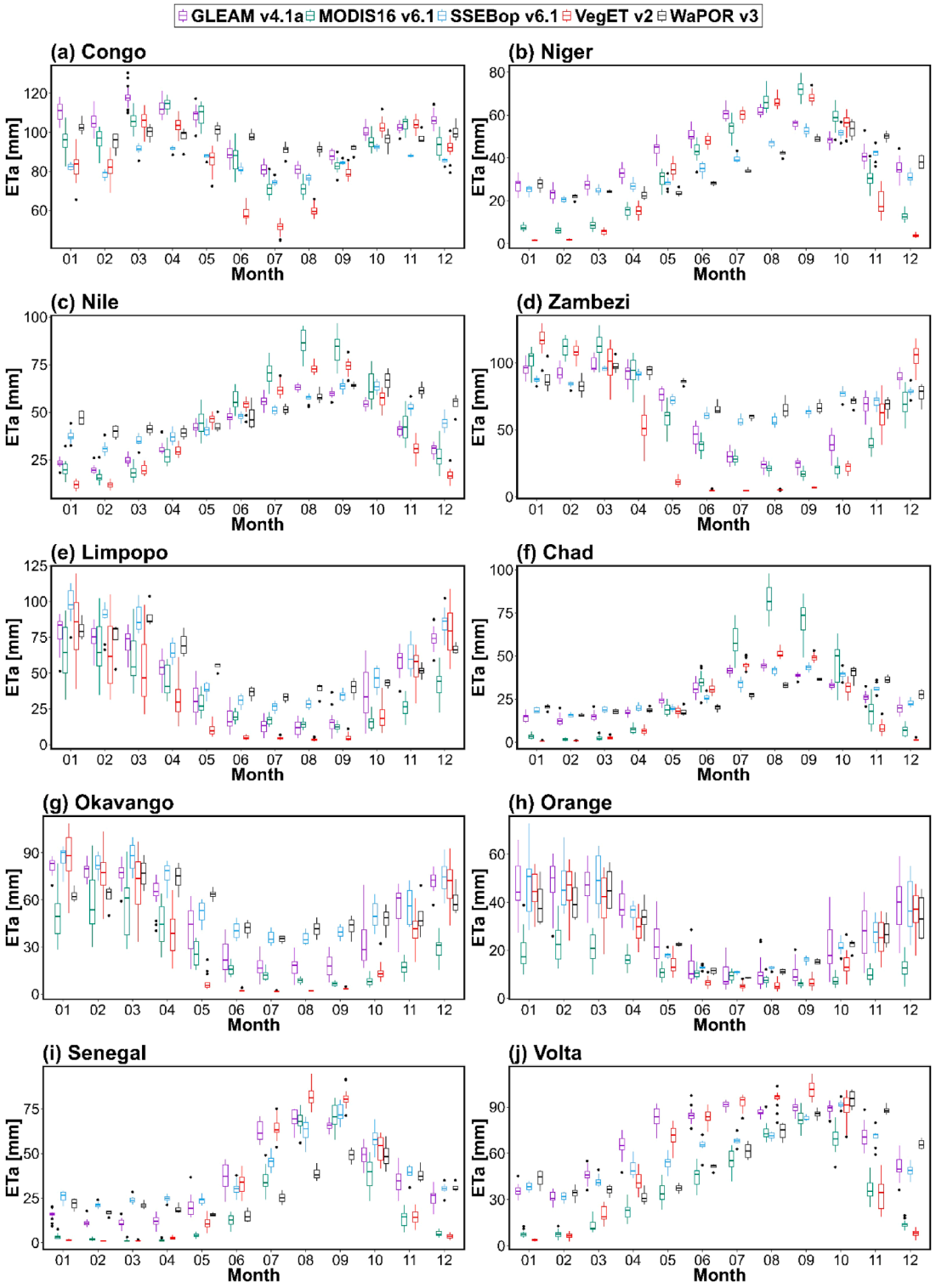

Fig. 13. Box plots of monthly *ETa* estimate for the periods 2003–2021 (MODIS16 v6.1, and GLEAM v4.1a), 2018–2021 (WaPOR v3) and 2013–2021 (SSEBop v6.1) across major river basins in Africa. ETa estimates are compared between the VegET model and four remote sensing ET products (GLEAM, MODIS16, SSEBop, WaPOR). The interquartile range shows the variability of each product's estimates, with outliers represented by black dots.

overestimation is particularly pronounced during periods of active crop growth or potential irrigation demand, underscoring WaPOR's unique retrieval behavior in heavily managed landscapes. VegET v2 aligns most closely with MODIS16 v6.1, GLEAM v4.1a, and SSEBop v6.1 across a wide array of land use and cover classes, consistently showing high correlation, near-unity slopes, and moderate RMSE (∼15–20 mm.month^{-1}). WaPOR v3 typically diverges in agricultural and built-up regions, where it tends to estimate higher *ETa*, leading to lower correlation and elevated RMSE. Collectively, these comparisons indicate that while all products capture broad *ETa* patterns across different LULC types, divergences emerge in zones of concentrated human activity or dense vegetation, where differences in retrieval algorithms and water use assumptions become most apparent` (Fig. 10).

3.5. Comparison of ETa across major basins

Fig. 11 shows monthly *ETa* scatter plots for each remote sensing dataset versus VegET v2, revealing overall strong agreement in large basins such as the Congo and Nile River Basins. GLEAM v4.1a and SSEBop v6.1 typically exhibit the highest correlations with VegET (r ≈ 0.79–0.89), near-unity slopes (∼1.0), and moderate RMSE values (e.g., 19–24 mm.month^{-1}). MODIS16 v6.1 also demonstrates high alignment (r ≈ 0.86), although it displays slightly greater dispersion in basins with strong seasonal variation (e.g., Limpopo, Okavango), resulting in an RMSE around 18 mm.month^{-1} . WaPOR v3 generally shows lower correlation (r ≈ 0.67) and a higher RMSE (∼28–30 mm.month^{-1}), indicating a tendency to overestimate *ETa* in certain river basins characterized by wetter climates or complex hydrological conditions (e.g., the Congo and Okavango River Basins). The Taylor diagrams (Fig. 12) indicate that VegET v2 and GLEAM v4.1a generally showed higher correlations and closer agreement with the reference, while SSEBop v6.1 and MODIS16 v6.1 exhibited larger deviations in standard deviation and RMSE when averaged across all basins during 2013–2021.

Monthly box plots (Fig. 13) of each basin further highlight seasonal variability in *ETa* estimates. In high-*ETa* basins like the Congo and Niger River Basins, VegET, GLEAM, and SSEBop generally group together, with moderate interquartile ranges and higher peak *ETa* during rainy seasons. WaPOR's estimates for these basins often exceed those of the other products, resulting in broader distributions and outlier points. Smaller or more arid basins such as the Okavango and Chad River Basins similarly show that while VegET, SSEBop, MODIS16, and GLEAM share broadly similar cycles, WaPOR diverges more frequently, especially during transition months between dry and wet seasons. Time series plots (Figure A6) underscore these seasonal and interannual patterns from 2003 onward. In the Congo and Nile River Basins, all products capture pronounced wet-season *ETa* peaks, yet WaPOR tends to produce higher maxima, while MODIS16 occasionally dips below the group average during peak growth periods. In contrast, SSEBop, VegET, and GLEAM typically track each other closely throughout most seasons. VegET v2 maintains strong agreement with GLEAM, SSEBop, and MODIS16 across most of Africa's major basins, as evidenced by correlation coefficients often exceeding 0.80 and RMSE values in the range of 18–24 mm.month^{-1} . WaPOR v3, though broadly consistent in certain basins, shows more pronounced deviations in humid or hydrologically complex regions (e.g., Congo and Okavango River Basins), leading to lower correlation (r ≈ 0.67) and higher RMSE (≳28 mm month^{-1}). This basic level analysis underscores both the strengths and limitations of each product under differing hydrological regimes, illuminating where model assumptions and retrieval algorithms exert the greatest influence on *ETa* estimation.

3.6. Application of VegET ETa for drought monitoring using ETDI

The annual average *ETDI* maps presented in Appendix C (Figure C.1) illustrate the spatial distribution of drought and wetness conditions across Africa from 2002 to 2021. Over this 20-year period, distinct patterns emerge, highlighting persistent drought conditions in arid regions such as the Sahel and southern Africa, where *ETDI* values frequently fall below −2, indicating severe to

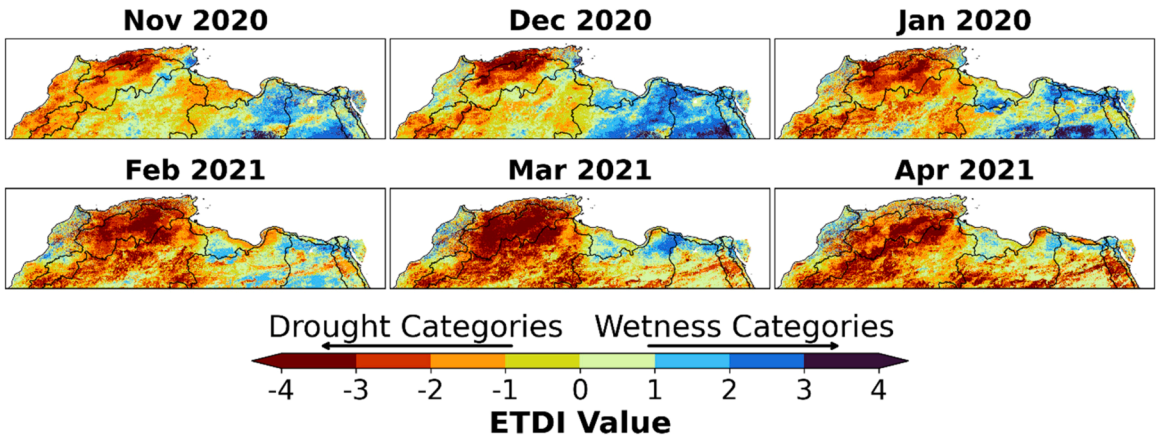

Fig. 14. Monthly Evapotranspiration Deficit Index (*ETDI*) maps from November 2020 to April 2021, zoomed in on Northern Africa, the Maghreb region. The color scale indicates the range of *ETDI* values, with negative values representing drought conditions and positive values indicating wetness. These maps capture the seasonal variation in water stress, with drought conditions becoming more severe during the late winter and early spring of 2021.

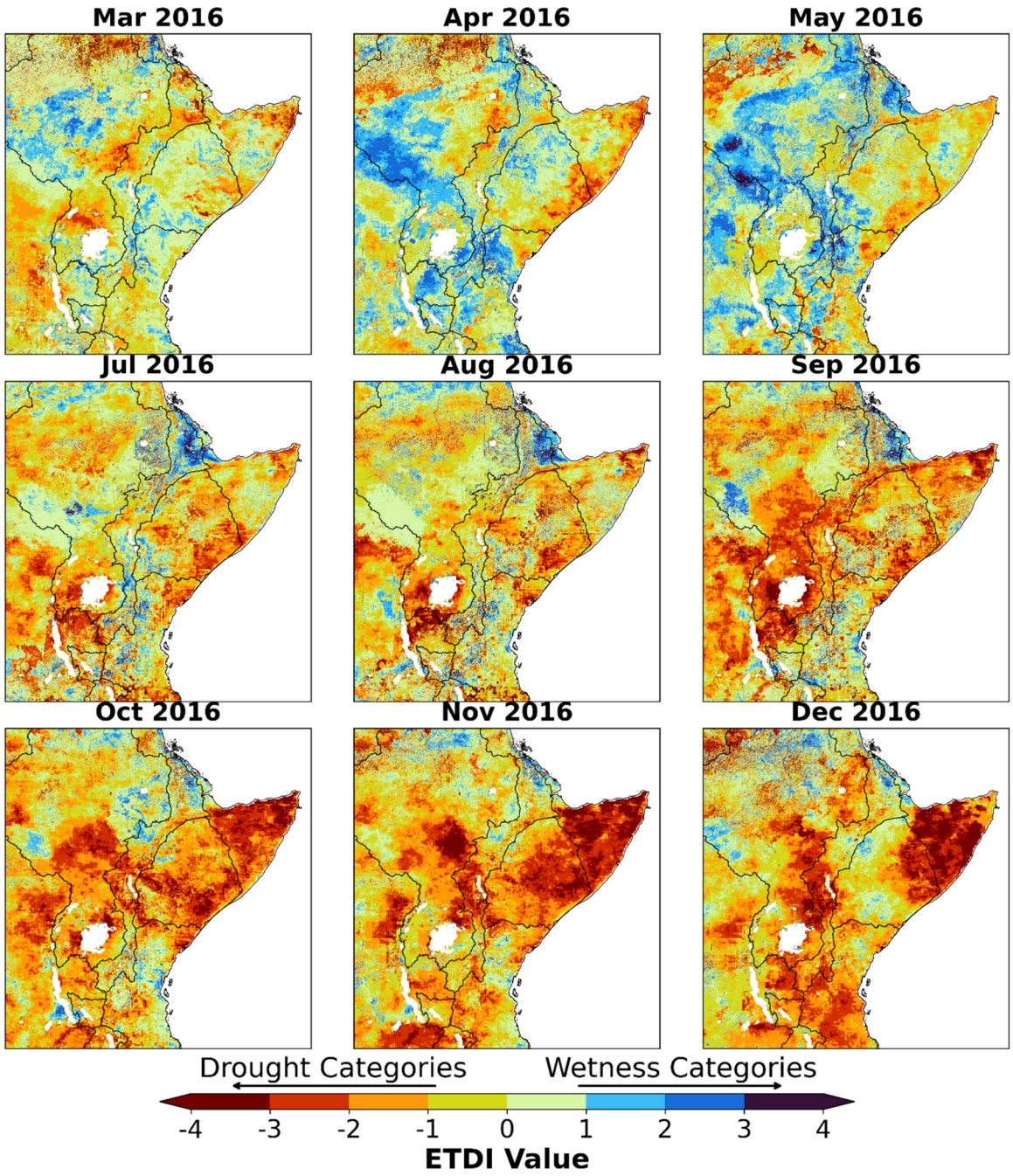

Fig. 15. Monthly Evapotranspiration Deficit Index (*ETDI*) maps for the Horn of Africa in 2016, covering the three main rainy seasons: boreal spring (March to May), boreal summer (July to September), and boreal autumn (October to December). The color scale shows the *ETDI* values, with negative values indicating drought conditions and positive values indicating wetness. The progression of drought and wetness conditions over the year highlights the seasonal variability of water stress across the region.

extreme drought. Conversely, regions such as central Africa and parts of Madagascar show recurring wetness, with *ETDI* values exceeding 2, suggesting consistent above-average moisture availability. The maps also capture inter-annual variability, such as the widespread wet conditions observed in 2007 and 2010, contrasted with severe drought conditions in 2017 and 2021.

The monthly *ETDI* maps for northern Africa shown in Fig. 14 illustrate the progression of drought conditions in the Maghreb region from November 2020 to April 2021. The rainy season, typically extending from October to March, experienced below-average rainfall during this period, in the core winter months of December 2020 to February 2021. The *ETDI* values during these months indicate increasing drought severity, with much of Morocco, Algeria, and Tunisia experiencing moderate to extreme drought, as indicated by

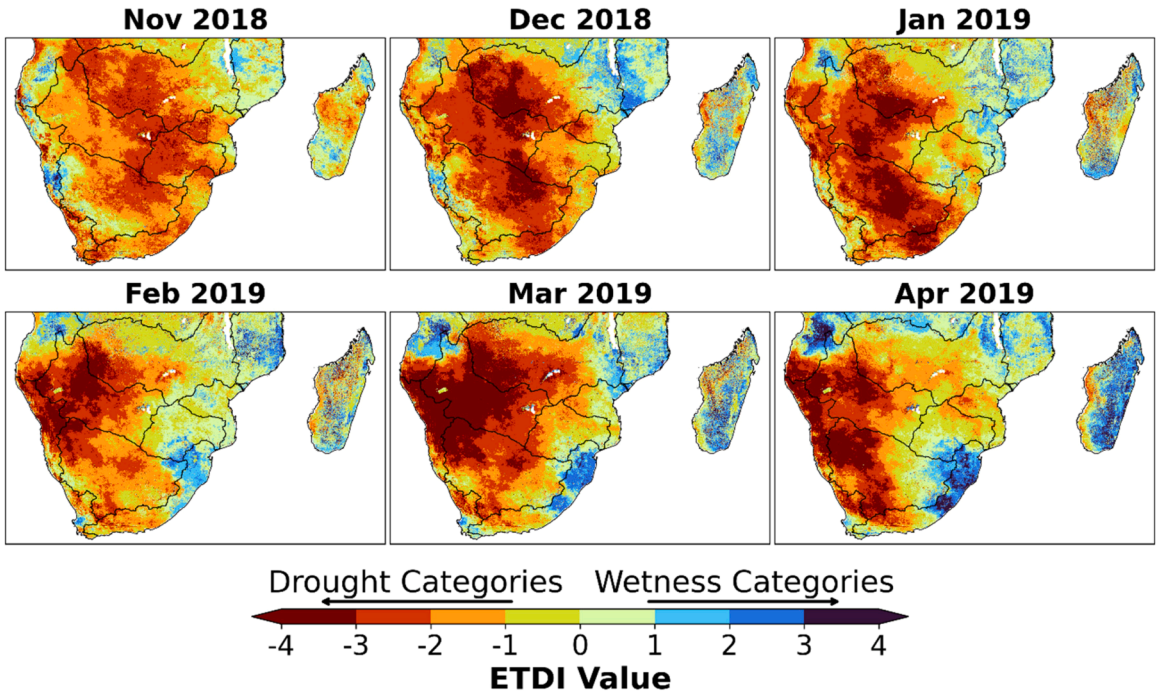

Fig. 16. Monthly Evapotranspiration Deficit Index (*ETDI*) maps for Southern Africa from November 2018 to April 2019. These maps capture the austral summer rainy season, showing the progression of drought and wetness conditions across the region. The color scale indicates *ETDI* values, with negative values representing drought conditions and positive values indicating wetness.

values falling below −2. By March and April 2021, *ETDI* values remained predominantly in the drought range, highlighting the persistence of water stress in the region despite the expected rainfall. The southern parts of the Maghreb, closer to the Sahara, also experienced extreme drought conditions.

Fig. 15 presents the monthly *ETDI* maps for the Horn of Africa throughout 2016, showcasing the distinct patterns during the region's three main rainy seasons: boreal spring (March to May), boreal summer (July to September), and boreal autumn (October to December). During the boreal spring, in March and April, the *ETDI* maps reveal widespread wet conditions, especially in southern Ethiopia and parts of Kenya, with values exceeding 2, indicating above-average moisture. However, by the boreal summer, dry conditions dominate, in Somalia and northeastern Ethiopia, where *ETDI* values fall below −2, signaling severe drought conditions. In the boreal autumn, drought conditions intensify in October and November, with large areas of Somalia, eastern Ethiopia, and northern Kenya experiencing extreme drought as indicated by *ETDI* values below −3. These patterns are consistent with the region's dependence on the short rains during autumn to alleviate the water deficit from the dry summer months. However, the late onset and variability of the autumn rains in 2016 contributed to prolonged drought conditions, exacerbating water scarcity and impacting agriculture and livelihoods across the region.

The monthly *ETDI* maps for southern Africa during November 2018–April 2019 (Fig. 16) provide a detailed view of drought dynamics during the austral summer rainy season. The results indicate widespread drought conditions across much of the region, in South Africa, Namibia, Botswana, and Zimbabwe. Starting in November 2018, large parts of the region exhibited *ETDI* values below −2, signifying severe drought, which persisted into December and January. The period from February through April 2019 shows some localized wetness in parts of Madagascar and Mozambique, likely related to tropical cyclones and other weather systems, while the core inland areas remained under severe drought. This period coincides with a documented drought event in southern Africa, exacerbating food insecurity, water shortages, and agricultural losses, especially in South Africa, Namibia, and Zimbabwe. The *ETDI* maps highlight the regional variability of drought severity, with some regions, coastal areas, experiencing slightly more favorable moisture conditions compared to the interior regions. The persistent drought across central Southern Africa during the peak of the rainy season underscores the ongoing vulnerability of the region to water scarcity and climate variability.

4. Discussion

This study represents one of the first applications of VegET at continental scale in Africa, providing a hydrologically grounded ETa

dataset that complements existing remote sensing products. The systematic evaluation against flux towers and four widely used ETa products across diverse climatic zones, land use classes, and major river basins reveals that the choice of modeling framework—water balance versus energy balance versus hybrid—systematically influences ETa magnitude and seasonality, with implications that vary by hydroclimatic regime. The following sections interpret these differences in terms of underlying mechanisms, compare them with published findings, and discuss their implications for drought monitoring and water resource management.

4.1. Performance in arid and semi-arid zones

In arid and semi-arid regions, VegET tends to produce lower ETa than WaPOR and SSEBop, particularly during dry seasons. This divergence is mechanistically linked to the models' contrasting treatment of soil moisture constraints. VegET's water-balance framework explicitly limits ETa when root-zone moisture falls below the maximum allowable depletion threshold (Ks → 0), producing estimates that track precipitation-driven soil moisture closely, consistent with evidence that surface soil moisture information can identify transitions between water- and energy-limited evapotranspiration regimes (Dong et al., 2022). This behavior is consistent with Adeyeri and Ishola (2021), who identified rainfall as the primary driver of ETa variability in the Sahel. In contrast, energy-balance products like WaPOR and SSEBop derive ETa primarily from thermal signatures and vegetation indices, which may remain elevated even when soil moisture is depleted—for example, through residual canopy greenness or warm bare-soil temperatures—leading to overestimation in water-limited environments (Blatchford et al., 2020; Trambauer et al., 2014). GLEAM, which assimilates satellite-derived soil moisture, occupies an intermediate position and captures short-term ETa fluctuations effectively but exhibits increased variability during wet-dry transitions (Martens et al., 2017). These findings suggest that in water-limited environments, the accuracy of ETa estimates depends less on the sophistication of the atmospheric forcing and more on how accurately the model represents soil water availability and its control on plant-accessible moisture. Integrating ground-based soil moisture observations or satellite-derived root-zone moisture products could improve VegET's accuracies in these zones, as demonstrated by Kiptala et al. (2013) for SEBAL-based approaches in East Africa.

4.2. Performance in humid and tropical zones

In humid tropical regions such as the Congo River Basin and coastal West Africa, VegET, MODIS16, and GLEAM converge closely, demonstrating that when water is not limiting, ETa is primarily controlled by available energy and vegetation cover—processes that all three frameworks capture through vegetation indices and radiation inputs. This convergence across fundamentally different modeling approaches (water balance, Penman-Monteith, Priestley-Taylor) provides mutual corroboration of ETa magnitudes in these regions. WaPOR, however, tends to overestimate ETa in humid zones, likely because its vegetation-index emphasis does not fully account for canopy interception partitioning and may attribute intercepted rainfall evaporation to transpiration (Blatchford et al., 2020).

A distinct challenge in the Congo River Basin is precipitation recycling, where land-surface evapotranspiration sustains a substantial fraction of regional rainfall (Brubaker et al., 1992; Eltahir and Bras, 1994). VegET, as a one-dimensional soil-column model, does not represent this atmospheric feedback, which may contribute to underestimation during peak wet seasons when recycled moisture amplifies precipitation and, consequently, ETa. Additionally, VegET's soil stress coefficient (Ks) responds to root-zone depletion rather than surface water ponding or rapid infiltration events characteristic of high-intensity tropical rainfall, potentially limiting its responsiveness to short-term moisture pulses. Despite these limitations, the close agreement with MODIS16 and GLEAM indicates that VegET provides reliable ETa estimates in humid environments when appropriately calibrated, and its water-balance framework offers the added value of internally consistent runoff and recharge fields that purely diagnostic remote sensing products cannot provide.

4.3. Impact of land use and irrigation practices

Land use exerts a strong influence on ETa model performance across Africa. In rainfed agricultural areas, VegET's NDVI-derived crop coefficients effectively capture seasonal vegetation water demand, consistent with Pòças et al. (2020), who demonstrated that phenology-based coefficients reliably represent crop water requirements across diverse cropping systems. However, in irrigated regions—such as the Nile Delta and parts of North Africa—all precipitation-driven models face a fundamental limitation: irrigation water inputs are not represented in their forcing data. VegET, which derives soil moisture exclusively from precipitation, will systematically underestimate ETa in irrigated areas because the additional water supply is unaccounted for. Conversely, WaPOR's reliance on vegetation indices can lead to overestimation in irrigated zones because elevated NDVI from irrigation-sustained vegetation is interpreted as high transpiration demand regardless of the water source (Blatchford et al., 2020). This asymmetry highlights a structural gap: neither precipitation-driven nor vegetation-index-driven approaches alone can accurately capture ETa in managed landscapes without explicit irrigation information. Integrating irrigation maps or satellite-derived soil moisture anomalies, as demonstrated by Kiptala et al. (2013) using SEBAL in East Africa, could help bridge this gap for future VegET applications.

4.4. Temporal and seasonal variability

All models capture the broad seasonal cycle of ETa across Africa, with peaks corresponding to rainy seasons. However, inter-model divergence increases during intra-seasonal transitions and extreme events, revealing how different frameworks handle temporal dynamics. VegET and SSEBop track seasonal trends consistently in semi-arid regions because both respond to surface conditions—soil moisture for VegET, land surface temperature for SSEBop—that indicate recent precipitation inputs. MODIS16, which relies primarily on atmospheric demand variables (vapor pressure deficit, air temperature), shows lower sensitivity to short-term soil moisture pulses and consequently underestimates ETa during brief wet spells in otherwise dry seasons. GLEAM's assimilation of satellite soil moisture provides increased intra-seasonal responsiveness but introduces additional variability during wet-dry transitions, consistent with Martens et al. (2017). These temporal characteristics have direct implications for drought monitoring: models that respond to soil moisture and vegetation phenology in near-real time—such as VegET and GLEAM—are likely better positioned to support early warning systems than those driven primarily by atmospheric variables.

4.5. Modeling frameworks and methodological insights

The systematic divergence among ETa products can be attributed to three fundamental differences in their modeling frameworks: (i) how ETa demand is defined—through atmospheric variables (MODIS16), thermal signatures (SSEBop), or vegetation phenology (VegET, WaPOR); (ii) how water availability constrains that demand—explicitly via soil moisture budgets (VegET, GLEAM) or implicitly via land surface temperature departures (SSEBop); and (iii) whether the model operates within a closed water balance (VegET) or as a diagnostic estimate (remote sensing products). These structural differences explain why products converge in humid energy-limited environments—where demand, not supply, controls ETa—but diverge substantially in water-limited regions where the representation of soil moisture stress becomes the dominant source of uncertainty. This finding is consistent with Jung et al. (2019), who showed that model parameterization accounts for over 90% of ETa uncertainty in West African humid zones, and with Trambauer et al. (2014), who documented large inter-product discrepancies in African arid zones. Future advancements should prioritize hybrid approaches that combine the spatial coverage of remote sensing with the water-balance consistency of hydrological models, potentially through data assimilation of satellite soil moisture into frameworks like VegET (Awada et al., 2022, 2024).

Our study results underscore that ETa intercomparisons should not be viewed solely as validation exercises, but as a way to understand how different modeling frameworks represent hydrological processes. For example, VegET's lower ETa relative to WaPOR in semi-arid zones demonstrates stricter water-balance constraints, which aligns with observed drought impacts. Conversely, agreement with MODIS16 and GLEAM in humid regions shows convergence across frameworks when water is not limiting. Because VegET is embedded within a full root-zone water balance framework, the *ETa* fields can be directly linked with runoff and recharge estimates. This aligns with recent continental-scale discharge modeling (Akpoti et al., 2024) where VegET runoff was routed with mizuRoute (Mizukami et al., 2016) to model pan-African discharge fields. Together, these applications highlight VegET's capability to support integrated hydrological assessments, from *ETa* to river discharge.

4.6. Limitations and uncertainties

Several limitations should be considered when interpreting the results of this study. First, VegET is a one-dimensional, precipitation-driven soil-water balance model that does not represent lateral water transfers, groundwater contributions, or irrigation inputs. In irrigated areas and regions with shallow water tables, this leads to systematic underestimation of *ETa* resulting from a lack of accounting for additional water sources beyond precipitation. Incorporating irrigation maps or satellite-derived soil moisture anomalies in future versions could partially address this gap. Second, VegET's reliance on NDVI-derived crop coefficients assumes that satellite-observed greenness is a reliable proxy for vegetation water demand. In regions with persistent cloud cover, such as the Congo River Basin, NDVI compositing artifacts can introduce noise into the Kcp signal, potentially affecting *ETa* seasonality. Third, the model does not explicitly represent canopy interception as a separate flux; instead, interception is parameterized through fixed maximum values for tree and herbaceous cover, which may not capture the variability of interception across different forest types and rainfall intensities.

Validation is constrained by the limited availability and spatial representativeness of eddy covariance (EC) flux towers in Africa. Only eight tower sites were available for this study, spanning a subset of the continent's climatic and land cover diversity. Key biomes—including tropical montane forests, and the Saharan fringe—remain unrepresented in the validation dataset. Furthermore, the spatial mismatch between EC tower footprints (typically 100–1000 m) and the 1-km VegET grid introduces scale-dependent uncertainty, particularly in heterogeneous landscapes where land cover varies within a single model pixel. EC data have associated uncertainties of 10–30% due to energy balance non-closure (Glenn et al., 2010, 2011), meaning that both the model and the reference data contribute to observed discrepancies.

Input data quality represents an additional source of uncertainty. Precipitation products used to force VegET, while state-of-the-art, exhibit well-documented biases in regions with sparse rain gauge networks, particularly in Central Africa, the Sahel, and highland

areas. Since VegET's soil moisture and ETa are directly driven by precipitation, these biases propagate into the ETa estimates. Similarly, the benchmark remote sensing products against which VegET is compared carry their own uncertainties, including sensitivity to cloud contamination, thermal calibration, and algorithm-specific assumptions—meaning that the intercomparison characterizes relative consistency among products rather than absolute accuracy. Finally, the study period (2000–2021) is defined by the availability of MODIS-era satellite data, which limits the ability to assess longer-term trends or pre-2000 baseline conditions. Despite these limitations, the consistency of VegET with flux tower observations and multiple independent remote sensing products across diverse environments supports its utility as a continental-scale hydrological ETa product for Africa.

4.7. Implications for drought monitoring and water resource management

The application of VegET-derived ETa in calculating the Evapotranspiration Deficit Index (ETDI) illustrates the utility of hydrologically grounded ETa compared to purely diagnostic remote sensing products. Unlike traditional drought indices that rely on potential evapotranspiration derived from temperature (e.g., SPI, PDSI), ETDI incorporates actual water consumption by vegetation, capturing the interplay between precipitation inputs, soil moisture depletion, and atmospheric demand (Narasimhan and Srinivasan, 2005). This is particularly relevant in Africa, where even minor deviations from seasonal rainfall norms can severely impact rainfed agricultural productivity. The ETDI results demonstrate the ability to capture region-specific drought dynamics: the 2015–2016 and 2018–2019 droughts in southern Africa, driven by El Niño-related precipitation deficits; the persistent seasonal water stress in the Horn of Africa (Nicholson, 2014); and the progressive drying in the Maghreb associated with declining winter rainfall and rising temperatures (Masih et al., 2014).

A key strength of using VegET ETa for ETDI is its internal consistency with the soil water balance: because ETa, runoff, and soil moisture are jointly simulated, drought signals in ETDI represent actual hydrological deficits rather than atmospheric proxies. This contrasts with meteorological drought indices that may underestimate agricultural impacts when precipitation deficits are partially offset by stored soil moisture, or overestimate impacts when antecedent conditions buffer the effect of a dry spell. As climate change intensifies the frequency and severity of droughts across Africa, integrating hydrological model-derived ETa into operational drought monitoring frameworks offers a pathway toward more physically grounded early warning systems for food security and water resource management.

5. Summary and conclusions

This work advances beyond a product evaluation by providing one of the first continental-scale hydrological simulations of *ETa* for Africa, validated against flux towers and benchmarked against four widely used satellite products. The integration with drought monitoring through ETDI demonstrates its operational value for water managers. Beyond *ETa*, the VegET framework links to runoff and discharge modeling (Akpoti et al., 2024), supporting basin-scale water accounting, agricultural water management, and climate resilience planning. For hydrologists and decision-makers, this study highlights VegET's utility as a model evaluation tool and a practical hydrological modeling framework for monitoring evapotranspiration and drought at continental scales. The study provides a comprehensive comparative analysis of the Agro-Hydrologic VegET model and four widely recognized remote sensing-based *ETa* products—MODIS16, SSEBop, WaPOR, and GLEAM—across various climatic zones, land use types, and spatial scales in Africa. The results reveal that no single *ETa* model consistently outperforms others across all regions, demonstrating the inherent complexities of estimating evapotranspiration in diverse environments.

In humid and tropical zones, such as the Congo River Basin and coastal West Africa, the VegET model demonstrates strong comparability with MODIS16 and GLEAM, effectively capturing the seasonal dynamics of *ETa*. This consistency can be attributed to the models' reliance on vegetation indices and water balance principles, which are appropriate in regions where water is not a limiting factor. However, some discrepancies arise, particularly during peak wet seasons, where models like WaPOR tend to overestimate *ETa* due to their over-reliance on vegetation indices, which may not fully account for canopy interception or other land surface processes. Moreover, VegET's reliance on soil moisture through the soil stress coefficient (Ks) may limit its ability to capture rapid changes in water availability, such as intense rainfall events and high precipitation recycling observed in tropical rainforests. In contrast, *ETa* values of VegET are lower in arid and semi-arid regions, such as the Sahel, where water is limited, and evapotranspiration is primarily constrained by soil moisture availability. Here, model like SSEBop, which is based on energy balance principles, generally provide the most accurate estimates of *ETa*, particularly in water-limited conditions. However, these models also exhibit increased variability during transitions between wet and dry periods, likely due to their sensitivity to short-term fluctuations in soil moisture and atmospheric demand. WaPOR, with its focus on agricultural water productivity, demonstrates high accuracy in irrigated regions but tends to overestimate *ETa* in areas where soil moisture limitations are not well represented.

Land use and land cover were also found to be critical factors influencing model performance. VegET, with its phenology-based approach, accurately estimated *ETa* in rainfed croplands and natural vegetation zones, where soil moisture from rainfall is a primary driver of *ETa*. However, its limitations become apparent in irrigated agricultural areas, particularly in North Africa and other regions relying on groundwater or supplemental irrigation. In these settings, VegET does not fully capture the complexities of managed

water use because it is specifically designed to estimate *ETa* based on soil moisture within a shallow 1-meter root zone driven by rainfall alone without accounting for additional water inputs from irrigation or groundwater sources. In these areas, WaPOR's design, which emphasizes agricultural water use, provides higher *ETa* estimates, but often at the cost of overestimations in dry seasons. The findings emphasize the importance of model calibration and the integration of multi-source data—including soil moisture observations, vegetation indices, and thermal infrared data—to improve *ETa* estimation across Africa's diverse landscapes. Given the variability in model performance, no single *ETa* product is universally superior. Instead, the strength of each model lies in its ability to capture specific environmental and land-use characteristics, underscoring the need for hybrid approaches that leverage the strengths of different methodologies.

Future research could focus on developing hybrid models that combine the strengths of precipitation-driven models like VegET with energy balance models like SSEBop and GLEAM. This will enable increased spatial and temporal resolution of *ETa* estimates, particularly in regions with high environmental variability. Furthermore, the incorporation of ground-based measurements is essential for validating and refining remote sensing estimates, especially in areas where remote sensing data may be limited or subject to bias. Expanding ground-based networks for soil moisture and vegetation monitoring will greatly enhance model accuracy and reliability, helping to close the gap between model predictions and observed *ETa* dynamics. In conclusion, increasing the accuracy and reliability of *ETa* models is key for supporting informed decision-making in water resource allocation, agricultural planning, and drought mitigation efforts. As Africa faces increasing challenges related to water scarcity, climate change, and population growth, robust and accurate *ETa* models are essential for ensuring the sustainable management of the continent's vital water resources. Advancing *ETa* modeling capabilities and integrating multi-source datasets, stakeholders can develop more effective strategies for managing water resources and adapting to the impacts of climate variability and change.

Furthermore, the application of VegET-derived actual evapotranspiration (*ETa*) in calculating drought indices like the Evapotranspiration Deficit Index (*ETDI*) highlights the potential for enhanced drought monitoring and management across Africa. Integrating both PET and *ETa*, *ETDI* provides a more accurate reflection of water stress experienced by vegetation, particularly in regions with highly variable climatic conditions. *ETDI* provides a more accurate representation of water stress experienced by vegetation, particularly in regions with highly variable climatic conditions. This approach allows for the timely detection of agricultural droughts, enabling stakeholders to implement mitigation strategies more effectively. As climate change continues to alter precipitation patterns and increase the frequency of extreme weather events, incorporating *ETa* into drought assessment frameworks becomes increasingly crucial for safeguarding food security and optimizing water resource allocation (Narasimhan and Srinivasan, 2005; Marshall et al., 2013). The enhanced precision in drought detection offered by models like VegET can significantly contribute to the development of resilient agricultural systems and inform policy decisions aimed at climate adaptation and sustainable resource management.

CRediT authorship contribution statement

Seid Abdulkarim: Writing – review & editing, Resources, Project administration, Funding acquisition. **Kirubel Mekonnen:** Writing – review & editing, Data curation. **Samuel Guug:** Writing – review & editing, Data curation. **Souleymane Sy:** Writing – review & editing, Data curation. **Velpuri Naga:** Writing – review & editing, Validation, Supervision, Resources, Project administration, Methodology, Conceptualization. **Vinay Nangia:** Writing – review & editing, Data curation. **Komlavi Akpoti:** Writing – review & editing, Writing – original draft, Visualization, Validation, Software, Methodology, Investigation, Formal analysis, Data curation, Conceptualization. **Parrish Gabriel:** Validation, Software. **Lahiru Madushanka:** Software, Data curation. **Tharindu Perera:** Software, Data curation. **Prabhath Paranamana:** Writing – review & editing, Software, Data curation. **Mulugeta Tadesse:** Writing – review & editing, Data curation. **Senay Gabriel:** Writing – review & editing, Validation, Software, Methodology. **Afua Owusu:** Writing – review & editing. **Stefanie Kagone:** Writing – review & editing, Software, Data curation. **Jan Bliefernicht:** Writing – review & editing, Data curation. **Mansoor Leh:** Writing – review & editing, Methodology.

Declaration of Competing Interest

The authors declare that they have no known competing financial interests or personal relationships that could have appeared to influence the work reported in this paper.

Acknowledgments

The authors would like to express their gratitude to the data providers and developers for making their datasets freely available. This research is conducted under the International Water Management Institute's Digital Innovations for Water Secure Africa (DIWASA) project. We sincerely thank The Leona M. and Harry B. Helmsley Charitable Trust for their generous financial support. The views expressed in this study are solely those of the authors and do not necessarily represent the views of the funding organizations but do represent the views of the U.S. Geological Survey. We also wish to extend our appreciation to the reviewers for their insightful edits and constructive feedback. Any mention of trade names, commercial products, or organizations is for descriptive purposes only and does not constitute endorsement by the U.S. Government.

Appendix A. Monthly Climatology of *ETa* products

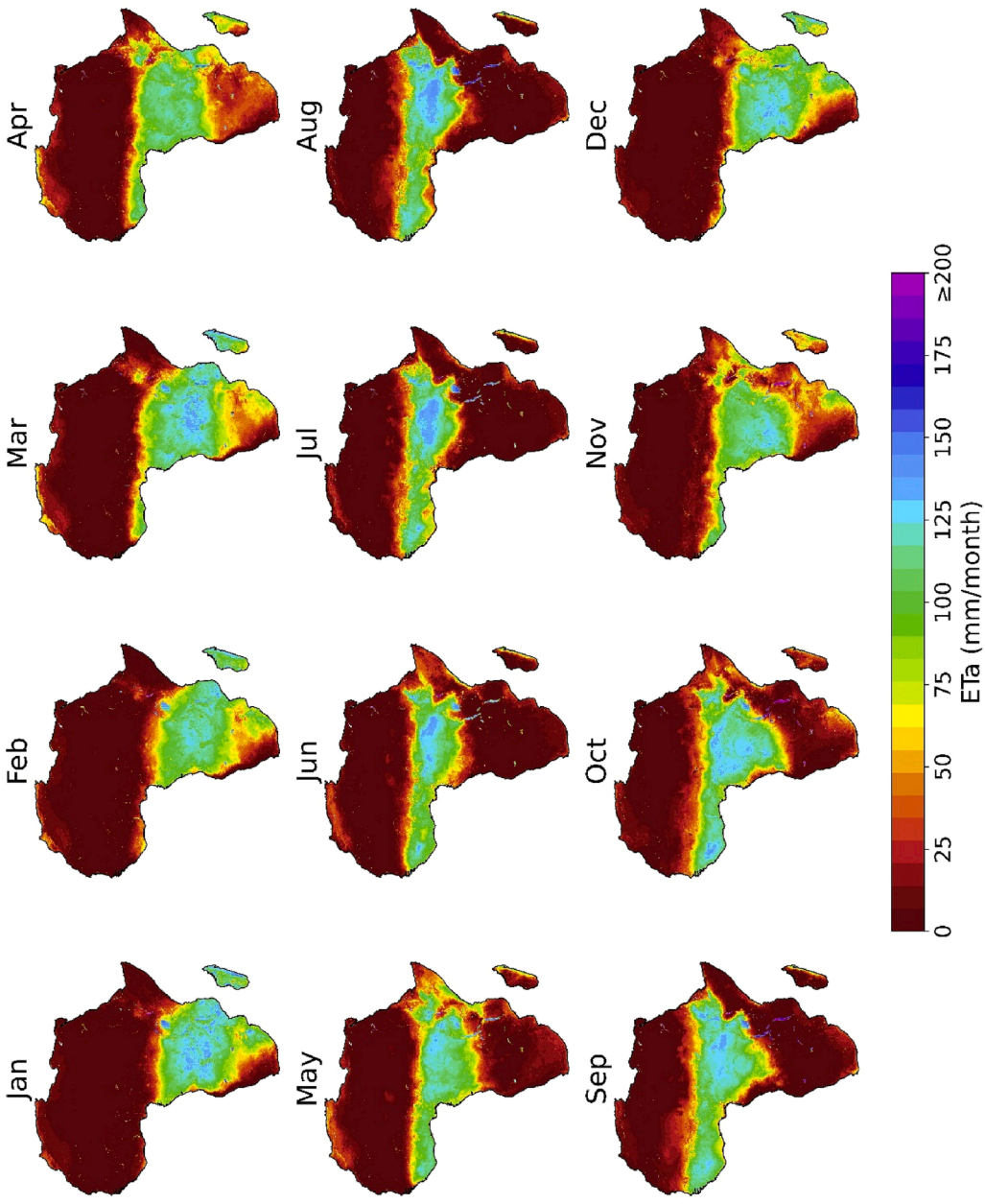

Figure A1. Monthly average ETa using VegET v2 for the period 2003–2021

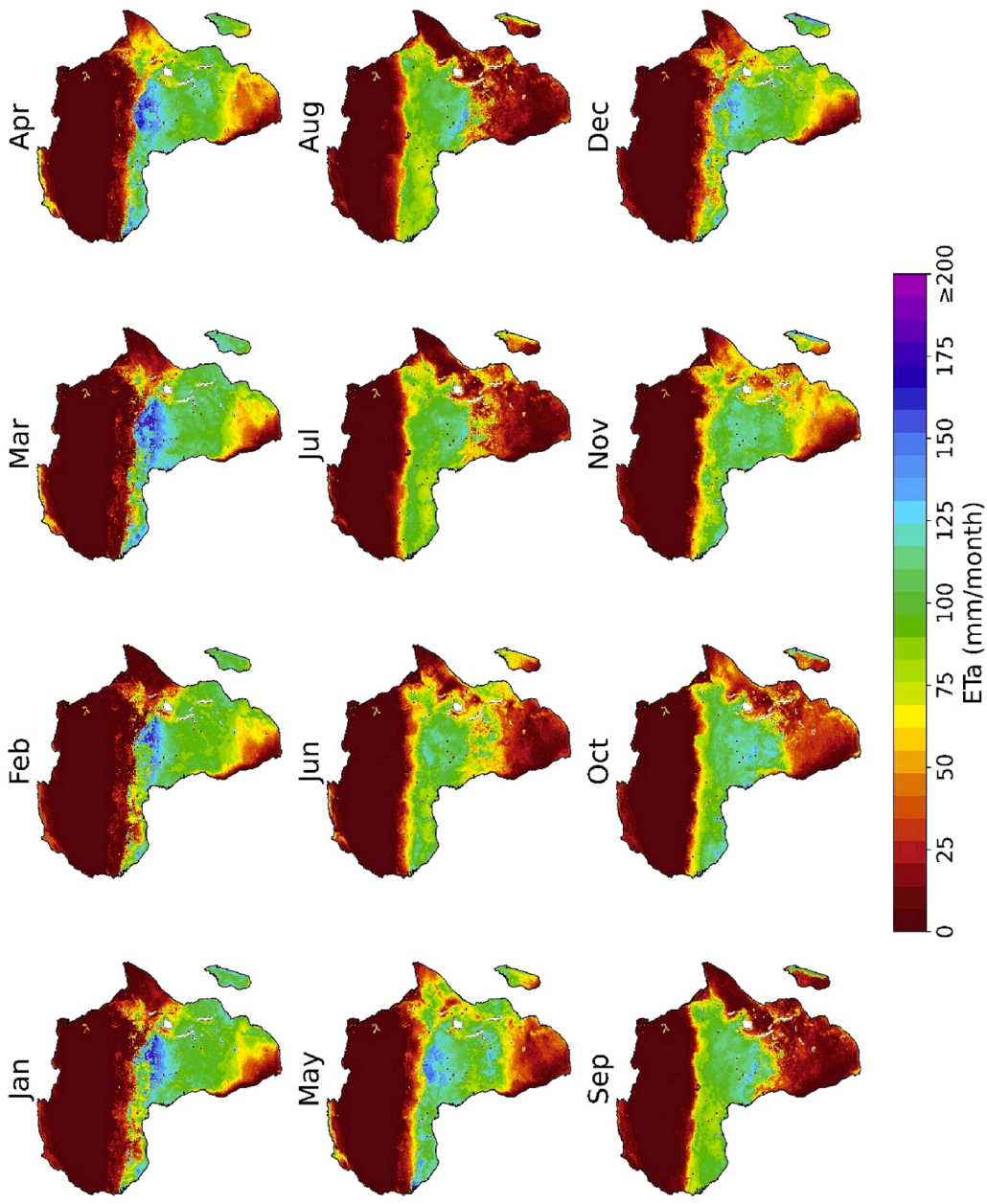

Figure A2. Monthly average ETa using GLEAMv4.1a for the period 2003–2021

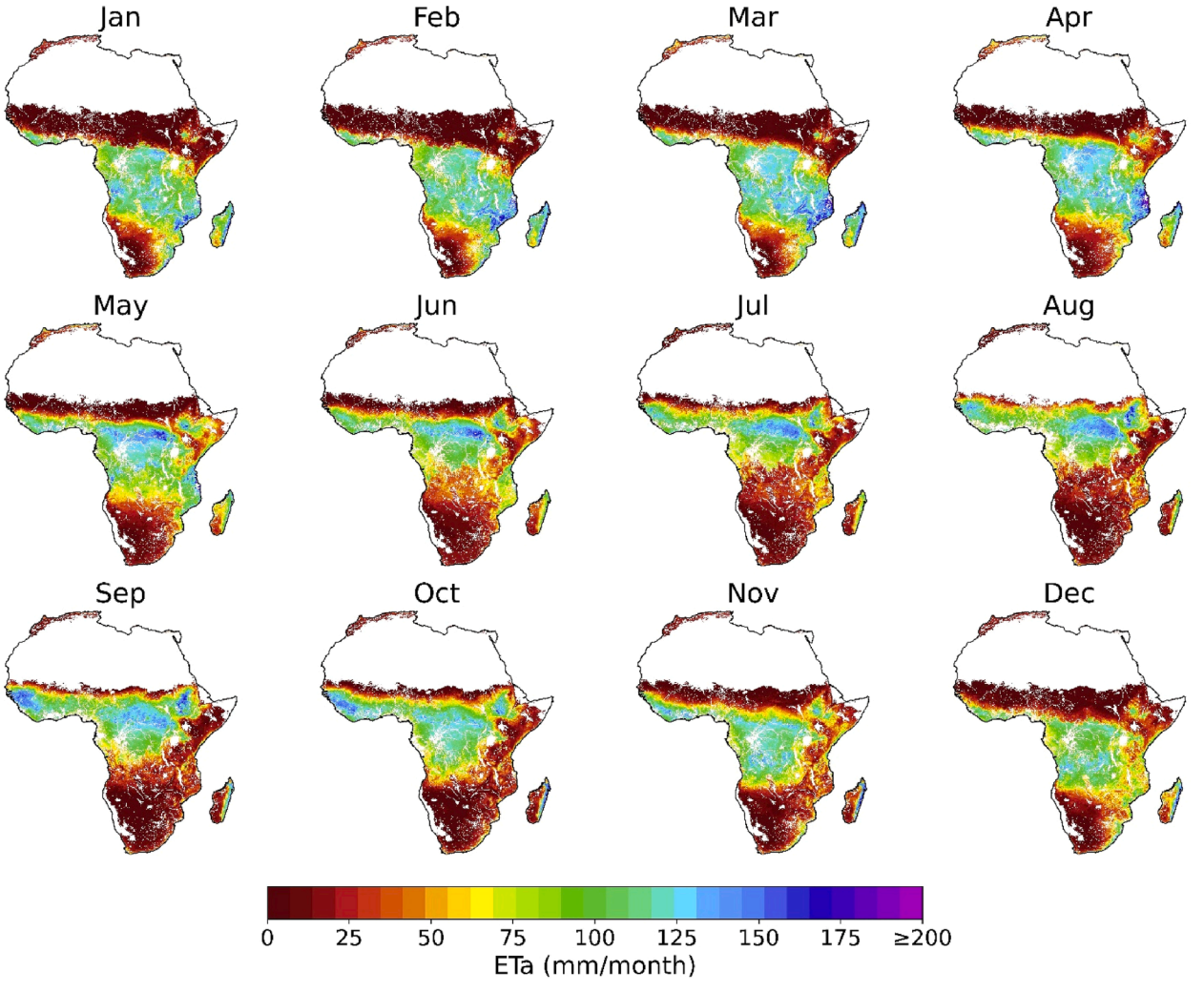

Figure A3. Monthly average ETa using MODIS v6.1 for the period 2003–2021. White spaces in the maps represent no data pixels in MODIS16 product

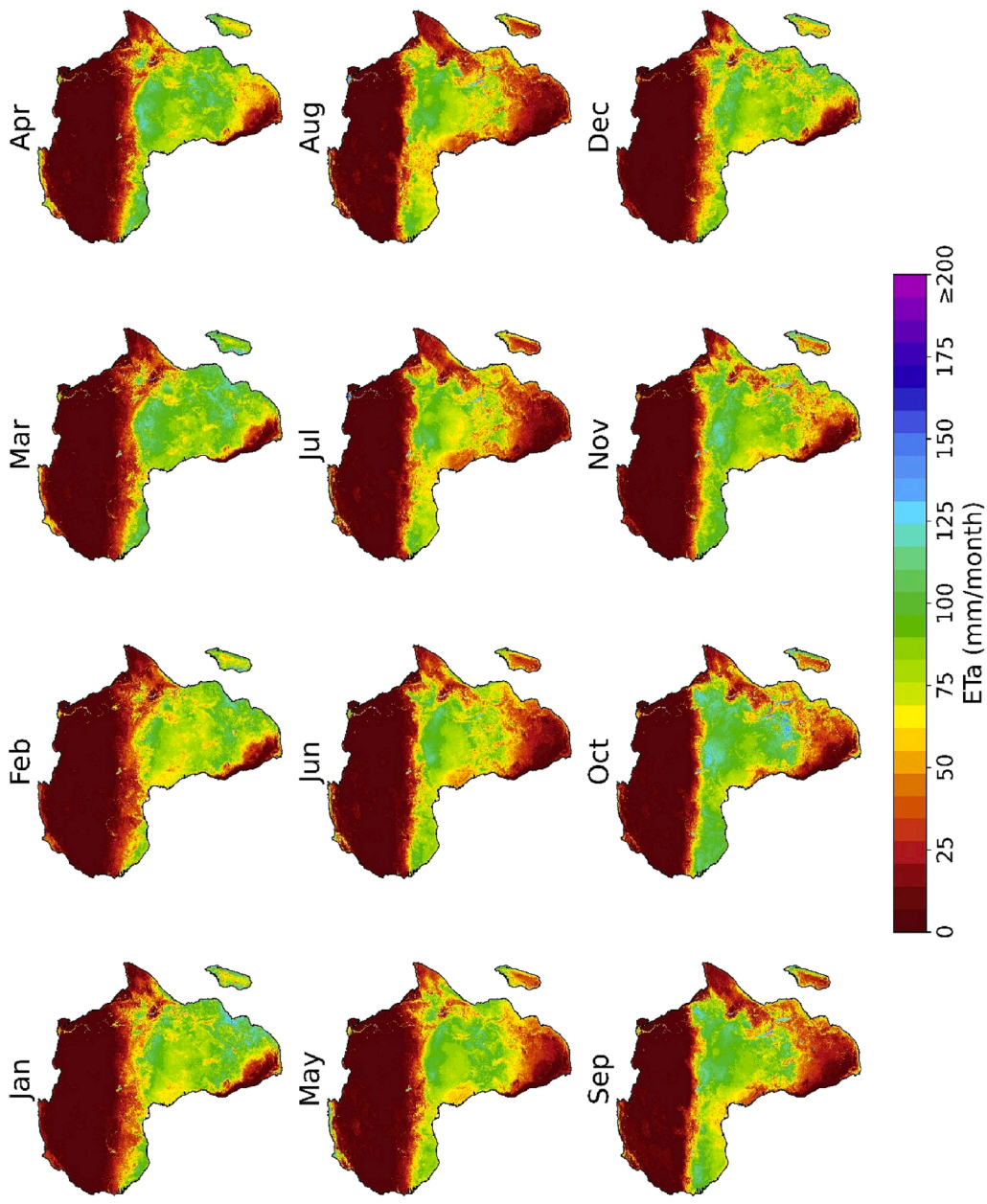

Figure A4. Monthly average ETa using SSEBop v6.1 for the period 2012–2021

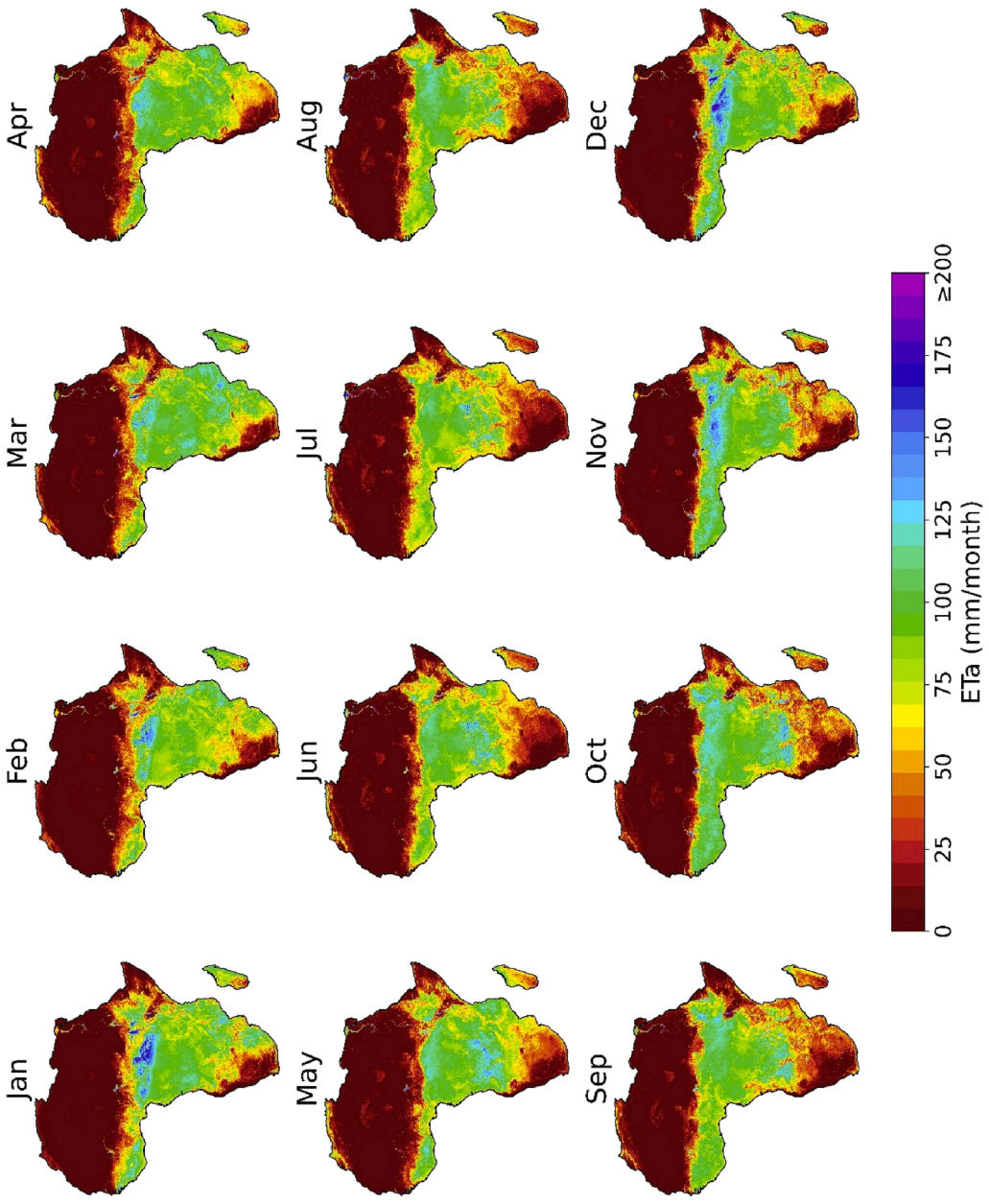

Figure A5. Monthly average ETa using WaPOR for the period 2018–2021

Appendix B. *ETa* comparison

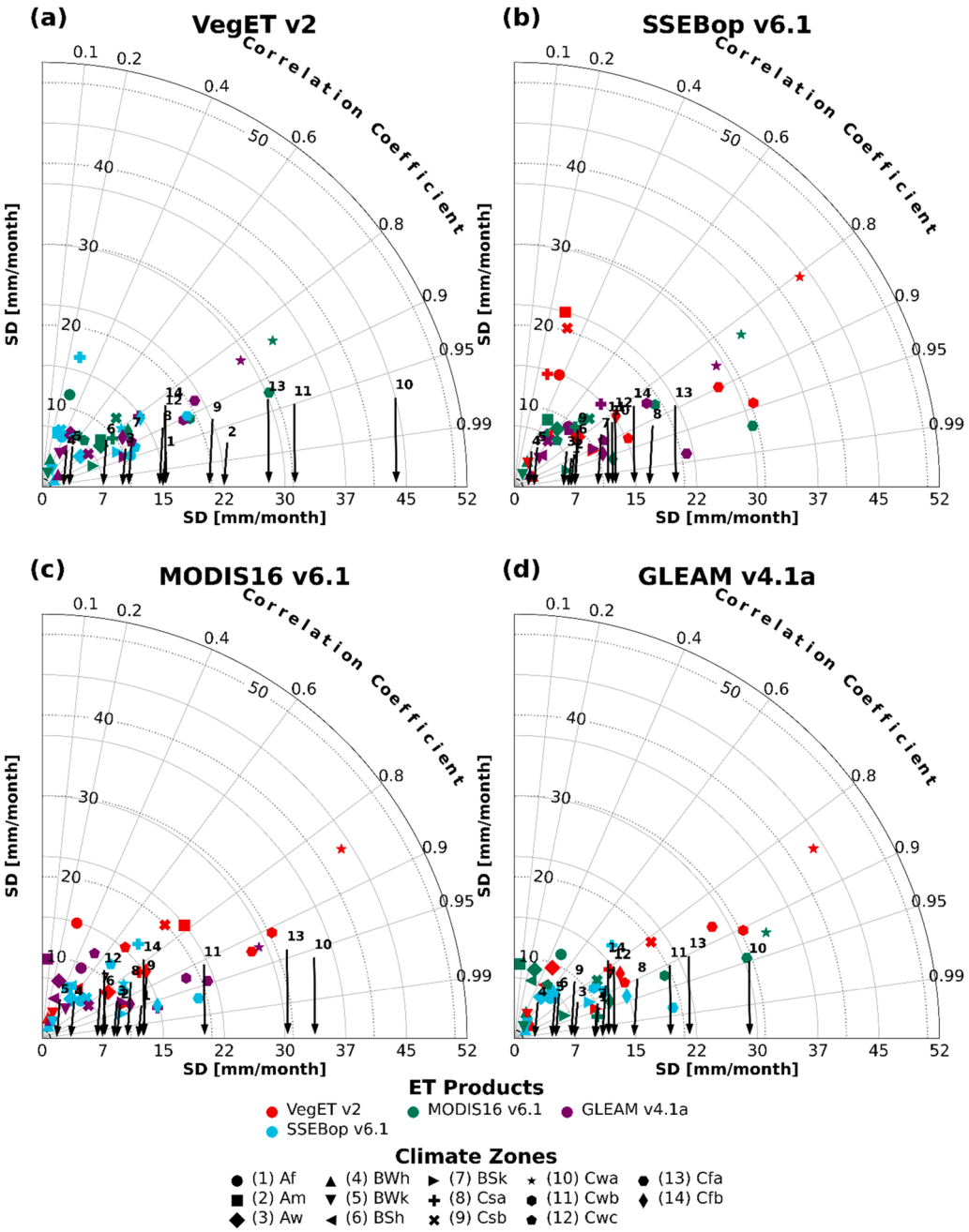

Figure B1. Taylor diagrams comparing actual evapotranspiration (*ETa*) estimates for various products (VegET v2, MODIS16 v6.1, WaPOR v3, and GLEAM v4.1a) across distinct climate zones for the period 2013–2021. The diagrams depict the standard deviation (SD) and correlation coefficient (R) of each product relative to the reference product. Reference points for individual climate zones are indicated by numbered arrows, corresponding to the following climate zones: (1) Af = Tropical, rainforest, (2) Am = Tropical, monsoon, (3) Aw = Tropical, savannah, (4) BSh = Arid, steppe, hot, (5) BSk = Arid, steppe, cold, (6) BWh = Arid, desert, hot, (7) BWk = Arid, desert, cold, (8) Cfa = Temperate, no dry season, hot summer, (9) Cfb = Temperate, no dry season, warm summer, (10) Csa = Temperate, dry summer, hot summer, (11) Csb = Temperate, dry summer, warm

summer, (12) Cwa = Temperate, dry winter, hot summer, (13) Cwb = Temperate, dry winter, warm summer, (14) Cwc = Temperate, dry winter, cold summer. The five panels (a-e) represent individual comparisons of each reference ET product against the others

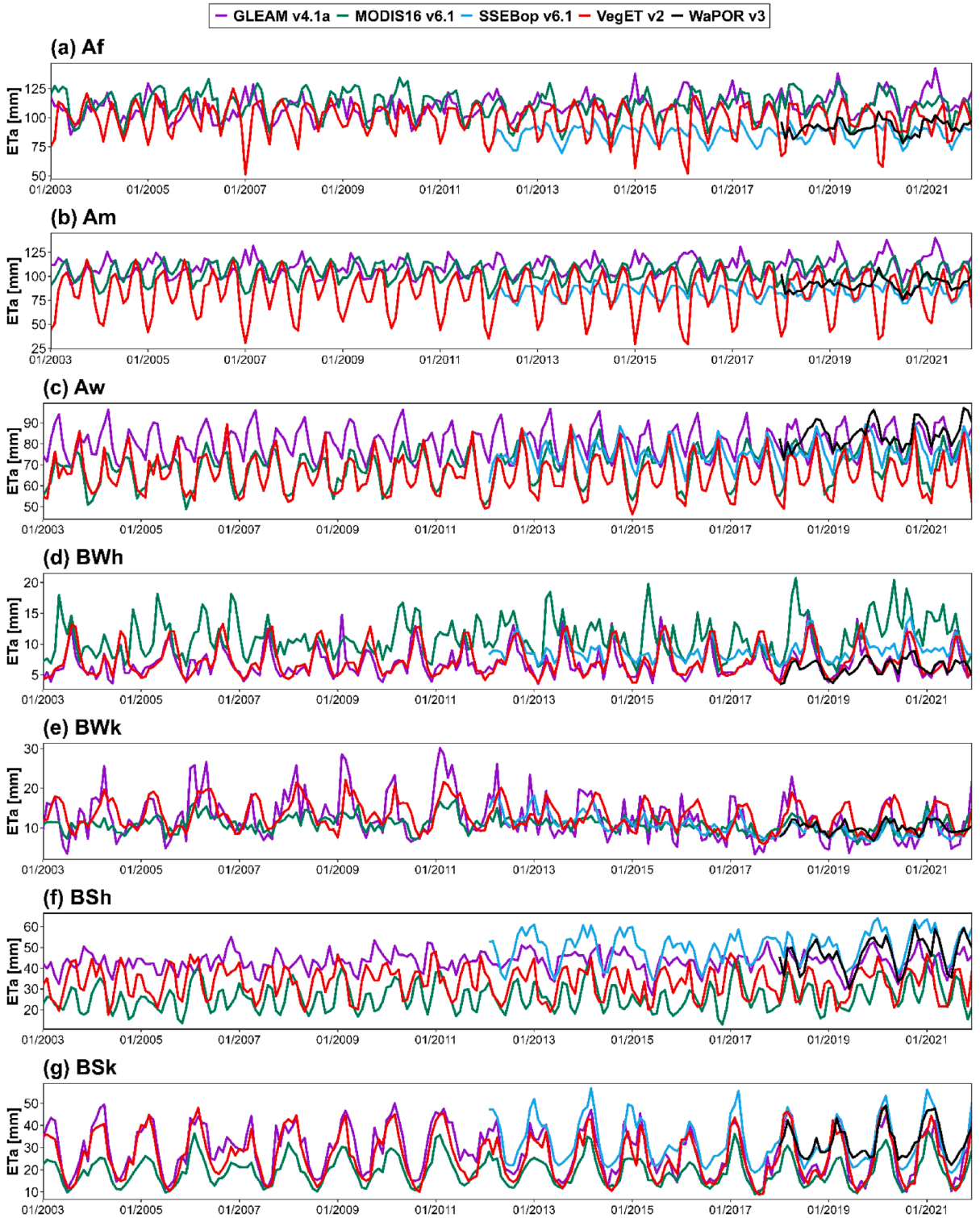

Figure B2. Temporal evolution of monthly actual evapotranspiration (*ETa*) estimates from the VegET v2 model and six remote sensing *ETa* products for the periods 2003–2021 (MODIS16 v6.1 and GLEAM v4.1a), 2018–2021 (WaPOR v3) and 2013–2021 (SSEBop v6.1) across major climate zones in Africa. Each panel shows the time series of *ETa* estimates for a specific climate zone, including tropical (a) rainforest (Af), (b) monsoon (Am), (c) savannah (Aw); arid (d) hot desert (BWh), (e) cold desert (BWk), (f) hot steppe (BSh), (g) cold steppe (BSk); temperate (h) dry summer, hot summer

(Csa), (i) dry summer, warm summer (Csb), (j) dry winter, hot summer (Cwa), (k) dry winter, warm summer (Cwb), (l) dry winter, cold summer (Cwc); and (m) no dry season, hot summer (Cfa), (n) no dry season, warm summer (Cfb)

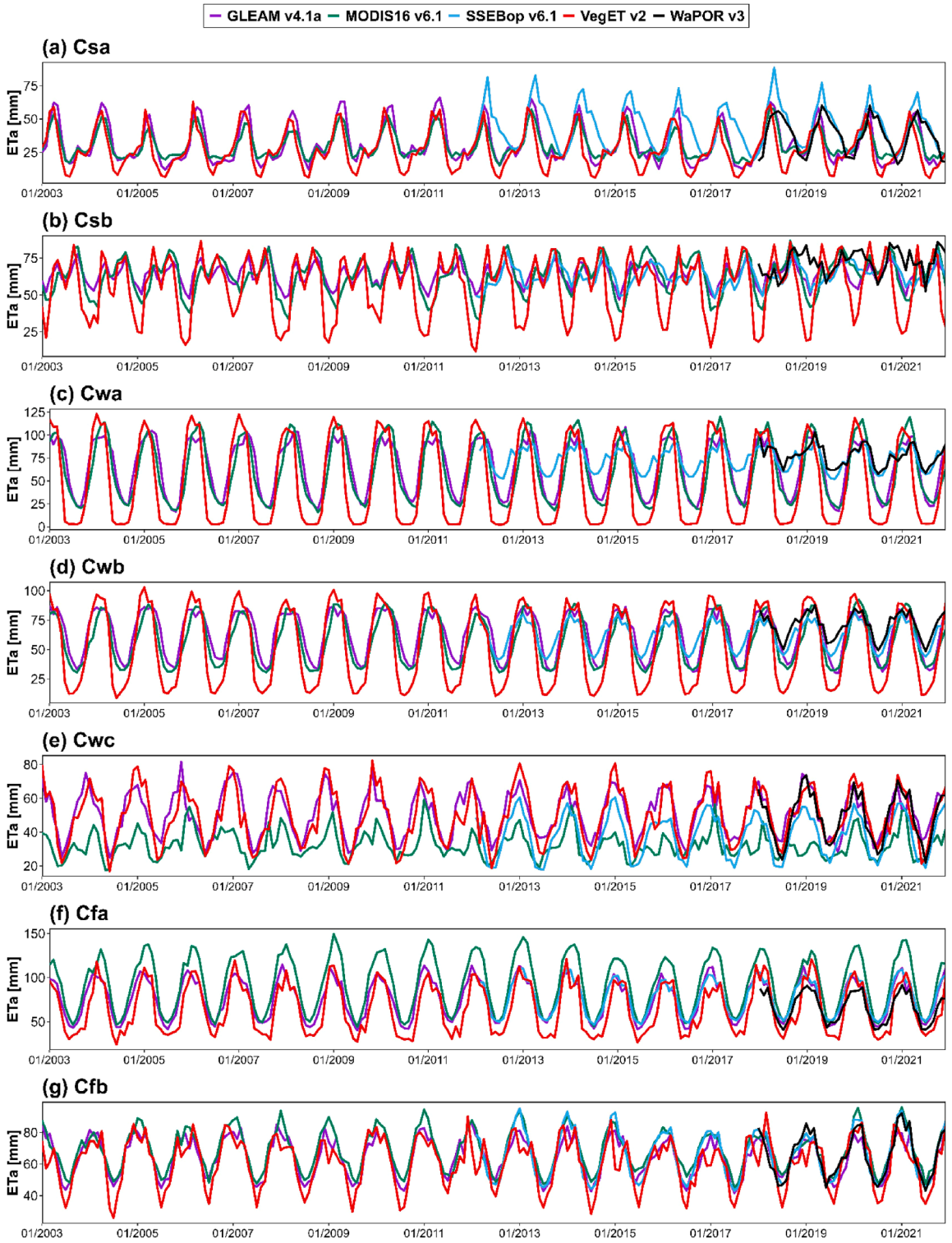

Figure B2. cont

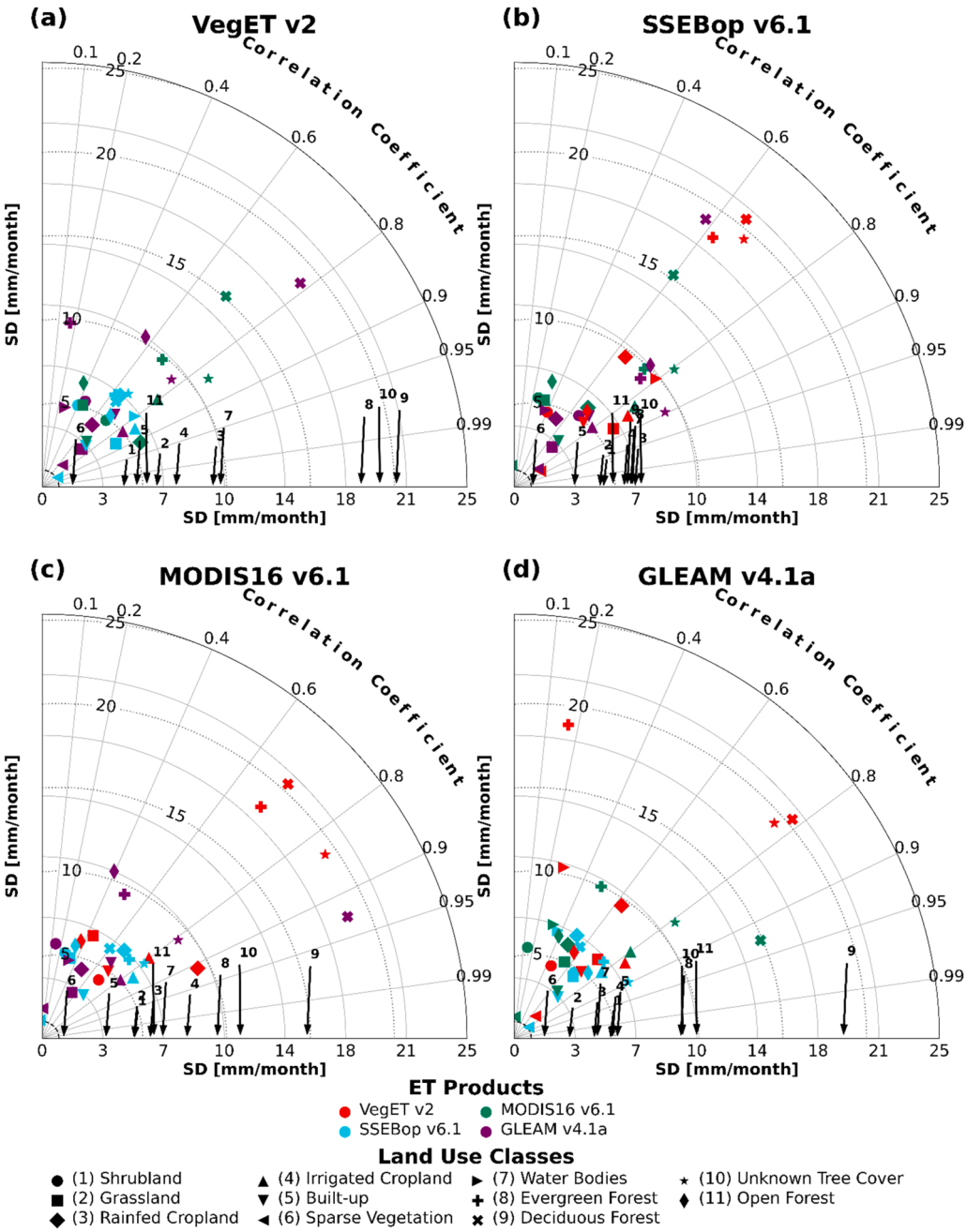

Figure B3. Taylor diagram comparing the performance of evapotranspiration (ET) products (VegET, SSEBop, MODIS16, WaPOR, and GLEAM) against VegET as the reference, for different land use classes across Africa for the period 2013–2021. The diagram evaluates the correlation coefficient and standard deviation of each product against VegET across the land use classes: Shrubland (Shr), Grassland (Gras), Rainfed/Fallow Cropland (RainC), Irrigated Cropland (IrriC), Built-up (Bup), Bare/Sparse Vegetation (BarV), Water Bodies (WaB), Evergreen Closed Forest (EvCF), Deciduous/Mixed Closed Forest (DMCF), Unknown Tree Cover (UTC), and Open Forest (OpF). The numbers on the x-axis correspond to different land use classes, with arrows indicating their respective positions. Each subplot represents a different ET product as the reference for comparison

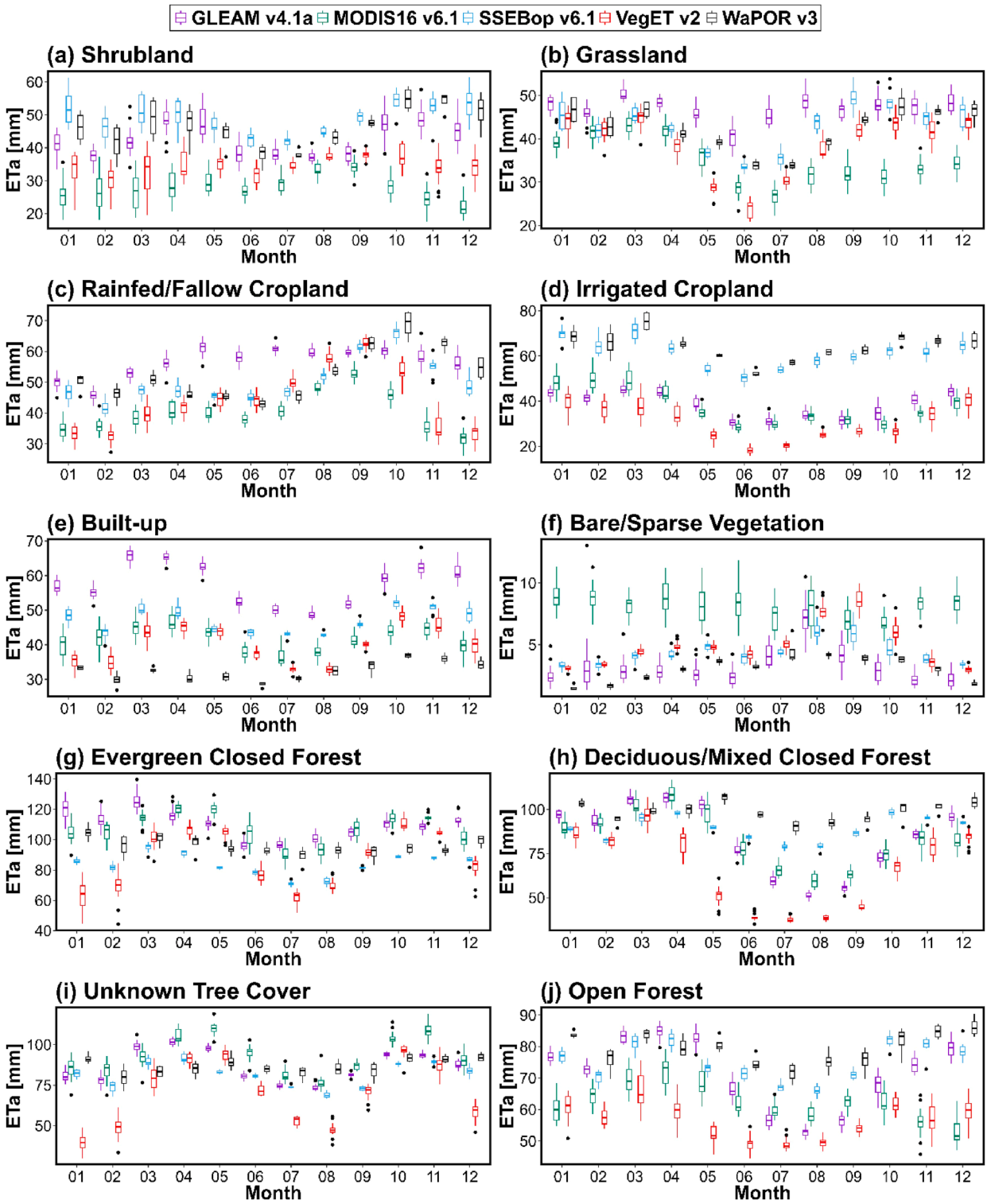

Figure B4. Monthly actual evapotranspiration (*ETa*) distribution across land use classes for Africa during the periods 2003–2021 (MODIS16 v6.1, and GLEAM v4.1a), 2018–2021 (WaPOR v3) and 2013–2021 (SSEBop v6.1). The box plots show the median, interquartile range, and outliers for each *ETa* products. The major land use classes include Shrubland, Grassland, Rainfed/Fallow Cropland, Irrigated Cropland, Built-up, Water Bodies, Evergreen Closed Forest, Deciduous/Mixed Closed Forest, Unknown Tree Cover, and Open Forest. The interquartile range shows the variability of each product's estimates, with outliers represented by black dots

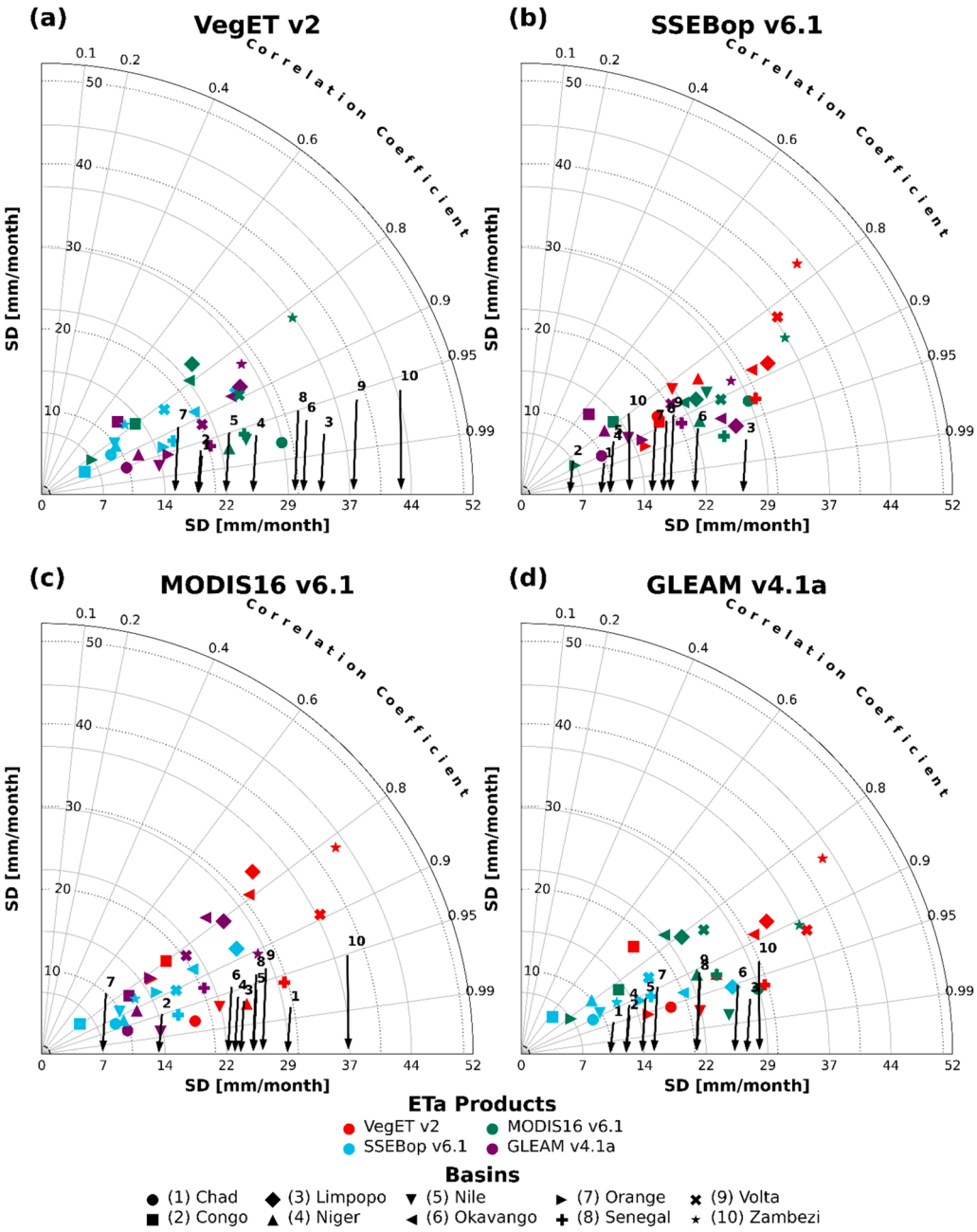

Figure B5. Taylor diagrams showing basin-specific comparisons of evapotranspiration (*ETa*) products (MODIS16 v6.1, WaPOR v3, and GLEAM v4.1a). Each panel presents a Taylor diagram with one *ETa* product as the reference dataset. The standard deviation (SD) and correlation coefficient are calculated for individual basins across Africa, represented by numbered markers

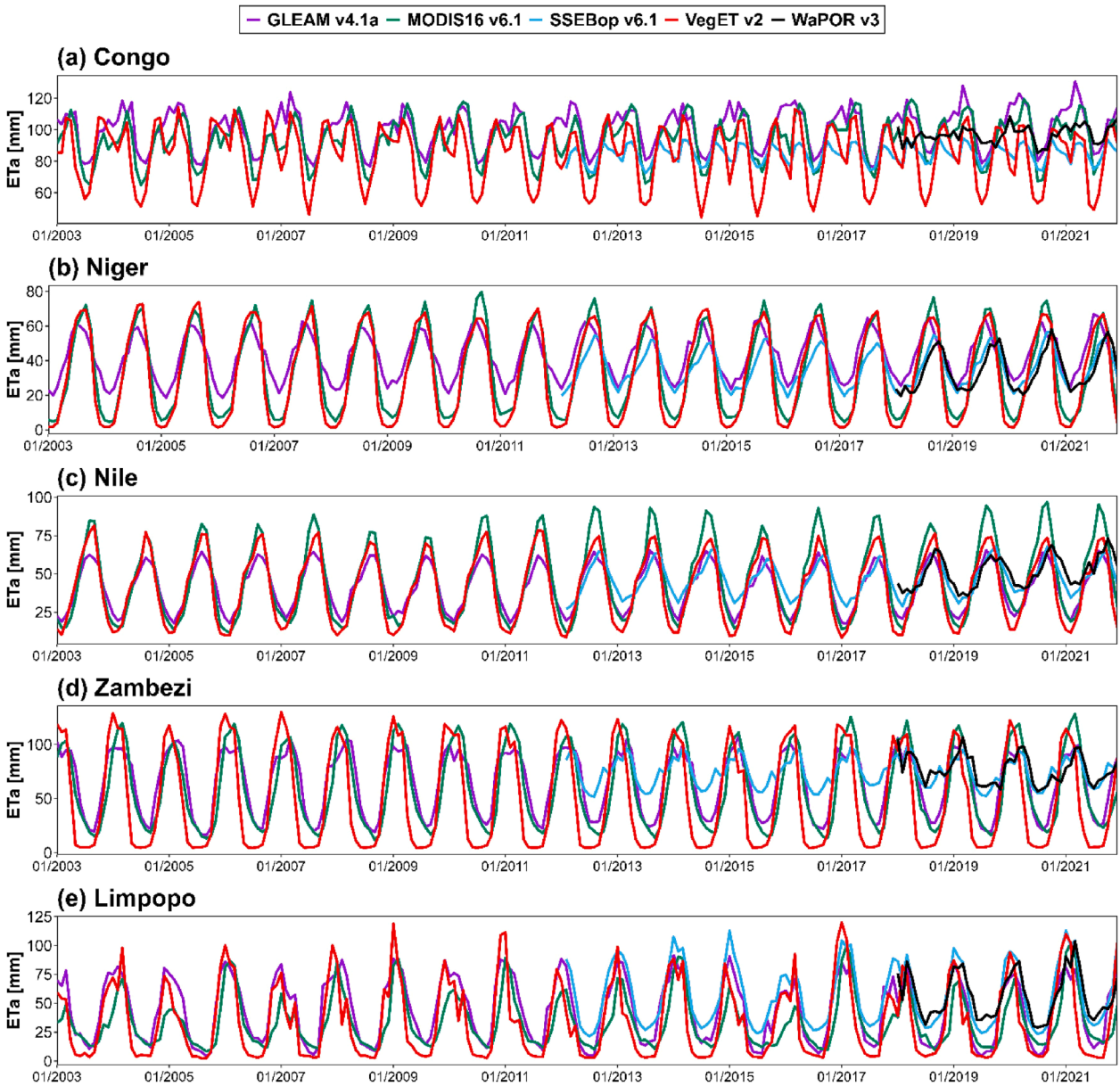

Figure B6. Temporal evolution of monthly *ETa* estimates from the VegET v2 model and six remote sensing *ETa* products for the periods 2003–2021 (MODIS16 v6.1, and GLEAM v4.1a), 2018–2021 (WaPOR v3) and 2013–2021 (SSEBop v6.1) across major basins in Africa

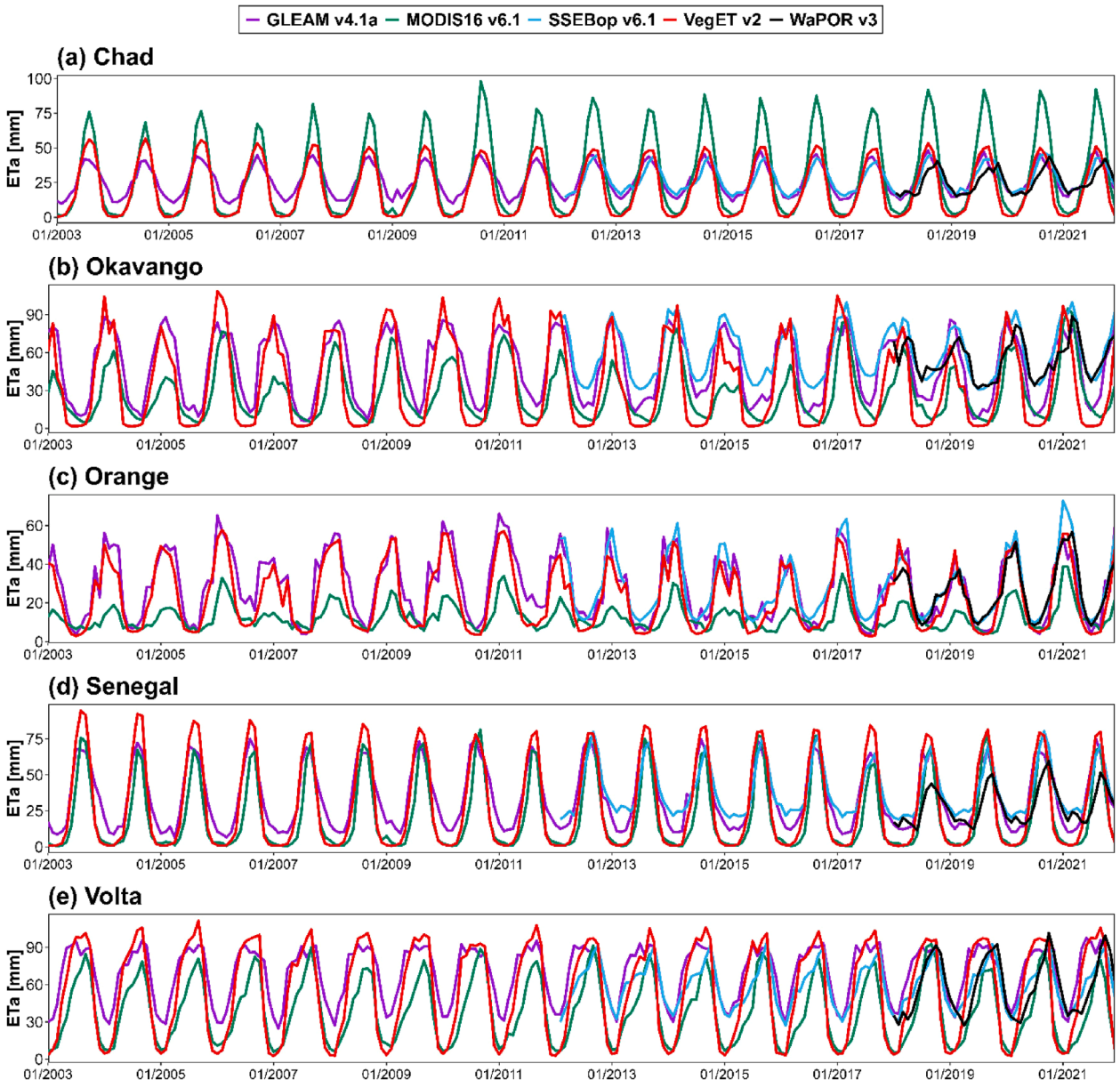

Figure B6. cont

Appendix C. Annual average Evapotranspiration Deficit Index (ETDI)

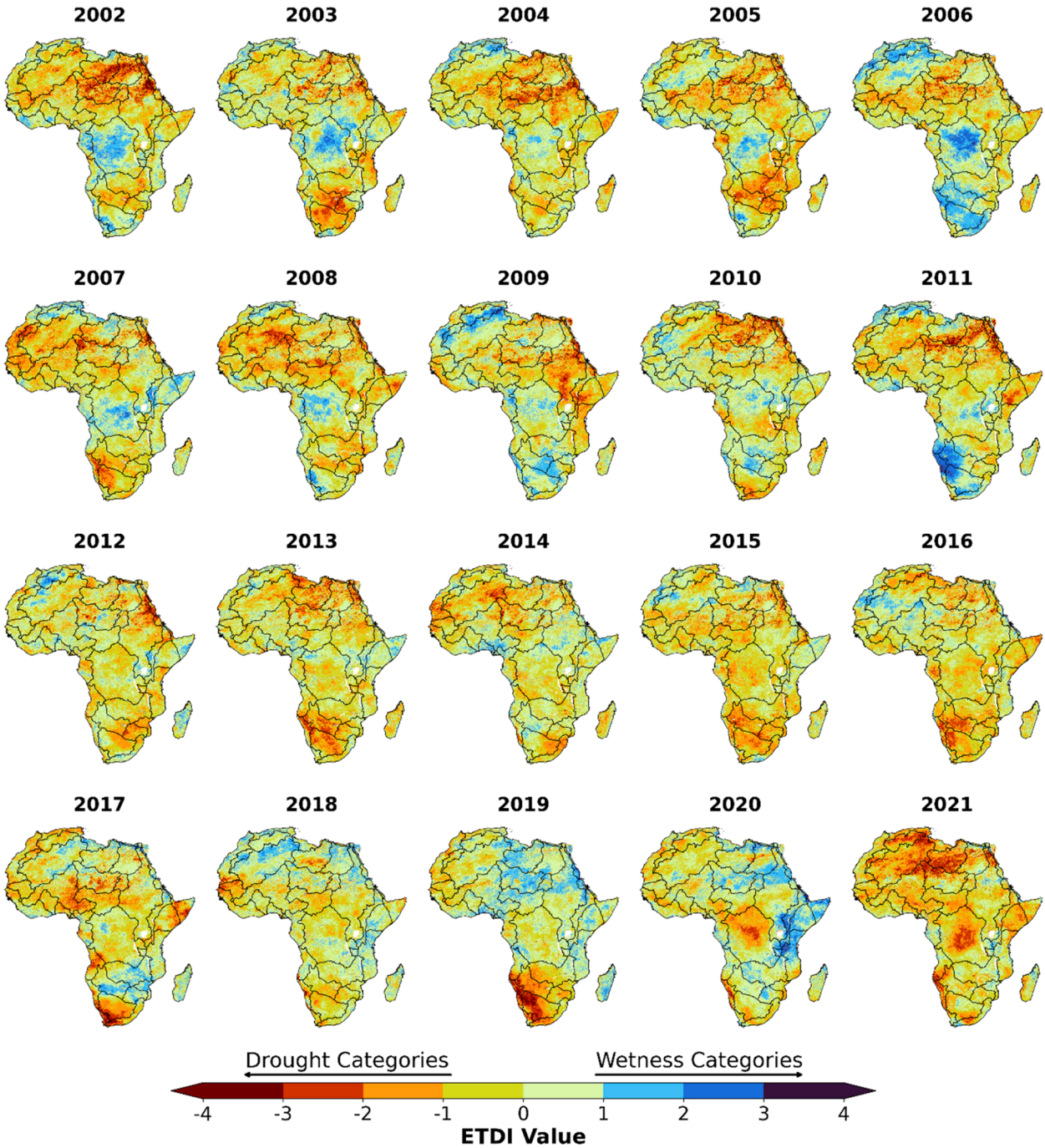

Figure C1. Annual average Evapotranspiration Deficit Index (ETDI) maps from 2002 to 2021 for Africa, generated using VegET *ETa* and GLEAM PET data. The color scale indicates the range of ETDI values, with negative values representing drought categories and positive values indicating wetness categories. These maps provide a visual representation of the spatial variability of drought and wetness conditions across the African continent over the 20-year period

Data Availability

Data will be made available on request.

References

Adeyeri, O.E., Ishola, K.A., 2021. Variability and trends of actual evapotranspiration over west africa: the role of environmental drivers. Agric. For. Meteorol. 308–309 (August), 108574. https://doi.org/10.1016/j.agrformet.2021.108574.

Akpoti, K., Antwi, E., Kabo-bah, A., 2016. Impacts of rainfall variability, land use and land cover change on stream flow of the Black Volta Basin, West Africa. Hydrology 3 (3), 26. https://doi.org/10.3390/hydrology3030026.

Akpoti, K., Velpuri, N., Mizukami, N., Kagone, S., Leh, M., Mekonnen, K., Owusu, A., Tinonetsana, P., Phiri, M., Madushanka, L., Perera, T., Paranamana, Prabhath, T., Parrish, G., Senay, G., Seid, A., 2024. Advancing Water Security in Africa with new high resolution discharge data. Sci. Data 1–38. https://doi.org/10.1038/s41597-024-04034-0.

Allen, R.G., Pereira, L.S., Raes, D., Smith, M., 1998. FAO Irrig. Drain. Pap. No. 56 - Crop Evapotranspiration (March).

Allen, R.G., Tasumi, M., Morse, A., Trezza, R., Wright, J.L., Bastiaanssen, W., Kramber, W., Lorite, I., Robison, C.W., 2007. Satellite-based energy balance for mapping evapotranspiration with internalized calibration (METRIC)—applications. J. Irrig. Drain. Eng. 133 (4), 395–406. https://doi.org/10.1061/(asce)0733-9437(2007)133:4(395).

Awada, H., Di Prima, S., Sirca, C., Giadrossich, F., Marras, S., Spano, D., Pirastru, M., 2022. A remote sensing and modeling integrated approach for constructing continuous time series of daily actual evapotranspiration. Agric. Water Manag. 260, 107320. https://doi.org/10.1016/j.agwat.2021.107320.

Awada, H., Sirca, C., Marras, S., Castellini, M., Spano, D., Pirastru, M., 2024. Modelling soil moisture and daily actual evapotranspiration: Integrating remote sensing surface energy balance and 1D Richards equation. Int. J. Appl. Earth Obs. Geoinf. 128, 103744. https://doi.org/10.1016/j.jag.2024.103744.

Bastiaanssen, W.G.M., 2000. SEBAL-based sensible and latent heat fluxes in the irrigated Gediz Basin, Turkey. J. Hydrol. 229 (1–2), 87–100. https://doi.org/10.1016/S0022-1694(99)00202-4.

Batjes, N.H. (2005). *ISRIC-WISE global data set of derived soil properties on a 0.5 by 0.5 ° grid (Version 3.0). Report 2005/08, ISRIC – World Soil Information, Wageningen* (with data set). https://doi.org/⟨https://www.isric.org/documents/document-type/isric-report-200508-isric-wise-global-data-set-derived-soil-properties-05⟩.

Bayat, B., Camacho, F., Nickeson, J., Cosh, M., Bolten, J., Vereecken, H., Montzka, C., 2021. Toward operational validation systems for global satellite-based terrestrial essential climate variables. Int. J. Appl. Earth Obs. Geoinf. 95 (September 2020), 102240. https://doi.org/10.1016/j.jag.2020.102240.

Beck, H.E., Zimmermann, N.E., McVicar, T.R., Vergopolan, N., Berg, A., Wood, E.F., 2018. Present and future Köppen-Geiger climate classification maps at 1-km resolution. Sci. Data 5, 180214. https://doi.org/10.1038/sdata.2018.214.

Blatchford, M.L., Mannaerts, C.M., Zeng, Y., Nouri, H., Karimi, P., 2019. Status of accuracy in remotely sensed and in-situ agricultural water productivity estimates: a review. Remote Sens. Environ. 234 (September), 111413. https://doi.org/10.1016/j.rse.2019.111413.

Biradar, C., Krishna, G., Govind, A., Nangia, V., Gamal, R., Zitouna, R., Jomaa, I., Mazahrih, N., Mansouri, A., El Meknassi, E., Haddad, M., Steduto, P., Swelam, A., Zaib, N. *Comparing Actual Evapotranspiration Retrieved Through Various Remote Sensing based Models with Ground Measured Data, Technical Report.International Center for Agricultural Research in the Dry Areas (ICARDA), Cairo, Egypt. ICARDA, 2 Port Said St, Victoria Square, Ismail El-Shaaer Building, Maadi, Cairo, Egypt*. https://hdl.handle.net/20.500.11766/66958.

Blatchford, M.L., Mannaerts, C.M., Njuki, S.M., Nouri, H., Zeng, Y., Pelgrum, H., Wonink, S., Karimi, P., 2020. Evaluation of WaPOR V2 evapotranspiration products across Africa. Hydrol. Process. 34 (15), 3200–3221. https://doi.org/10.1002/hyp.13791.

Bliefernicht, J., Berger, S., Salack, S., Guug, L., Hingerl, D.H., Heinzeller, M., Mauder, R., Steinbrecher, G., Waongo, E., Waongo, M., Steup, A.Y., Bossa, M., Quansah, A.A., Gessner, K., Knauer, A., Straub, R., Schönrock, R., Kunkel, E.C., Okogbue, A., Barry, Kunstmann. H., 2018. The WASCAL Hydrometeorological Observatory in the Sudan Savanna of Burkina Faso. Vadose Zone J. https://doi.org/10.2136/vzj2018.03.0065.

Bo, L., Qi, H., Wenpeng, W., Xiaofan, Z., Jianqing, Z., 2011. Variation of actual evapotranspiration and its impact on regional water resources in the Upper Reaches of the Yangtze River. Quat. Int. 244 (2), 185–193. https://doi.org/10.1016/j.quaint.2011.02.039.

Brubaker, K.L., Entekhabi, D., Eagleson, P.S., 1992. Estimation of continental precipitation recycling. J. Clim. 6 (6), 1077–1089. https://doi.org/10.1175/1520-0442(1993)006<1077:EOCPR>2.0.CO;2.

Chen, B., Black, T.A., Coops, N.C., Hilker, T., Trofymow, J.A., Morgenstern, K., 2009. Assessing tower flux footprint climatology and scaling between remotely sensed and eddy covariance measurements. Bound. -Layer. Meteorol. 130 (2), 137–167. https://doi.org/10.1007/s10546-008-9339-1.

Chiti, T., Certini, G., Grieco, E., Valentini, R., 2010. The role of soil in storing carbon in tropical rainforests: The case of Ankasa Park, Ghana. Plant and Soil 331 (1), 453–461. https://doi.org/10.1007/s11104-009-0265-x.

De Groen, M.M., Savenije, H.H., 2006. A monthly interception equation based on the statistical characteristics of daily rainfall. Water Resour. Res. 42 (12). https://doi.org/10.1029/2006WR005013.

Didan, K., 2015. MOD13Q1 MODIS/Terra Vegetation Indices 16-Day L3 Global 250m SIN Grid. NASA LP DAAC. https://doi.org/10.5067/MODIS/MOD13Q1.006.

Dile, Y.T., Ayana, E.K., Worqlul, A.W., Xie, H., Srinivasan, R., Lefore, N., You, L., Clarke, N., 2020. Evaluating satellite-based evapotranspiration estimates for hydrological applications in data-scarce regions: A case in Ethiopia. Sci. Total Environ. 743, 140702. https://doi.org/10.1016/j.scitotenv.2020.140702.

Dong, J., Dirmeyer, P.A., Lei, F., Anderson, M.C., Holmes, T.R.H., Hain, C., Crow, W.T., 2020. Soil Evaporation Stress Determines Soil Moisture-Evapotranspiration Coupling Strength in Land Surface Modeling. Geophys. Res. Lett. 47 (21), 1–11. https://doi.org/10.1029/2020GL090391.

Dong, J., Akbar, R., Short Gianotti, D.J., Feldman, A.F., Crow, W.T., Entekhabi, D., 2022. Can Surface soil moisture information identify evapotranspiration regime transitions? Geophys. Res. Lett. 49 (7). https://doi.org/10.1029/2021GL097697.

Drusch, M., Del Bello, U., Carlier, S., Colin, O., Fernandez, V., Gascon, F., Hoersch, B., Isola, C., Laberinti, P., Martimort, P., Meygret, A., Spoto, F., Sy, O., Marchese, F., Bargellini, P., 2012. Sentinel-2: ESA's optical high-resolution mission for GMES operational services. Remote Sens. Environ. 120, 25–36. https://doi.org/10.1016/j.rse.2011.11.026.

Dzikiti, S., Jovanovic, N.Z., Bugan, R.D., Ramoelo, A., Majozi, N.P., Nickless, A., Cho, M.A., Le Maitre, D.C., Ntshidi, Z., Pienaar, H.H., 2019. Comparison of two remote sensing models for estimating evapotranspiration: algorithm evaluation and application in seasonally arid ecosystems in South Africa. J. Arid Land 11 (4), 495–512. https://doi.org/10.1007/s40333-019-0098-2.

Eltahir, E.A., Bras, R.L., 1994. Precipitation recycling in the Amazon basin. Q. J. R. Meteorol. Soc. 120 (518), 861–880. https://doi.org/10.1002/qj.49712051806.

European Space Agency (ESA), 2021. Copernicus Sentinel-2 (processed by ESA), MSI Level-2A BOA Reflectance Product. Collection 1 [Data set]. European Space Agency. https://doi.org/10.5270/S2_-znk9xsj.

FAO & IHE Delft. (2019). *Technical report on the data quality of the WaPOR FAO database version 1.0*. Rome. 134 pp.

Fuentes, I., Vervoort, R.W., McPhee, J., 2024. Global evapotranspiration models and their performance at different spatial scales: contrasting a latitudinal gradient against global catchments. J. Hydrol. 628. https://doi.org/10.1016/j.jhydrol.2023.130477.

Funk, C., Peterson, P., Landsfeld, M., Pedreros, D., Verdin, J., Shukla, S., Husak, G., Rowland, J., Harrison, L., Hoell, A., Michaelsen, J., 2015. The climate hazards infrared precipitation with stations - a new environmental record for monitoring extremes. Sci. Data 2, 1–21. https://doi.org/10.1038/sdata.2015.66.

Gerrits, A.M.J., Pfister, L., Savenije, H.H.G., 2010. Spatial and temporal variability of canopy and forest floor interception in a beech forest. Hydrol. Process. 24 (21), 3011–3025. https://doi.org/10.1002/hyp.7712.

Glenn, E.P., Nagler, P.L., Huete, A.R., 2010. Vegetation index methods for estimating evapotranspiration by remote sensing. Surv. Geophys. 31 (6), 531–555. https://doi.org/10.1007/s10712-010-9102-2.

Glenn, E.P., Doody, T.M., Guerschman, J.P., Huete, A.R., King, E.A., Mcvicar, T.R., Van Dijk, A.I.J.M., Van Niel, T.G., Yebra, M., Zhang, Y., 2011. Actual evapotranspiration estimation by ground and remote sensing methods: the Australian experience. Hydrol. Process. 25 (26), 4103–4116. https://doi.org/10.1002/hyp.8391.

Glenn, E.P., Neale, C.M.U., Hunsaker, D.J., Nagler, P.L., 2011. Vegetation index-based crop coefficients to estimate evapotranspiration by remote sensing in agricultural and natural ecosystems. Hydrol. Process. 25 (26), 4050–4062. https://doi.org/10.1002/hyp.8392.

Gonzalez-Dugo, M.P., Neale, C.M.U., Mateos, L., Kustas, W.P., Prueger, J.H., Anderson, M.C., Li, F., 2009. A comparison of operational remote sensing-based models for estimating crop evapotranspiration. Agric. For. Meteorol. 149 (11), 1843–1853. https://doi.org/10.1016/j.agrformet.2009.06.012.

Guerschman, J.P., McVicar, T.R., Vleeshower, J., Van Niel, T.G., Peña-Arancibia, J.L., Chen, Y., 2022. Estimating actual evapotranspiration at field-to-continent scales by calibrating the CMRSET algorithm with MODIS, VIIRS, Landsat and Sentinel-2 data. J. Hydrol. 605 (August 2021). https://doi.org/10.1016/j.jhydrol.2021.127318.

Ha, W., Kolb, T.E., Springer, A.E., Dore, S., O'Donnell, F.C., Martinez Morales, R., Masek Lopez, S., Koch, G.W., 2015. Evapotranspiration comparisons between eddy covariance measurements and meteorological and remote-sensing-based models in disturbed ponderosa pine forests. Ecohydrology 8 (7), 1335–1350. https://doi.org/10.1002/eco.1586.

Hansen, M.C., DeFries, R.S., Townshend, J.R.G., Carroll, M., Dimiceli, C., Sohlberg, R.A., 2003. Global percent tree cover at a spatial resolution of 500 meters: First results of the MODIS vegetation continuous fields algorithm. Earth Interact. 7 (10), 1–15. https://doi.org/10.1175/1087-3562(2003)007<0001:gptcaa>2.0.co;2.

Hingerl, L., Bliefernicht, J., Guug, S., Sy, S., Neidl, F., Jagdhuber, T., Kunstmann, H., 2025. Comparative analysis of land-atmosphere interactions across three contrasting ecosystems in the West Sudanian Savanna. J. Hydrol.: Reg. Stud. 61, 102751. https://doi.org/10.1016/j.ejrh.2025.102751.

Hobbins, M., Dewes, C., Jansma, T., 2023. Global reference evapotranspiration for food-security monitoring (ver. 2.0, October 2023): U.S. Geological Survey data release. https://doi.org/10.5066/P9IIQMV1.

Hssaine, B.A., Merlin, O., Rafi, Z., Ezzahar, J., Jarlan, L., Khabba, S., Er-Raki, S., 2018. Calibrating an evapotranspiration model using radiometric surface temperature, vegetation cover fraction and near-surface soil moisture data. Agric. For. Meteorol. 256–257 (March), 104–115. https://doi.org/10.1016/j.agrformet.2018.02.033.

Huang, D., Wang, J., Khayatnezhad, M., 2021. Estimation of Actual Evapotranspiration Using Soil Moisture Balance and Remote Sensing. Iran. J. Sci. Technol. - Trans. Civ. Eng. 45 (4), 2779–2786. https://doi.org/10.1007/s40996-020-00575-7.

Hulley, G., Hook, S., 2018. VIIRS/NPP Land Surface Temperature and Emissivity Daily L3 Global 1km SIN Grid Day V001 [Data set]. NASA EOSDIS Land Process. Distrib. Act. Arch. Cent. https://doi.org/10.5067/VIIRS/VNP21A1D.001.

Jin, X., Schaepman, M.E., Clevers, J.G.P.W., Su, Z.B., 2009. Impact and consequences of evapotranspiration changes on water resources availability in the arid Zhangye Basin, China. Int. J. Remote Sens. 30 (12), 3223–3238. https://doi.org/10.1080/01431160802559053.

Jung, H.C., Getirana, A., Arsenault, K.R., Holmes, T.R.H., McNally, A., 2019. Uncertainties in Evapotranspiration Estimates over West Africa. Remote Sens. 11 (8), 892. https://doi.org/10.3390/rs11080892.

Justice, C.O., Román, M.O., Csiszar, I., Vermote, E.F., Wolfe, R.E., Hook, S.J., Friedl, M., Wang, Z., Schaaf, C.B., Miura, T., Tschudi, M., Riggs, G., Hall, D.K., Lyapustin, A.I., Devadiga, S., Davidson, C., Masuoka, E.J., 2013. Land and cryosphere products from Suomi NPP VIIRS: Overview and status. J. Geophys. Res. Atmospheres 118 (17), 9753–9765. https://doi.org/10.1002/jgrd.50771.

Katul, G.G., Oren, R., Manzoni, S., Higgins, C., Parlange, M.B., 2012. Evapotranspiration: A process driving mass transport and energy exchange in the soil-plant-atmosphere-climate system. Rev. Geophys. 50 (3). https://doi.org/10.1029/2011RG000366.

Kiptala, J.K., Mohamed, Y., Mul, M.L., Van Der Zaag, P., 2013. Mapping evapotranspiration trends using MODIS and SEBAL model in a data scarce and heterogeneous landscape in Eastern Africa. Water Resour. Res. 49 (12), 8495–8510. https://doi.org/10.1002/2013WR014240.

Lan, X., Liu, Z., Chen, X., Lin, K., Cheng, L., 2021. Trade-off between carbon sequestration and water loss for vegetation greening in China. Agric. Ecosyst. Environ. 319 (June), 107522. https://doi.org/10.1016/j.agee.2021.107522.

Liu, Q., Liang, L., Mcvicar, T.R., Wang, X., Li, C., Xia, X., 2024. Globally assessing how evapotranspiration feedbacks govern the impacts of multi-year droughts. J. Hydrol. 641 (March), 131852. https://doi.org/10.1016/j.jhydrol.2024.131852.

Majozi, N.P., Mannaerts, C.M., Ramoelo, A., Mathieu, R., Mudau, A.E., Verhoef, W., 2017. An intercomparison of satellite-based daily evapotranspiration estimates under different eco-climatic regions in South Africa. Remote Sens. 9 (4), 1–21. https://doi.org/10.3390/rs9040307.

Marshall, M., Tu, K., Funk, C., Michaelsen, J., Williams, P., Williams, C., Ardö, J., Boucher, M., Cappelaere, B., De Grandcourt, A., Nickless, A., Nouvellon, Y., Scholes, R., Kutsch, W., 2013. Improving operational land surface model canopy evapotranspiration in Africa using a direct remote sensing approach. Hydrol. Earth Syst. Sci. 17 (3), 1079–1091. https://doi.org/10.5194/hess-17-1079-2013.

Martens, B., Miralles, D.G., Lievens, H., Van Der Schalie, R., De Jeu, R.A.M., Fernández-Prieto, D., Beck, H.E., Dorigo, W.A., Verhoest, N.E.C., 2017. GLEAM v3: Satellite-based land evaporation and root-zone soil moisture. Geosci. Model Dev. 10 (5), 1903–1925. https://doi.org/10.5194/gmd-10-1903-2017.

Masih, I., Maskey, S., Mussá, F.E.F., Trambauer, P., 2014. A review of droughts on the African continent: A geospatial and long-term perspective. Hydrol. Earth Syst. Sci. 18 (9), 3635–3649. https://doi.org/10.5194/hess-18-3635-2014.

Mekonnen, K., Manohar, N., Leh, M., Akpoti, K., Owusu, A., Tinonetsana, P., Hamouda, T., Ghansah, B., 2023. Accuracy of satellite and reanalysis rainfall estimates over Africa: A multi-scale assessment of eight products for continental applications. J. Hydrol. Reg. Stud. 49 (April), 101514. https://doi.org/10.1016/j.ejrh.2023.101514.

Merbold, L., Ardö, J., Arneth, A., Scholes, R.J., Nouvellon, Y., De Grandcourt, A., Archibald, S., Bonnefond, J.M., Boulain, N., Brueggemann, N., Bruemmer, C., Cappelaere, B., Ceschia, E., El-Khidir, H.A.M., El-Tahir, B.A., Falk, U., Lloyd, J., Kergoat, L., Le Dantec, V., Kutsch, W.L., 2009. Precipitation as driver of carbon fluxes in 11 African ecosystems. Biogeosciences 6, 1027–1041. https://doi.org/10.5194/bg-6-1027-2009.

Miralles, D.G., Holmes, T.R.H., De Jeu, R.A.M., Gash, J.H., Meesters, A.G.C.A., Dolman, A.J., 2011. Global land-surface evaporation estimated from satellite-based observations. Hydrol. Earth Syst. Sci. 15 (2), 453–469. https://doi.org/10.5194/hess-15-453-2011.

Mizukami, N., Clark, M.P., Sampson, K., Nijssen, B., Mao, Y., Mcmillan, H., Viger, R.J., Markstrom, S.L., Hay, L.E., Woods, R., Arnold, J.R., Brekke, L.D., 2016. mizuRoute version 1: a river network routing tool for a continental domain water resources applications. Geosci. Model Dev. 9 (6), 2223–2238. https://doi.org/10.5194/gmd-9-2223-2016.

Mu, Q., Zhao, M., Running, S.W., 2011. Improvements to a MODIS global terrestrial evapotranspiration algorithm. Remote Sens. Environ. 115 (8), 1781–1800. https://doi.org/10.1016/j.rse.2011.02.019.

Nadolski, L., Bliefernicht, J., Petrovic, D., Rauch, M., Sy, S., Guug, S., Steinbrecher, R., Neidl, F., Hingerl, L., Kunstmann, H., 2024. Exploring and closing the energy balance of eddy covariance measurements along a land use gradient in the West African Sudanian savanna. Front. Water 6. https://doi.org/10.3389/frwa.2024.1393884.

Nagappan, M., Gopalakrishnan, V., Alagappan, M., 2020. Prediction of reference evapotranspiration for irrigation scheduling using machine learning. Hydrol. Sci. J. 65 (16), 2669–2677. https://doi.org/10.1080/02626667.2020.1830996.

Narasimhan, B., Srinivasan, R., 2005. Development and evaluation of Soil Moisture Deficit Index (SMDI) and Evapotranspiration Deficit Index (ETDI) for agricultural drought monitoring. Agric. For. Meteorol. 133 (1–4), 69–88. https://doi.org/10.1016/j.agrformet.2005.07.012.

Nicholson, S.E., 2014. A detailed look at the recent drought situation in the Greater Horn of Africa. J. Arid Environ. 103, 71–79. https://doi.org/10.1016/j.jaridenv.2013.12.003.

Oki, T., Kanae, S., 2006. Global Hydrological Cycles and World Water Resources. Science 313, 1068–1072. https://doi.org/10.1126/science.1128845.

Owusu, A., Kagone, S., Leh, M., Velpuri, N.M., Gumma, M.K., Ghansah, B., Mohammed, I., 2024. A framework for disaggregating remote-sensing cropland into rainfed and irrigated classes at continental scale. Int. J. Appl. Earth Obs. Geoinf. 126, 103607. https://doi.org/10.1016/j.jag.2023.103607.

Pôças, I., Calera, A., Campos, I., Cunha, M., 2020. Remote sensing for estimating and mapping single and basal crop coefficientes: A review on spectral vegetation indices approaches. In: Agricultural Water Management, 233. Elsevier B.V. https://doi.org/10.1016/j.agwat.2020.106081

Pokorny, J., 2009. Evapotranspiration. In: Likens, G.E. (Ed.), Encyclopedia of inland waters, 2. Academic Press, pp. 292–303. https://doi.org/10.1016/B978-0-12-409548-9.11182-0.

Pool, S., Francés, F., Garcia-Prats, A., Pulido-Velazquez, M., Sanchis-Ibor, C., Schirmer, M., Yang, H., Jiménez-Martínez, J., 2021. From flood to drip irrigation under climate change: impacts on evapotranspiration and groundwater recharge in the mediterranean region of Valencia (Spain). Earth'S. Future 9 (5), 1–20. https://doi.org/10.1029/2020EF001859.

Senay, G.B., 2008. Modeling landscape evapotranspiration by integrating land surface phenology and a water balance algorithm. Algorithms 1 (2), 52–68. https://doi.org/10.3390/a1020052.

Senay, G.B., Leake, S., Nagler, P.L., Artan, G., Dickinson, J., Cordova, J.T., Glenn, E.P., 2011. Estimating basin scale evapotranspiration (ET) by water balance and remote sensing methods. Hydrol. Process. 25 (26), 4037–4049. https://doi.org/10.1002/hyp.8379.

Senay, G.B., Bohms, S., Singh, R.K., Gowda, P.H., Velpuri, N.M., Alemu, H., Verdin, J.P., 2013. Operational evapotranspiration mapping using remote sensing and weather datasets: a new parameterization for the SSEB Approach. J. Am. Water Resour. Assoc. 49 (3), 577–591. https://doi.org/10.1111/jawr.12057.

Senay, G.B., Friedrichs, M., Morton, C., Parrish, G.E.L., Schauer, M., Khand, K., Kagone, S., Boiko, O., Huntington, J., 2022. Mapping actual evapotranspiration using Landsat for the conterminous United States: Google Earth Engine implementation and assessment of the SSEBop model. Remote Sens. Environ. 275 (March 2021), 113011. https://doi.org/10.1016/j.rse.2022.113011.

Senay, G.B., Kagone, S., Parrish, G.E.L., Khand, K., Boiko, O., Velpuri, N.M., 2023. Improvements and evaluation of the agro-hydrologic VegET model for large-area water budget analysis and drought monitoring. Hydrology 10 (8). https://doi.org/10.3390/hydrology10080168.

Sun, Z., Gebremichael, M., Ardö, J., Nickless, A., Caquet, B., Merboldh, L., Kutschi, W., 2012. Estimation of daily evapotranspiration over Africa using MODIS/Terra and SEVIRI/MSG data. Atmos. Res. 112, 35–44. https://doi.org/10.1016/j.atmosres.2012.04.005.

Tagesson, T., Fensholt, R., Guiro, I., Rasmussen, M.O., Huber, S., Mbow, C., Ardö, J., 2015. Ecosystem properties of semiarid savanna grassland in West Africa and its relationship with environmental variability. Glob. Change Biol. 21 (1), 250–264. https://doi.org/10.1111/gcb.12734.

Tagesson, T., Fensholt, R., Cappelaere, B., Mougin, E., Horion, S., Kergoat, L., Ardö, J., 2016. Spatiotemporal variability in carbon exchange fluxes across the Sahel. Agric. For. Meteorol. 226, 108–118. https://doi.org/10.1016/j.agrformet.2016.05.013.

Tang, R., Peng, Z., Liu, M., Li, Z.L., Jiang, Y., Hu, Y., Huang, L., Wang, Y., Wang, J., Jia, L., Zheng, C., Zhang, Y., Zhang, K., Yao, Y., Chen, X., Xiong, Y., Zeng, Z., Fisher, J.B., 2024. Spatial-temporal patterns of land surface evapotranspiration from global products. Remote Sens. Environ. 304 (May 2023), 114066. https://doi.org/10.1016/j.rse.2024.114066.

Taylor, K.E., 2001. Summarizing multiple aspects of model performance in a single diagram. J. Geophys. Res. Atmospheres 106 (D7), 7183–7192. https://doi.org/10.1029/2000JD900719.

Te Wierik, S.A., Keune, J., Miralles, D.G., Gupta, J., Artzy-Randrup, Y.A., Gimeno, L., Nieto, R., Cammeraat, L.H., 2022. The Contribution of Transpiration to Precipitation Over African Watersheds. Water Resour. Res. 58 (11). https://doi.org/10.1029/2021WR031721.

Thompson, J.R., Green, A.J., Kingston, D.G., 2014. Potential evapotranspiration-related uncertainty in climate change impacts on river flow: An assessment for the Mekong River basin. J. Hydrol. 510, 259–279. https://doi.org/10.1016/j.jhydrol.2013.12.010.

Trambauer, P., Maskey, S., Winsemius, H., Werner, M., Uhlenbrook, S., 2013. A review of continental scale hydrological models and their suitability for drought forecasting in (sub-Saharan) Africa. Phys. Chem. Earth 66, 16–26. https://doi.org/10.1016/j.pce.2013.07.003.

Trambauer, P., Dutra, E., Maskey, S., Werner, M., Pappenberger, F., Van Beek, L.P.H., Uhlenbrook, S., 2014. Comparison of different evaporation estimates over the African continent. Hydrol. Earth Syst. Sci. 18 (1), 193–212. https://doi.org/10.5194/hess-18-193-2014.

Valentini, R., Giacomo Nicolini, Paolo Stefani, Agnès De Grandcourt, Silvio, Stivanello., 2016. FLUXNET FLUXNET2015 GH-Ank Ankasa Dataset. Inf. Orig. Res. Organ.(s). https://doi.org/10.18140/FLX/1440229.

Van Der Ent, R.J., Savenije, H.H.G., Schaefli, B., Steele-Dunne, S.C., 2010. Origin and fate of atmospheric moisture over continents. Water Resour. Res. 46 (9), 1–12. https://doi.org/10.1029/2010WR009127.

Velpuri, N.M., Senay, G.B., Singh, R.K., Bohms, S., Verdin, J.P., 2013. A comprehensive evaluation of two MODIS evapotranspiration products over the conterminous United States: Using point and gridded FLUXNET and water balance ET. Remote Sens. Environ. 139, 35–49. https://doi.org/10.1016/j.rse.2013.07.013.

Vicente-Serrano, S.M., Beguería, S., López-Moreno, J.I., 2010. A multiscalar drought index sensitive to global warming: The standardized precipitation evapotranspiration index. J. Clim. 23 (7), 1696–1718. https://doi.org/10.1175/2009JCLI2909.1.

Vinukollu, R.K., Wood, E.F., Ferguson, C.R., Fisher, J.B., 2011. Global estimates of evapotranspiration for climate studies using multi-sensor remote sensing data: Evaluation of three process-based approaches. Remote Sens. Environ. 115 (3), 801–823. https://doi.org/10.1016/j.rse.2010.11.006.

Wan, Z., 2014. New refinements and validation of the collection-6 MODIS land-surface temperature/emissivity product. Remote Sens. Environ. 140, 36–45. https://doi.org/10.1016/j.rse.2013.08.027.

Wan, Z., Hook, S., Hulley, G., 2021. MOD11A1 MODIS/Terra Land Surface Temperature/Emissivity Daily L3 Global 1km SIN Grid V061 [Data set]. NASA EOSDIS Land Process. Distrib. Act. Arch. Cent. https://doi.org/10.5067/MODIS/MOD11A1.061.

Wang, K., Dickinson, R.E., 2012. A review of global terrestrial evapotranspiration: Observation, modeling, climatology, and climatic variability. Rev. Geophys. 50 (2). https://doi.org/10.1029/2011RG000373.

Weerasinghe, I., Bastiaanssen, W., Mul, M., Jia, L., Van Griensven, A., 2020. Can we trust remote sensing evapotranspiration products over Africa. Hydrol. Earth Syst. Sci. 24 (3), 1565–1586. https://doi.org/10.5194/hess-24-1565-2020.

Werth, D., Avissar, R., 2004. The regional evapotranspiration of the Amazon. J. Hydrometeorol. 5 (1), 100–109. https://doi.org/10.1175/1525-7541(2004)005<0100:TREOTA>2.0.CO;2.

Wu, R., Liu, Y., Xing, X., 2021. Evaluation of evapotranspiration deficit index for agricultural drought monitoring in North China. J. Hydrol. 596 (October 2020), 126057. https://doi.org/10.1016/j.jhydrol.2021.126057.

Xu, C.Y., Singh, V.P., 2005. Evaluation of three complementary relationship evapotranspiration models by water balance approach to estimate actual regional evapotranspiration in different climatic regions. J. Hydrol. 308 (1–4), 105–121. https://doi.org/10.1016/j.jhydrol.2004.10.024.

Yang, Y., Anderson, M.C., Gao, F., Wood, J.D., Gu, L., Hain, C., 2021. Studying drought-induced forest mortality using high spatiotemporal resolution evapotranspiration data from thermal satellite imaging. Remote Sens. Environ. 265, 112640. https://doi.org/10.1016/j.rse.2021.112640.

Zhang, K., Kimball, J.S., Running, S.W., 2016. A review of remote sensing based actual evapotranspiration estimation. Wiley Interdiscip. Rev. Water 3 (6), 834–853. https://doi.org/10.1002/wat2.1168.

Zhang, Y., Peña-Arancibia, J.L., McVicar, T.R., Chiew, F.H.S., Vaze, J., Liu, C., Lu, X., Zheng, H., Wang, Y., Liu, Y.Y., Miralles, D.G., Pan, M., 2016. Multi-decadal trends in global terrestrial evapotranspiration and its components. Sci. Rep. 6 (December 2015), 1–12. https://doi.org/10.1038/srep19124.

Zhao, M., A, G., Liu, Y., Konings, A.G., 2022. Evapotranspiration frequently increases during droughts. Nat. Clim. Change 12 (11), 1024–1030. https://doi.org/10.1038/s41558-022-01505-3.

Kutsch, W. L., Lutz, M., & Olaf, K. (2016). *FLUXNET FLUXNET2015 ZM-Mon Mongu Dataset Description*. doi:10.18140/FLX/1440189.